4. Steady Rolling with creepage and spin: asymptotic theories.

In this chapter and the next we will treat the problem of the transmission of tangential forces during rolling.

Consider two bodies of revolution which are pressed together by a normal force N, and which roll steadily over each other, see Fig. 6.

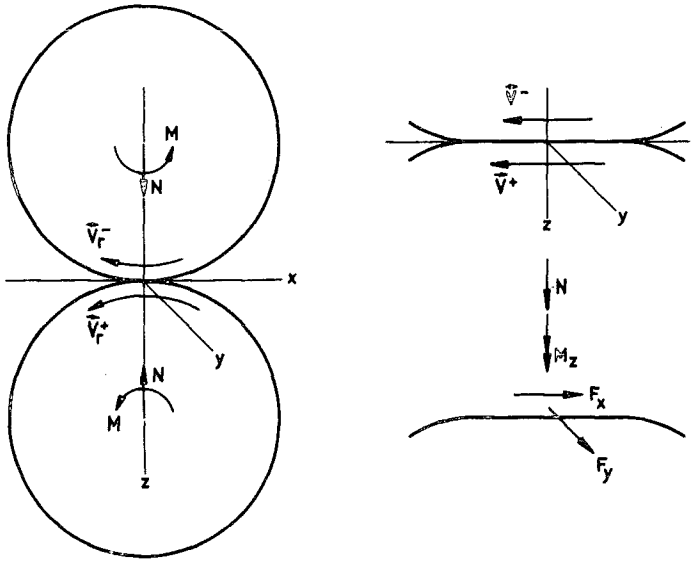

Fig. 6. Two bodies rolling over each other.

Owing to the normal force, a contact area is formed along which the bodies touch. If the conformity of the bodies is not too strong, and the changes of curvature are small, the contact area and the normal pressure transmitted across it are given by the HERTZ theory which we treated in detail in 3.221. According to this theory, the contact area is an ellipse with semi-axes a and b,

$$E = \{x,y,z:\ (x/a)^2+(y/b)^2 \leq 1,\ z=0\}\ , \tag{4.1}$$

while the distribution of normal stress is given by

$$Z = \frac{3N}{2\pi ab}\sqrt{1-(x/a)^2-(y/b)^2}. \tag{4.2}$$

The formulae by means of which the semi-axes a and b can be computed from N and from the radii of curvature R_x^+, R_y^+, R_x^-, R_y^- are given in 3.221. When the bodies are rolling steadily, their parallel circles are almost parallel, so that according to 3.221 the axes of the

contact ellipse are very nearly oriented along the rolling direction and perpendicular to it. So, if we take the axial direction of the ellipse as x and y axes, as we did throughout this work, the rolling direction very nearly coincides with one of these, so that we can assume without loss of generality that it is the positive x-axis.

In addition to the normal load, a tangential force can be transmitted from one body to the other, owing to friction. When the tangential load is below its maximal COULOMB value, that is, $|(F_x,F_y)|<\mu N$, μ: coeff. of friction, slip occurs in part of the contact area called the area of slip E_g, while in the remainder of the contact area, the locked area or area of adhesion E_h, there is no relative velocity of one body with respect to the other. This is a consequence of the fact that the elastic deformation of the bodies modifies the velocity pattern near the contact area. In the area of slip E_g, work is done by friction; macroscopically, this results in a difference of the overall circumferential velocity of the bodies. This difference is determined by means of the quantities called creepage and spin, which are defined in (4.14).

In the present chapter, we first set up the boundary conditions both for steady and unsteady rolling (sec. 4.1). In sec. 4.2, we consider the various symmetries present in the problem, and we introduce a number of dimensionless parameters. In sec. 4.3 we generalize the theory of DE PATER [1] and KALKER [1] on DE PATER's asymptotic case of infinitesimal creepage and spin, to elliptic contact areas. This is an application of the load-displacement equations of ch. 2. In 4.4 we present the theory of LUTZ [1,2,3] and WERNITZ [1,2] on LUTZ's asymptotic case of infinite creepage and spin, in a slightly generalized form.

4.1. Boundary conditions.

For the problem of elasticity and the solution of the boundary value problem, the bodies will be approximated by half-spaces. The boundary conditions are set up for the finite bodies, but we will already utilize the coordinate system of the half-spaces.

A cartesian coordinate system (0; x,y,z) is introduced in the following manner. The plane z=0 is the boundary of the half-spaces,

$z \geq 0$ is the lower half-space. The bodies touch each other along an elliptical contact area E, see 3.221. We take the centre of the ellipse as origin, and the axes of the ellipse as the coordinate axes x and y,

$$E = \{x,y,z: (x/a)^2+(y/b)^2 \leq 1,\ z=0\}. \tag{4.3}$$

The positive x-axis coincides approximately with the rolling direction, which is always the case when two bodies of revolution roll steadily over each other, as we pointed out in sec. 4.

The material of the bodies flows through this coordinate system. We take the undeformed state so, that at infinity the deformed and the undeformed state coincide, in other terms, the elastic displacement $\underline{u}^{\pm} = (u^{\pm},v^{\pm},w^{\pm})$ vanishes at infinity. In this undeformed state, the bodies intersect. This intersection is countered by the elastic deformation, as a consequence of which the contact area forms. According to 3.221, only the difference $w = w^{+}-w^{-}$ of the z-component of the displacement is involved in the formation of the contact area. As we have seen in (2.15c) and (2.10a), this difference is unaffected by the tangential tractions acting in the contact area, when the elastic constants of the bodies are the same. That means that contact area and normal pressure can be calculated as if the tangential tractions were absent. In the case that the elastic constants are not the same, we assume that the contact area E and the normal pressure Z are not significantly altered by the tangential tractions (X,Y), see sec. 2.1.

Regarding the tangential tractions, we only take the effect of dry friction into account. This means that the contact area is divided into a region of slip E_g where the tangential traction $|(X,Y)|=\mu Z$, and is directed along the local slip, and a locked region E_h where the slip vanishes, and $|(X,Y)| \leq \mu Z$. We assume that the coefficient of friction is independent of the slip, in particular, that the coefficient of friction which prevails in the locked region is the same as that in the slip region.

We observe that the slip is of central importance in the boundary conditions, and we proceed to find an expression for it. Consider a particle of the bodies which lies at a certain time t in

the point $\underline{x} = (x,y,z)$ in the undeformed state. The position in the deformed state is $\underline{x} + \underline{u}^{\pm} = (x+u^{\pm}, y+v^{\pm}, z+w^{\pm})$. The velocity of the particle is found by differentiation with respect to time. In the undeformed state the velocity is

$$\underline{V}_u = \frac{d\underline{x}}{dt} = \left(\frac{dx}{dt} , \frac{dy}{dt} , \frac{dz}{dt} \right), \tag{4.4}$$

and in the deformed state,

$$\underline{V}_d = \frac{d\underline{x}}{dt} + \frac{d\underline{u}}{dt} = \underline{V}_u + \frac{\partial \underline{u}}{\partial t} + (\underline{V}_u.\mathrm{grad})\underline{u}. \tag{4.5}$$

Let the superscript $^+$ refer to the lower body, and the superscript $^-$ to the upper body. We define the slip as the velocity of the upper body with respect to the lower body in the deformed state. It is:

$$\left.\begin{aligned} \underline{V}(x,y,0) = \underline{V}_d^- - \underline{V}_d^+ = (\underline{V}_u^+ - \underline{V}_u^-) + \frac{\partial(\underline{u}^- - \underline{u}^+)}{\partial t} + \\ + \tfrac{1}{2}(\{\underline{V}_u^- + \underline{V}_u^+\}.\mathrm{grad})(\underline{u}^- - \underline{u}^+) + \tfrac{1}{2}(\{\underline{V}_u^- - \underline{V}_u^+\}.\mathrm{grad})(\underline{u}^+ + \underline{u}^-). \end{aligned}\right\} \tag{4.6}$$

Since $|\mathrm{grad}(\underline{u}^+ + \underline{u}^-)| \ll 1$, we may neglect the last term of the right hand side of (4.6) with respect to the first term. This gives

$$\left.\begin{aligned} \underline{V}(x,y,0) = (V_u^+ - V_u^-) - \frac{\partial \underline{u}}{\partial t} - \tfrac{1}{2}(\{\underline{V}_u^- + \underline{V}_u^+\}.\mathrm{grad})\underline{u}, \\ \underline{u} = \underline{u}^+ - \underline{u}^-. \end{aligned}\right\} \tag{4.7}$$

The z-component of $\underline{V}(x,y,0)$ vanishes in the half-space approximation; the (x,y) components of $\underline{V}(x,y,0)$ depend only on the differences $u=u^+-u^-$, $v=v^+-v^-$ of the (x,y) components of the elastic displacement at z=0. We saw in (2.11a,b), and (2.10a) that this difference is unaffected by the normal pressure Z, when the elastic displacements of both bodies are the same. We can then calculate the tangential tractions and the difference of the (x,y) components of the elastic displacement at the contact area, as if the normal pressure were absent. We will do this throughout this work. If we use the results so obtained also in the case of different elastic constants by using the combined modulus of rigidity G and POISSON's ratio σ of eq. (2.10), it should be kept in mind that we make an error. This error is not necessarily small, see sec. 2.1.

We can regard the velocity of the undeformed bodies in the half-

space approximation as a velocity at the origin and a rotation about the z-axis:

$$\left.\begin{aligned} \frac{dx^+}{dt} &= \frac{dx^+}{dt}\Big|_o - \Omega_z^+ y, \quad \frac{dy^+}{dt} = \frac{dy^+}{dt}\Big|_o + \Omega_z^+ x, \\ \frac{dx^-}{dt} &= \frac{dx^-}{dt}\Big|_o - \Omega_z^- y, \quad \frac{dy^-}{dt} = \frac{dy^-}{dt}\Big|_o + \Omega_z^- x. \end{aligned}\right\} \tag{4.8}$$

We define the rolling velocity $\underline{V}_r$, with magnitude V as the opposite of the mean velocity at the origin,

$$\underline{V}_r = -\tfrac{1}{2}\left(\left[\frac{dx^+}{dt} + \frac{dx^-}{dt}\right]_o, \left[\frac{dy^+}{dt} + \frac{dy^-}{dt}\right]_o\right), \quad V = |\underline{V}_r|. \tag{4.9}$$

In the steady rolling of two bodies of revolution over each other, the rolling velocity makes a small angle δ with the positive x-axis. We confine ourselves to this case of small δ. Then, we have:

$$\underline{V}_r \approx -(V, \delta V). \tag{4.10}$$

The creepage $\underline{\upsilon} = (\upsilon_x, \upsilon_y)$ is defined as follows:

$$\upsilon_x = \frac{1}{V}\left(\frac{dx^-}{dt} - \frac{dx^+}{dt}\right)\Big|_o, \quad \upsilon_y = \frac{1}{V}\left(\frac{dy^-}{dt} - \frac{dy^+}{dt}\right)\Big|_o. \tag{4.11}$$

We write for the rotations Ω_z^+ and Ω_z^-

$$\Omega_z^+ = \tfrac{1}{2}(\Phi-\phi)V, \quad \Omega_z^- = \tfrac{1}{2}(\Phi+\phi)V. \tag{4.12}$$

ϕ is called the spin, and the constant Φ has no special name. Note that ϕ and Φ are not dimensionless, but have the dimension of $(\text{length})^{-1}$. The velocity (4.8) of the undeformed bodies becomes:

$$\left.\begin{aligned} \frac{dx^+}{dt} &= -V - \tfrac{1}{2}V\upsilon_x - \tfrac{1}{2}(\Phi-\phi)yV, \quad \frac{dy^+}{dt} = -\delta V - \tfrac{1}{2}V\upsilon_y + \tfrac{1}{2}(\Phi-\phi)xV; \\ \frac{dx^-}{dt} &= -V + \tfrac{1}{2}V\upsilon_x - \tfrac{1}{2}(\Phi+\phi)yV, \quad \frac{dy^-}{dt} = -\delta V + \tfrac{1}{2}V\upsilon_y + \tfrac{1}{2}(\Phi+\phi)xV, \end{aligned}\right\} \tag{4.13}$$

and

$$\underline{V}_u^- - \underline{V}_u^+ = \left(\frac{d(x^- - x^+)}{dt}, \frac{d(y^- - y^+)}{dt}\right) = V(\upsilon_x - \phi y, \upsilon_y + \phi x), \tag{4.14a}$$

$$\underline{V}_u^- + \underline{V}_u^+ = -V(2+\Phi y, 2\delta - \Phi x). \tag{4.14b}$$

$(\underline{V}_u^- + \underline{V}_u^+)$ is multiplied in (4.7) by a term of order grad $\underline{u}$. So we may neglect δ with respect to 1 when we insert (4.14b) in (4.7). We also assume that the angle between the rolling axes of the upper and the lower body and the z-axis is not small, that is, the rolling

axes are not almost vertical. In that case, the horizontal component of rotation Ω_x is larger or has the same order of magnitude as Ω_z, or ΦV. But $V = O(\rho\Omega_x)$, where ρ is the characteristic length of the bodies, see (3.38). Therefore, Φx and Φy are at most of the order of magnitude x/ρ, y/ρ. In the contact area we have that x/ρ and y/ρ are $O(\ell/\rho)$, with ℓ the major semi-axis of the contact ellipse, which is small with respect to unity when the bodies are counterformal. Hence we may also neglect the terms Φy and Φx when we insert (4.14b) into (4.7):

$$\left(\underline{V}_{-u}^{+} + \underline{V}_{-u}^{-} \right) = (-2V,0) \text{ when inserted in (4.7).} \tag{4.14c}$$

So, (4.7) becomes

$$\underline{V}(x,y,0) = V\,\underline{s}(x,y,0) = V(s_x,s_y,0),\ \underline{s}\text{: relative slip} \tag{4.15a}$$

$$\left.\begin{aligned} s_x &= v_x - \phi y - \frac{1}{V}\frac{\partial u}{\partial t} + \frac{\partial u}{\partial x}\ , \\ s_x &= v_y + \phi x - \frac{1}{V}\frac{\partial v}{\partial t} + \frac{\partial v}{\partial x}\ ; \end{aligned}\right\} \text{ unsteady rolling} \tag{4.15b}$$

$$s_x = v_x - \phi y + \frac{\partial u}{\partial x}\ ,\ s_y = v_y + \phi x + \frac{\partial v}{\partial x}\ \text{: steady rolling.} \tag{4.15c}$$

The boundary conditions can now be formulated.

$$\text{Stresses and displacements vanish at infinity;} \tag{4.16a}$$

$$\left.\begin{aligned} &Z = 0 \text{ on } z = 0, \text{ outside } E; \\ &Z = G\, f_{00}\sqrt{1-(x/a)^2-(y/b)^2},\ f_{00} = \frac{3N}{2\pi abG} \text{ inside } E; \end{aligned}\right\} \tag{4.16b}$$

$$X = Y = 0 \text{ on } z = 0, \text{ outside } E; \tag{4.16c}$$

$$\left.\begin{aligned} &(X,Y) = \mu G\, f_{00}\sqrt{1-(x/a)^2-(y/b)^2}\,(w_x,w_y) \text{ in region of slip } E_g, \\ &\text{with } \mu\text{: coeff. of friction, } w_x = s_x/s,\ w_y = s_y/s,\ s = \sqrt{s_x^2+s_y^2}\ , \\ &\underline{s} \text{ given in (4.15).} \end{aligned}\right\} \tag{4.16d}$$

$$s_x = s_y = 0,\ |(X,Y)| \le \mu Z \text{ in region of adhesion } E_h. \tag{4.16e}$$

4.2. Considerations of symmetry. New dimensionless parameters.

Let us define

$$X' = \frac{2\pi abG}{3\mu N}\,X,\quad Y' = \frac{2\pi abG}{3\mu N}\,Y \tag{4.17a}$$

$$(v_x', v_y', \phi') = \frac{2\pi abG}{3\mu N}\,(v_x, v_y, \phi). \tag{4.17b}$$

Then it follows from HOOKE's law and from the fact that we neglect the influence of the normal pressure Z on the displacement differences u and v, that the displacement differences due to (X',Y') are

$$(u', v') = \frac{2\pi abG}{3\mu N}\,(u, v), \tag{4.17c}$$

where (u,v) are the displacement differences due to (X,Y). Hence,

$$\left.\begin{aligned} s_x' &= v_x' - \phi' y - \frac{1}{V}\frac{\partial u'}{\partial t} + \frac{\partial u'}{\partial x} = \frac{2\pi abG}{3\mu N}\, s_x, \\ s_y' &= v_y' + \phi' x - \frac{1}{V}\frac{\partial v'}{\partial t} + \frac{\partial v'}{\partial x} = \frac{2\pi abG}{3\mu N}\, s_y. \end{aligned}\right\} \tag{4.17d}$$

Clearly,

$$w_x' = w_x,\quad w_y' = w_y. \tag{4.17e}$$

If

$$\left.\begin{aligned} (X', Y') &= G\sqrt{1-(x/a)^2-(y/b)^2}\,(w_x', w_y') && \text{in } E_g, \\ s_x' &= s_y' = 0,\quad |(X', Y')| \le G\sqrt{1-(x/a)^2-(y/b)^2} && \text{in } E_h, \end{aligned}\right\} \tag{4.18}$$

then it is clear that (4.16a,c,d,e) are satisfied by (X,Y). So we have only to solve (4.18) to obtain the solution for any coefficient of friction and normal load. Also, we have only to consider a single value of G, further we can choose the unit of length arbitrarily, so that we have to consider only one contact area with the prescribed ratio of the axes. In accordance with this, we introduce new dimensionless parameters. We consider $f_x = F_x/\mu N$, $f_y = F_y/\mu N$, $m_z = M_z/\mu Nc$, $c = \sqrt{ab}$, (see 3.50). Let F_x', F_y', and M_z' be the total force and torsional couple connected with (X',Y'); then

$$\left.\begin{aligned} f_x = F_x/\mu N &= \frac{3\mu N}{2\pi abG} \times \frac{F_x'}{\mu N} = \frac{3F_x'}{2\pi c^2 G}\,; \\ f_y = F_y/\mu N &= \frac{3\mu N}{2\pi abG} \times \frac{F_y'}{\mu N} = \frac{3F_y'}{2\pi c^2 G}\,; \\ m_z = M_z/\mu Nc &= \frac{3\mu N}{2\pi abG} \times \frac{M_z'}{\mu Nc} = \frac{3M_z}{2\pi c^3 G}\,. \end{aligned}\right\} \tag{4.19}$$

We also introduce new dimensionless parameters for creepage and spin:

$$\left.\begin{aligned} &\frac{1}{\rho} = \tfrac{1}{4}\Big(\frac{1}{R_x^+} + \frac{1}{R_x^-} + \frac{1}{R_y^+} + \frac{1}{R_y^-}\Big), \text{ see (3.38)};\\ &\xi = \frac{\upsilon_x \rho}{\mu c}, \quad \eta = \frac{\upsilon_y \rho}{\mu c}, \quad \chi = \frac{\phi\rho}{\mu}, \quad c = \sqrt{ab}. \end{aligned}\right\} \tag{4.20}$$

We express ξ, η and χ in υ_x', υ_y', and ϕ' of (4.17b). We make use of (3.51):

$$\left.\begin{aligned} &\xi = \frac{\upsilon_x \rho}{\mu c} = \frac{3N\mu}{2\pi abG}\frac{\rho}{\mu c}\upsilon_x' = \frac{2\sqrt{g}}{(1-\sigma)\underline{E}}\upsilon_x', \quad \eta = \frac{2\sqrt{g}}{(1-\sigma)\underline{E}}\upsilon_y',\\ &\chi = \frac{\phi\rho}{\mu} = \frac{2c\sqrt{g}}{(1-\sigma)\underline{E}}\phi' = \frac{2s}{(1-\sigma)\underline{E}}\phi', \text{ s: minor semi-axis of E.} \end{aligned}\right\} \tag{4.21}$$

We observe that $c\phi'$ and $s\phi'$ are dimensionless.

In the following, we suppose that (X',Y') and (u',v') satisfy the boundary conditions (4.18). Let

$$X^{(2)} = -X', \quad Y^{(2)} = -Y', \tag{4.22a}$$

$$\upsilon_x^{(2)} = -\upsilon_x', \quad \upsilon_y^{(2)} = -\upsilon_y', \quad \phi^{(2)} = -\phi'. \tag{4.22b}$$

From (4.22a) it follows that the corresponding displacement differences $u^{(2)}$ and $v^{(2)}$ satisfy

$$u^{(2)} = -u', \quad v^{(2)} = -v', \tag{4.22c}$$

so that it follows from (4.22b) and (4.22c) that

$$s_x^{(2)} = -s_x, \quad s_y^{(2)} = -s_y \Longrightarrow w_x^{(2)} = -w_x', \quad w_y^{(2)} = -w_y'; \tag{4.22d}$$

hence the boundary conditions are satisfied by $(X^{(2)},Y^{(2)},u^{(2)},v^{(2)})$ with the creepage and spin of (4.22b). The areas of slip and adhesion are the same as in the solution (X',Y',u',v'), and we have that

$$\left.\begin{aligned} f_x &= f_x(-\xi,-\eta,-\chi) = -f_x(\xi,\eta,\chi),\\ f_y &= f_y(-\xi,-\eta,-\chi) = -f_y(\xi,\eta,\chi),\\ m_z &= m_z(-\xi,-\eta,-\chi) = -m_z(\xi,\eta,\chi). \end{aligned}\right\} \tag{4.22e}$$

Let

$$X^{(3)}(x,y) = -X'(x,-y), \quad Y^{(3)}(x,y) = Y'(x,-y). \tag{4.23a}$$

Then, according to (2.15a,b),

$$u^{(3)}(x,y) = -u'(x,-y), \quad v^{(3)}(x,y) = v'(x,-y). \tag{4.23b}$$

When

$$\upsilon_x^{(3)} = -\upsilon_x', \quad \upsilon_y^{(3)} = \upsilon_y', \quad \phi^{(3)} = \phi' \ , \tag{4.23c}$$

it is easy to see that

$$s_x^{(3)}(x,y) = -s_x'(x,-y), \ s_y^{(3)}(x,y) = s_y'(x,-y), \tag{4.23d}$$

so that

$$w_x^{(3)}(x,y) = -w_x(x,-y), \ w_y^{(3)}(x,y) = w_y'(x,-y). \tag{4.23e}$$

We conclude that $(X^{(3)},Y^{(3)},u^{(3)},v^{(3)})$ satisfy the boundary conditions (4.18), with areas of adhesion and slip which are the mirror images with respect to the x-axis of the E_h and E_g corresponding to (X',Y'). Moreover, it is easily verified from

$$(F_x,F_y) = \iint_E (X,Y)dxdy, \ M_z = \iint_E (xY-yX)dxdy \tag{4.24}$$

that

$$f_x(\xi,\eta,\chi) = -f_x(-\xi,\eta,\chi), \ f_y(\xi,\eta,\chi) = f_y(-\xi,\eta,\chi), \ m_z(\xi,\eta,\chi) = m_z(-\xi,\eta,\chi). \tag{4.23f}$$

Let

$$X^{(4)}(x,-y) = X'(x,y), \ Y^{(4)}(x,-y) = -Y'(x,y), \tag{4.25a}$$

$$\upsilon_x^{(4)} = \upsilon_x', \quad \upsilon_y^{(4)} = -\upsilon_y', \quad \phi^{(4)} = -\phi' \ . \tag{4.25b}$$

It follows from (2.15a,b) that the corresponding surface displacement differences

$$u^{(4)}(x,y) = u'(x,-y), \ v^{(4)}(x,y) = -v'(x,-y), \tag{4.25c}$$

so that

$$s_x^{(4)}(x,y) = s_x'(x,-y), \ s_y^{(4)}(x,y) = -s_y'(x,-y), \tag{4.25d}$$

$$\Longrightarrow w_x^{(4)}(x,y) = w_x'(x,-y), \ w_y^{(4)}(x,y) = -w_y'(x,-y), \tag{4.25e}$$

So the system $(X^{(4)},Y^{(4)},u^{(4)},v^{(4)})$ satisfies the boundary conditions (4.18) for the creepage and spin as given in (4.25b), and with locked area and slip area which are the mirror image with respect to the x-axis of the E_h and E_g corresponding to (X',Y',u',v'). Again it is readily verified from (4.25a) and (4.24) that

$$\left.\begin{aligned} f_x(\xi,\eta,\chi) &= f_x(\xi,-\eta,-\chi), \\ f_y(\xi,\eta,\chi) &= -f_y(\xi,-\eta,-\chi), \\ m_z(\xi,\eta,\chi) &= -m_z(\xi,-\eta,-\chi). \end{aligned}\right\} \tag{4.25f}$$

As a corrollary of (4.23) we have

$$\left.\begin{aligned} \xi = 0 \Longrightarrow X'(x,y) &= X^{(3)}(x,y) = -X'(x,-y), \\ Y'(x,y) &= Y^{(3)}(x,y) = Y'(x,-y), \\ s'_x(x,y) &= s^{(3)}(x,y) = -s'_x(x,-y), \\ s'_y(x,y) &= s^{(3)}(x,y) = s'_x(x,-y), \\ f_x(0,\eta,\chi) &= 0, \\ E_h \text{ and } E_g &\text{ symmetric with respect to the x-axis.} \end{aligned}\right\} \tag{4.26}$$

We see from (4.26) that when $\xi = 0$, traction and slip are mirror antisymmetric about the x-axis.

As a corrollary of (4.25) we have

$$\left.\begin{aligned} \eta = \chi = 0 \Longrightarrow X'(x,y) &= X^{(4)}(x,y) = X'(x,-y), \\ Y'(x,y) &= Y^{(4)}(x,y) = -Y'(x,-y), \\ s'_x(x,y) &= s_x^{(4)}(x,y) = s_x^{(4)}(x,-y), \\ s'_y(x,y) &= s_y^{(4)}(x,y) = -s_y^{(4)}(x,-y), \\ f_y(\xi,0,0) &= m_z(\xi,0,0) = 0, \\ E_h \text{ and } E_g &\text{ symmetric with respect to the x-axis.} \end{aligned}\right\} \tag{4.27}$$

We see from (4.27) that when $\eta = \chi = 0$, traction and slip are mirror symmetric about the x-axis.

We summarize (4.22e), (4.23f), and (4.25f):

$$\left.\begin{aligned} f_x(\xi,\eta,\chi) &= -f_x(-\xi,\eta,\chi) = f_x(\xi,-\eta,-\chi) = -f_x(-\xi,-\eta,-\chi), \\ f_y(\xi,\eta,\chi) &= f_y(-\xi,\eta,\chi) = -f_y(\xi,-\eta,-\chi) = -f_y(-\xi,-\eta,-\chi), \\ m_z(\xi,\eta,\chi) &= m_z(-\xi,\eta,\chi) = -m_z(\xi,-\eta,-\chi) = -m_z(-\xi,-\eta,-\chi). \end{aligned}\right\} \tag{4.28}$$

Finally, it should be observed that the method used here for symmetries about the x-axis cannot be used for symmetries about the

y-axis. To see this, one might propose the following relationship:

$$X^{(5)}(x,y) = -X'(-x,y), \quad Y^{(5)}(x,y) = Y^{(5)}(-x,y).$$

Then indeed

$$u^{(5)}(x,y) = -u'(-x,y), \; v^{(5)}(x,y) = v'(-x,y),$$

but

$$\frac{\partial u^{(5)}(x,y)}{\partial x} = + \frac{\partial u'(-x,y)}{\partial x}, \quad \frac{\partial v^{(5)}(x,y)}{\partial x} = - \frac{\partial v'(-x,y)}{\partial x},$$

so that the signs of $(s_x^{(5)}, s_y^{(5)})$ do not match those of $(X^{(5)}, Y^{(5)})$.

4.3. The limiting case of infinitesimal creepage and spin.

When creepage and spin are absent, it follows from (4.15) that the relative slip (s_x, s_y) is given by

$$s_x = - \frac{1}{V} \frac{\partial u}{\partial t} + \frac{\partial u}{\partial x}, \quad s_y = - \frac{1}{V} \frac{\partial v}{\partial t} + \frac{\partial v}{\partial x}, \tag{4.29}$$

so that we can satisfy the adhesion condition $s_x = s_y = 0$ (4.16e) throughout the contact area by setting $u = v = 0$, from which it follows that $X = Y = 0$ (all in case of elastic symmetry). Therefore, the adhesion area covers the whole contact area and there is no slip.

As a consequence it is to be expected that when creepage and spin do not vanish but are very small, the adhesion area covers nearly the entire contact area. Accordingly it was proposed by DE PATER in 1957 to treat the case that creepage and spin are so small that the adhesion area can be approximated by the entire contact area. So, the boundary conditions (4.16) become

Stresses and displacements vanish at infinity; (4.30a)

$Z = 0$ on $z = 0$, outside E,

$$Z = G f_{00} \sqrt{1-(x/a)^2-(y/b)^2}, \; f_{00} = \frac{3N}{2\pi abG} \text{ inside E;} \tag{4.30b}$$

$X = Y = 0$ on $z = 0$, outside E; (4.30c)

$$\left.\begin{aligned} s_x &\equiv v_x - \phi y - \frac{1}{V} \frac{\partial u}{\partial t} + \frac{\partial u}{\partial x} = 0, \\ s_y &\equiv v_y + \phi x - \frac{1}{V} \frac{\partial v}{\partial t} + \frac{\partial v}{\partial x} = 0. \end{aligned}\right\} \tag{4.30d}$$

Condition (4.30a) is satisfied if we use the integral representations (2.7) and (2.13) of BOUSSINESQ-CERRUTTI for the connection between

surface tractions and displacements. Conditions (4.30b) define the HERTZ problem which we treated in 3.221. We will consider only the case of steady rolling, so that $\frac{\partial u}{\partial t} = \frac{\partial v}{\partial t} = 0$, and (4.30d) becomes

$$s_x \equiv \upsilon_x - \phi y + \frac{\partial u}{\partial x} = 0, \quad s_y \equiv \upsilon_y + \phi x + \frac{\partial v}{\partial x} = 0 \quad \text{inside E.} \tag{4.30e}$$

We integrate (4.30e) with respect to x, to find u and v:

$$u = -x\upsilon_x + \phi xy + f(y), \quad v = -\upsilon_y x - \tfrac{1}{2}\phi x^2 + g(y) \text{ in E,} \tag{4.31}$$

where f(y) and g(y) are arbitrary, differentiable functions of y. In order to apply the theory of the load-displacement equations, which is based on the integral representation of BOUSSINESQ-CERRUTTI, so that (4.30a) is satisfied, and in which the surface outside the ellipse E is free of traction (cond. (4.30c)), we approximate f(y) and g(y) by polynomials:

$$\left.\begin{aligned} u &= -\upsilon_x x + \phi xy + \sum_{n=0}^{M} a_{on}\, y^n, \\ v &= -\upsilon_y x - \tfrac{1}{2}\phi x^2 + \sum_{n=0}^{M} b_{on}\, y^n. \end{aligned}\right\} \quad \text{in E} \tag{4.32}$$

By increasing M, we can approximate f and g as closely as we like. The coefficients a_{on} and b_{on} are (2M+2) parameters which are still free. To (u,v) correspond the tangential tractions (X,Y) of the form

$$(X,Y) = \{1-(x/a)^2-(y/b)^2\}^{-\frac{1}{2}} \sum_{p=0}^{M} \sum_{q=0}^{M-p} (d_{pq}, e_{pq}) x^p y^q, \tag{4.33}$$

where the (d_{pq}, e_{pq}) are uniquely determined by υ_x, υ_y, ϕ and the (2M+2) parameters a_{on} and b_{on}. This means that we can assume (2M+2) relations between the (d_{pq}, e_{pq}).

In order to find these relations, we first attempt to bring X and Y in a form in which there is no singularity at the edge of the contact area:

$$(X,Y) = \{1-(x/a)^2-(y/b)^2\}^{+\frac{1}{2}} \sum_{p=o}^{M-2} \sum_{q=0}^{M-p-2} (d'_{pq}, e'_{pq}) x^p y^q, \tag{4.34}$$

and compare the number of coefficients in (4.33) and (4.34). In (4.33), there are (M+1)(M+2) coefficients, while (4.34) contains (M-1)M coefficients. In order that (4.33) can be brought into the form (4.34), there must exist (M+1)(M+2)-(M-1)M=4M+2 relations

between the coefficients of (4.33), which is about double the number of parameters (a_{on},b_{on}). So it would seem to be impossible to bring (4.33) in the form (4.34).

Another argument which points in the same direction is the following. Let us suppose that POISSON's ratio $\sigma = 0$. Then, according to (2.15a,b),

$$u(x,y)= \frac{1}{\pi G} \iint_E X(x',y') \frac{dx'dy'}{R} , \quad v(x,y)= \frac{1}{\pi G} \iint_E Y(x',y') \frac{dx'dy'}{R} ,$$

$$R = \sqrt{(x-x')^2+(y-y')^2}.$$

It is easy to see that when X is even in x, u will be even in x. For,

$$\begin{aligned} u(-x,y) &= \frac{1}{\pi G} \int_{-b}^{b} dy' \int_{-a\sqrt{1-(y'/b)^2}}^{a\sqrt{1-(y'/b)^2}} \frac{X(x',y')dx'dy'}{\sqrt{(x+x')^2+(y-y')^2}} \\ &= \frac{1}{\pi G} \int_{-b}^{b} dy' \int_{-a\sqrt{1-(y'/b)^2}}^{a\sqrt{1-(y'/b)^2}} \frac{X(-x',y')dx'dy'}{\sqrt{(x-x')^2+(y-y')^2}} \\ &= \frac{1}{\pi G} \iint_E \frac{X(x',y')dx'dy'}{R} = u(x.v). \end{aligned}$$

The converse, viz. that to an u which is even in x corresponds an X which is also even in x, follows from the (assumed) uniqueness. In the same way it can be shown that to an u which is odd in x corresponds an X which is odd in x. Now, $u = -v_x x$ is odd in x, and it is a polynomial, so it gives rise to an X which is odd in x and which has a singularity on the edge of the contact area, the strength of which is an odd function of x. $u = f(y)$ gives rise to an X with a singularity (if any) which is even in x. So these singularities can never cancel each other. The same holds for $v = -v_y x$ and for $u = \phi xy$. Finally, the singularities due to $u = -v_x x$ and to $u = \phi xy$ cannot cancel each other, since the former is even in y and the latter is odd in y. The conclusion is that there will be a singularity in (X,Y) at the edge of the contact area when $\sigma = 0$, and hence there is a strong presumption that the same happens when $\sigma \neq 0$.

The two arguments above point to two things: firstly, that it is impossible to have no area of slip whenever there is creepage and/or spin, and secondly, that if we assume as an approximation that there is no area of slip, we must accept a solution with an infinite traction at the edge of the contact area.

The first conclusion has a simple physical explanation. It is that there is a rate of dissipation connected with creepage and spin, of magnitude $(F_x v_x + F_y v_y + M_z \phi)V$, where (F_x, F_y) is the resultant tangential force and M_z is the resulting torsional couple about the z-axis, transmitted at the contact area. Since the elastic field is conservative, and the absence of an area of slip means that there is no dissipation by friction, the hypothesis that there is no area of slip leads to a contradiction.

As to the second conclusion we observe that there is also a rate of dissipation connected with the solution in which there is a stress singularity at the edge, and no slip in the contact area. This constitutes a paradox. It was pointed out by JOHNSON [3], pg. 797, that a comparable paradox occurs in aerofoil theory.

So we have found that the surface traction goes to infinity at the edge of the contact area. On the other hand, we still have the (2M+2) parameters a_{on} and b_{on}, and the only boundary condition which we did not use is COULOMB's friction law. The conclusion is that the parameters a_{on} and b_{on} must be determined by an application of the friction law, interpreted to fit our problem.

The friction law states in the first place that the tangential traction $|(X,Y)|$ may not exceed a finite multiple of the normal pressure Z: $|(X,Y)| \leq \mu Z$. This part of the friction law is violated near the edge of the contact area, if the traction goes to infinity there. So it is plausible to suppose that an infinite traction at a point should be interpreted as an indication that it belongs to the area of slip. We will show in 4.31 that the slip area does not border on the leading edge of the contact area in our approximation. Hence we must have that the strength of the singularity (X^e, Y^e) vanishes at the leading edge:

$$\left.\begin{aligned} (X^e,Y^e) &= 0 \quad \text{on leading edge of E,} \\ (X^e,Y^e) &= \lim_{(x,y)\to \text{ edge from inside}} (X,Y)\sqrt{1-(x/a)^2-(y/b)^2} \end{aligned}\right\} \quad (4.35)$$

The question arises whether this last condition indeed suffices to remove the undeterminateness of the boundary conditions (4.30). In the case of a circular contact area and vanishing POISSON's ratio

we succeeded in determining the solution in terms of an infinite series of spheroidal harmonics, the coefficients of which were stated explicitly (see KALKER [1], p. 171, eq. (8.10)). It was found that the problem is indeed completely determined by the conditions (4.30) and (4.35). Although this does not constitute a proof, there is a strong presumption that the conditions (4.30) and (4.35) indeed completely define the more general problem ($\sigma \neq 0$, elliptical contact area) we have here.

In the case of a finite number of the parameters a_{on}, b_{on}, it is impossible to satisfy (4.35). We then approximate (4.35) by the demand that (a_{on},b_{on}) are chosen so as to minimize the integral

$$\left.\begin{array}{l} \int_{-\pi/2}^{\pi/2} \{(X^e)^2 + (Y^e)^2\}\, d\psi = \text{minimal},\ x = a\cos\psi,\ y = b\sin\psi; \\ (X^e,Y^e) \text{ given by (4.35).} \end{array}\right\} \quad (4.36)$$

Since (X^e,Y^e) depend linearly on the parameters (a_{on},b_{on}), condition (4.36) furnishes us with the following (2M+2) linear equations in the (2M+2) unknowns (a_{on},b_{on}):

$$\left.\begin{array}{l} \int_{-\pi/2}^{\pi/2} \{X^e \frac{\partial X^e}{\partial a_{on}} + \frac{\partial Y^e}{\partial a_{on}}\} d\psi = \int_{-\pi/2}^{\pi/2} \{X^e \frac{\partial X^e}{\partial b_{on}} + Y^e \frac{\partial Y^e}{\partial b_{on}}\} d\psi = 0,\ n=0,\ldots,M, \\ X^e,Y^e: \text{ linearly dependent on } (a_{on},b_{on}), \\ \qquad \frac{\partial X^e}{\partial a_n}, \ldots,\ldots,\ldots \text{ independent of } (a_{on},b_{on}). \end{array}\right\} \quad (4.37)$$

4.31. Proof that no slip takes place at the leading edge, when creepage and spin are infinitesimal.

As we pointed out in 4.3, an infinite traction at a point of the edge on the contact area means that this point belongs to the slip area E_g. COULOMB's law also states that the slip is in the same direction as the tangential traction. To obtain an insight into the slip at the traction singularity, we determine the limiting behaviour of s_x and s_y as we approach the edge of the contact area from the outside since $s_x = s_y = 0$ inside the contact area.

We can express the slip in the traction by means of (2.16):

$$\left.\begin{aligned} s_x(x',y') &= v_x - \phi y' + \\ &+ \frac{1}{\pi G}\frac{\partial}{\partial x'}\iint_E \left[X(x,y)\left\{\frac{1-\sigma}{R} + \frac{\sigma(x-x')^2}{R^3}\right\} + Y(x,y)\,\frac{\sigma(x-x')(y-y')}{R^3}\right]dxdy, \\ s_y(x',y') &= v_y + \phi x + \\ &+ \frac{1}{\pi G}\frac{\partial}{\partial x'}\iint_E \left[Y(x,y)\left\{\frac{1-\sigma}{R} + \frac{\sigma(y-y')^2}{R^3}\right\} + X(x,y)\,\frac{\sigma(x-x')(y-y')}{R^3}\right]dxdy \\ R &= \sqrt{(x-x')^2+(y-y')^2}, \quad E: \text{ contact area.} \end{aligned}\right\} \tag{4.38}$$

Since (x',y') lies outside the contact area, we may interchange differentiation with respect to x' and integration:

$$\left.\begin{aligned} s_x(x',y') &= v_x - \phi y' + \\ &+ \frac{1}{\pi G}\iint_E \left[X(x,y)\left\{\frac{(1-3\sigma)(x-x')}{R^3} + \frac{3\sigma(x-x')^3}{R^5}\right\} + \right. \\ &\qquad \left. + \sigma Y(x,y)\left\{-\frac{y-y'}{R^3} + \frac{3(x-x')^2(y-y')}{R^5}\right\}\right]dxdy, \\ s_y(x',y') &= v_y + \phi x' + \\ &+ \frac{1}{\pi G}\iint_E \left[Y(x,y)\left\{\frac{(1-\sigma)(x-x')}{R^3} + \frac{3\sigma(x-x')(y-y')^2}{R^5}\right\} + \right. \\ &\qquad \left. + \sigma X(x,y)\left\{-\frac{y-y'}{R^3} + \frac{3(x-x')^2(y-y')}{R^5}\right\}\right]dxdy \end{aligned}\right\} \tag{4.39}$$

We assume that the tangential traction has an inverse square root behaviour at the edge of the contact area,

$$\left.\begin{aligned} X(x,y) &= X'(x,y)\{1-(x/a)^2-(y/b)^2\}^{-\frac{1}{2}}, \\ Y(x,y) &= Y'(x,y)\{1-(x/a)^2-(y/b)^2\}^{-\frac{1}{2}}, \end{aligned}\right\} \tag{4.40}$$

where $X'(x,y)$ and $Y'(x,y)$ are continuously differentiable functions. Now it will be shown later in this section that when the distance u' of (x',y') to E approaches zero, see fig. 7, then the relative slip is given by

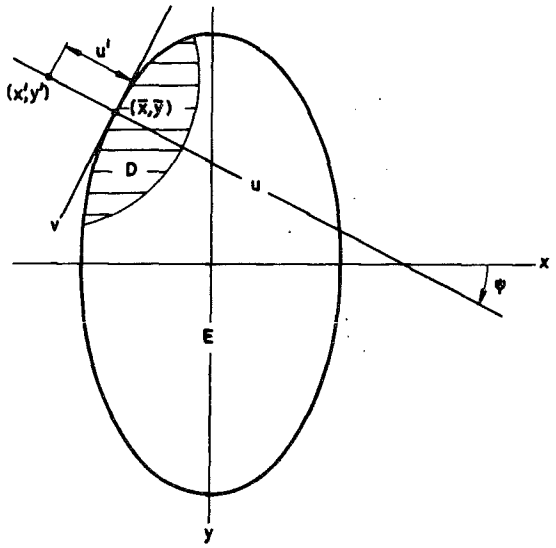

Fig. 7. The contact area with the u,v-axes.

$$\left.\begin{aligned} s_x(x',y') &= \cos\psi\Big\{\frac{2X'(\bar{x},\bar{y})}{GB\sqrt{u'}}(1-\sigma\cos^2\psi)-\frac{2\sigma Y'(\bar{x},\bar{y})}{GB\sqrt{u'}}\cos\psi\sin\psi\Big\}+0(1)\\ s_y(x',y') &= \cos\psi\Big\{\frac{2Y'(\bar{x},\bar{y})}{GB\sqrt{u'}}(1-\sigma\sin^2\psi)-\frac{2\sigma X'(\bar{x},\bar{y})}{GB\sqrt{u'}}\cos\psi\sin\psi\Big\}+0(1)\\ &u'\text{: distance of } (x',y') \text{ to E, } B=\sqrt{2}\sqrt[4]{(x'/a^2)^2+(y'/b^2)^2},\\ &\psi\text{ : angle between pos. x-axis and inner normal on edge of E}\\ &\quad\text{which passes through } (x',y');\\ &(\bar{x},\bar{y})\text{: intersection of this normal with the ellipse;}\\ &0(1)\text{ : any bounded function.} \end{aligned}\right\}\quad(4.41)$$

When POISSON's ratio $\sigma=0$, s_x and s_y become

$$\left.\begin{aligned} s_x(x',y') &= \frac{2X'(\bar{x},\bar{y})}{GB\sqrt{u'}}\cos\psi+0(1),\\ s_y(x',y') &= \frac{2Y'(\bar{x},\bar{y})}{GB\sqrt{u'}}\cos\psi+0(1), \end{aligned}\right\}\quad(4.42)$$

from which we see that the vector (s_x,s_y) is parallel to the tangential traction (X,Y) as $u'\to 0$, when, at any rate, $(X',Y')\neq(0,0)$ or, in other terms, when the traction goes to infinity at the edge. The vector has the same sense as (X',Y') when $\cos\psi>0$, and the opposite sense when $\cos\psi<0$. It is easy to see from fig. 7 that $\cos\psi>0$ when (x',y') approaches the trailing edge $x<0$, and that

$\cos\psi<0$ when (x',y') approaches the leading edge $x>0$. It is thus plausible to suppose that at the leading edge the slip would be opposite to the tangential traction, if the traction goes to infinity there; according to the friction law, this should not happen, and therefore the traction singularity should be removed from the leading edge.

When POISSON's ratio $\sigma\neq 0$, the slip and the tangential traction are not precisely parallel, but we can show that at the leading edge they are almost opposite, and at the trailing edge almost in the same sense. In order to show this, we calculate the angle θ between slip and traction from (4.41). After some calculation we obtain:

$$\cos\theta = \frac{Xs_x + Ys_y}{|(X,Y)||(s_x,s_y)|} = \frac{\{X^2+Y^2-\sigma(X\cos\psi+Y\sin\psi)^2\}\,\mathrm{sign}(\cos\psi)}{\sqrt{X^2+Y^2}\,\sqrt{X^2+Y^2-\sigma(2-\sigma)(X\cos\psi+Y\sin\psi)^2}} \qquad (4.43)$$

where we dropped the prime of X' and Y'. We denote by D the ratio

$$D = (X\cos\psi + Y\sin\psi)^2/(X^2+Y^2). \qquad (4.44a)$$

Since $(X\cos\psi + Y\sin\psi)$ is the component of (X,Y) in the direction $(\cos\psi, \sin\psi)$,

$$0 \leq D \leq 1. \qquad (4.44b)$$

In this notation, $\cos\theta$ becomes

$$\cos\theta = \frac{(1-\sigma D)\,\mathrm{sign}(\cos\psi)}{\sqrt{1-\sigma(2-\sigma)D}}\,. \qquad (4.45)$$

It can be shown without difficulty that the absolute value $|\cos\theta|$ reaches a maximum of 1 when D=0 or D=1, and a minimum of $\frac{2\sqrt{1-\sigma}}{2-\sigma}$ when $D = \frac{1}{2-\sigma}$. When $\sigma=0$, the minimum equals unity as we knew already. When $\sigma=\frac{1}{4}$, the minimum is 0.987, corresponding to an angle of 9°; when $\sigma=\frac{1}{2}$, the minimum is 0.941, corresponding to an angle of 20°. As a consequence of this and of the presence of $\mathrm{sign}(\cos\psi)$ in the expression for $\cos\theta$, we have that on the leading edge the angle θ is nearly 180°, and on the trailing edge it is nearly zero. Numerically we have:

$$\left.\begin{aligned} &\text{at the leading edge:} \quad 180^\circ - \theta_m \leq \theta \leq 180^\circ + \theta_m, \\ &\text{at the trailing edge:} \quad -\theta_m \leq \theta \leq \theta_m, \\ &\theta_m = 0 \text{ for } \sigma = 0;\ \theta_m = 9^\circ \text{ for } \sigma = \tfrac{1}{4};\ \theta_m = 20^\circ \text{ for } \sigma = \tfrac{1}{2}. \end{aligned}\right\} \qquad (4.46)$$

The conclusion is again that the traction singularity should be

removed from the leading edge of the contact area.

In the remainder of this section we will establish (4.41). We see from (4.39) and (4.41) that this task consists in calculating the part that behaves as $1/\sqrt{u'}$ (see fig. 7 and (4.41)) as the distance u' from (x',y') to E goes down to zero, of integrals of the following type:

$$I(x',y') = \iint_E \frac{f(x,y)(x-x')^m(y-y')^n}{R^{m+n+2}\sqrt{1-(x/a)^2-(y/b)^2}}\,dxdy, \quad \begin{matrix} R\text{: see (2.9)}, \\ E\text{: see (1.5a)}, \end{matrix} \tag{4.47}$$

where f(x,y) is a continuously differentiable function, and (x',y') is a point outside the elliptic area E. We shall show that $|I(x',y')| \to \infty$ as (x',y') approaches the elliptic area E, and we shall calculate the singular part of I.

In our coordinate system, we take the minor semi-axis of E as the unit of length. From (x',y') we drop a normal on the ellipse, see fig. 7; the point of intersection is $(\bar{x},\bar{y})$. It is clear that the contribution to the integral of the domain of integration outside a neighbourhood of (x',y') with radius δ is bounded. We denote by D this neighbourhood in so far it intersects with the elliptic area E. D is shown shaded in fig. 7. We also denote a bounded function by O(1). So we obtain

$$I(x',y') = \iint_D \frac{f(x,y)(x-x')^m(y-y')^n}{R^{m+n+2}\sqrt{1-(x/a)^2-(y/b)^2}}\,dxdy + O(1). \tag{4.48}$$

We introduce the cartesian coordinate system (u,v) into this integral, which has $(\bar{x},\bar{y})$ as origin, and the positive u-axis of which coincides with the inner normal to the ellipse at $(\bar{x},\bar{y})$, see fig. 7. Let ψ be the angle between the positive x-axis and the positive u-axis. Then:

$$\left.\begin{aligned}
&x-\bar{x} = u\cos\psi - v\sin\psi,\ y-\bar{y} = u\sin\psi + v\cos\psi;\\
&\text{the point } (x',y') \text{ has in the } (u,v) \text{ coordinate system}\\
&\qquad \text{the coordinates } (-u',0);\\
&u' \text{ is the distance from } (x',y') \text{ to E, } u'>0;\\
&x-x' = (u+u')\cos\psi - v\sin\psi,\ y-y' = (u+u')\sin\psi + v\cos\psi;\\
&R^2 = (u+u')^2+v^2;\ dxdy = dudv;\\
&f(x,y) = f(\bar{x},\bar{y}) + O\left(\sqrt{u^2+v^2}\right) = f(\bar{x},\bar{y}) + O\left(\sqrt{[u+u']^2+v^2}\right).
\end{aligned}\right\} \tag{4.49}$$

Also, since $(\bar{x},\bar{y})$ lies on the ellipse,

$$\left.\begin{aligned} 1-(x/a)^2-(y/b)^2 &= \frac{\bar{x}^2-x^2}{a^2}+\frac{\bar{y}^2-y^2}{b^2} = \frac{(\bar{x}-x)\{2\bar{x}-(\bar{x}-x)\}}{a^2}+\frac{(\bar{y}-y)\{2\bar{y}-(\bar{y}-y)\}}{b^2} = \\ &= -\Big(\frac{2\bar{x}\cos\psi}{a^2}+\frac{2\bar{y}\sin\psi}{b^2}\Big)u-\Big(-\frac{2\bar{x}\sin\psi}{a^2}+\frac{2\bar{y}\cos\psi}{b^2}\Big)v+h'(u,v), \end{aligned}\right\} \tag{4.50}$$

where $h'(u,v)$ is a homogeneous quadratic form in (u,v). So,

$$h'(u,v) = 0(u^2+v^2) = 0((u+u')^2+v^2) = 0(R^2) \text{ in } D, \tag{4.51}$$

where we made use of the fact that $u'>0$, and that $u>0$ in D. Also we have that the coefficient of v vanishes in (4.50), since the ellipse is tangent to the v-axis. That means according to (4.50), that

$$\left.\begin{aligned} &\frac{2\bar{x}}{a^2} = \alpha\cos\psi,\ \frac{2\bar{y}}{b^2} = \alpha\sin\psi,\ \alpha = \pm 2\sqrt{\frac{\bar{x}^2}{a^4}+\frac{\bar{y}^2}{b^4}} = \pm B^2\ (1+0(R)), \\ &B = \sqrt{2}\sqrt[4]{\Big(\frac{x'}{a^2}\Big)^2+\Big(\frac{y'}{b^2}\Big)^2}, \end{aligned}\right\} \tag{4.52}$$

so that (4.50) becomes

$$\left.\begin{aligned} 1-(x/a)^2-(y/b)^2 &= B^2\{u+h(u,v)\}(1+0(R)), \\ \text{with } h'(u,v) \quad &= B^2(1+0(R))h(u,v) = 0(R^2). \end{aligned}\right\}. \tag{4.53}$$

In (4.53) we chose the negative sign for α, since a point (x,y) with $v=0$, $0<u<<1$ lies inside the ellipse, so that $1-(x/a)^2-(y/b)^2>0$.

The integral (4.43) becomes with (4.49) and (4.53):

$$I(x',y') = \iint_D \frac{\{f(\bar{x},\bar{y})+0(R)\}\{(u+u')\cos\psi-v\sin\psi\}^m\{(u+u')\sin\psi+v\cos\psi\}^n}{B(1+0(R))\sqrt{u+h(u,v)}\ R^{m+n+2}}\,dudv+0(1). \tag{4.54}$$

Again we introduce a new coordinate system into this integral:

$$w = u+h(u,v),\ v = v; \tag{4.55}$$

we denote

$$\left.\begin{aligned} &r^2=(w+u')^2+v^2;\ \text{then, } h(u,v)=0(r^2),\ R^2=r^2(1+0(r)); \\ &dudv = \{1+0(r)\}dwdv; \\ &(u+u')\cos\psi-v\sin\psi=\{(w+u')\cos\psi-v\sin\psi\}(1+0(r)), \\ &(u+u')\sin\psi+v\cos\psi=\{(w+u')\sin\psi+v\cos\psi\}(1+0(r)), \\ &\text{all in D.} \end{aligned}\right\} \tag{4.56}$$

The integral becomes

$$\left.\begin{aligned} I(x',y') &= \iint_D \frac{\{f(\bar{x},\bar{y})+0(r)\}\{(w+u')\cos\psi-v\sin\psi\}^m}{B\sqrt{w}\ r^{m+n+2}} \times \\ &\quad \times \{(w+u')\sin\psi+v\cos\psi\}^n\{1+0(r)\}dvdw+0(1), \\ &= I'(x',y')+0(1), \\ I'(x',y') &= \iint_D \frac{f(\bar{x},\bar{y})\{(w+u')\cos\psi-v\sin\psi\}^m\{(w+u')\sin\psi+v\cos\psi\}^n}{B\sqrt{w}\ r^{m+n+2}}\ dvdw, \end{aligned}\right\} \quad (4.57)$$

since $\iint_D r^{m+n+1}/r^{m+n+2}\ dvdw = 0(1)$.

We observe that the domain of integration D lies in the half-plane $w \geq 0$. For $u' \geq 0$, the domain outside D, in so far as it lies in the half-plane $w \geq 0$, gives a finite contribution to the integral. So we can extend the integration to the whole half-plane $w \geq 0$:

$$I(x',y') = \int_0^\infty \frac{f(\bar{x},\bar{y})}{B\sqrt{w}}\ dw \int_{-\infty}^{\infty} \frac{\{(w+u')\cos\psi-v\sin\psi\}^m\{(w+u')\sin\psi+v\cos\psi\}^n}{r^{m+n+2}}\ dv+0(1) \quad (4.58)$$

We evaluate $\{(w+u')\cos\psi-v\sin\psi\}^m\{(w+u')\sin\psi+v\cos\psi\}^n$ by means of the binomial theorem. A typical integral is then

$$I(x',y',k,\ell) = \frac{f(\bar{x},\bar{y})}{B} \int_0^\infty \frac{dw}{\sqrt{w}} \int_{-\infty}^{\infty} \frac{(w+u')^k\ v^\ell\ dv}{\{(w+u')^2+v^2\}^{k/2+\ell/2+1}}\ . \quad (4.59)$$

By symmetry, this integral vanishes when ℓ is odd. When ℓ is even, we use the substitution

$$v = (w+u')\tan\theta,\ dv = \frac{w+u'}{\cos^2\theta}\ d\theta. \quad (4.60)$$

This gives

$$\left.\begin{aligned} I(x',y',k,\ell) &= \frac{f(\bar{x},\bar{y})}{B} \int_0^\infty \frac{dw}{(w+u')\sqrt{w}} \int_{-\pi/2}^{\pi/2} \sin^\ell\theta\cos^k\theta\ d\theta = \\ &= \frac{\pi f(\bar{x},\bar{y})}{B\sqrt{u'}} \frac{\Gamma\left(\frac{k+1}{2}\right)\Gamma\left(\frac{\ell+1}{2}\right)}{\Gamma\left(\frac{k+\ell+2}{2}\right)} \text{ when } \ell \text{ is even}, \\ &= 0 \qquad\qquad \text{when } \ell = \text{odd}. \end{aligned}\right\} \quad (4.61)$$

So as a final result from (4.58), (4.59) and (4.61) we obtain:

$$I(x',y') = \iint_E \frac{f(x,y)(x-x')^m(y-y')^n}{R^{m+n+2}\sqrt{1-(x/a)^2-(y/b)^2}}\,dxdy = \left.\begin{aligned} &= \frac{\pi f(\bar{x},\bar{y})}{2B\sqrt{u'}} \Big\{ \sum_{i=0}^{m} \sum_{j=0}^{n} \left[(-1)^i+(-1)^j\right] \binom{m}{i}\binom{n}{j} \frac{\Gamma\left(\frac{m+n-i-j+1}{2}\right)\Gamma\left(\frac{i+j+1}{2}\right)}{\Gamma\left(\frac{m+n+2}{2}\right)} \times \\ &\qquad \times \cos^{m+j-i}\psi \sin^{n+i-j}\psi \Big\} + O(1), \\ &B = \sqrt{2}\sqrt[4]{(x'/a^2)^2+(y'/b^2)^2}, \end{aligned}\right\} \quad (4.62)$$

$\bar{x}$, $\bar{y}$, u' and ψ, see fig. 7.

The expression (4.41) follows from (4.39) and from (4.62) after a straightforward, but somewhat laborious calculation, which we omit here.

4.32. Solution of the problem.

When we use the theory of the load-displacement equations, the boundary conditions (4.30a,c) are automatically satisfied, and the only boundary conditions left are (4.32) and (4.36).

We define

$$(X',Y') = \sum_{p=0}^{M} \sum_{q=0}^{M-p} (d_{pq},e_{pq})\, x^p y^q, \quad (4.63)$$

where the coefficients d_{pq}, e_{pq} depend uniquely on v_x, v_y, ϕ, a_{on}, b_{on} through the load-displacement equations (2.56), where we have, according to (4.32) in terms of the constants (a_{mn},b_{mn}) of (2.32):

$$\left.\begin{aligned} &a_{10} = -v_x,\ a_{11} = \phi\ ,\ a_{mn} = 0 \quad \text{otherwise, unless } m = 0; \\ &b_{10} = -v_y,\ b_{20} = -\tfrac{1}{2}\phi,\ b_{mn} = 0 \quad \text{otherwise, unless } m = 0. \end{aligned}\right\} \quad (4.64)$$

X and Y are given by

$$(X,Y) = G\sqrt{1-(x/a)^2-(y/b)^2}^{-1}\,(X',Y'), \quad (4.65)$$

so that according to the definition (4.35)

$$(X^e,Y^e) = G \lim_{x,y\to\text{edge}} (X',Y'). \quad (4.66)$$

According to the remarks made after (2.56), $(a_{2m+\varepsilon,2n+\omega}, b_{2m+\varepsilon',2n+\omega'})$ on the one hand, and $(d_{2p+\varepsilon,2q+\omega}, e_{2p+\varepsilon',2q+\omega'})$ on

the other hand belong to a closed system of equations for each of the four possible choices of (ε,ω). If we set M=2K+1, for instance, and

$$\left.\begin{aligned}
x_j^0 &= (1,x^2,y^2,x^4,x^2y^2,y^4, \ldots, y^{2K})\\
x_j^1 &= x(1,x^2,y^2,x^4,x^2y^2,y^4, \ldots, y^{2K})\\
x_j^2 &= y(1,x^2,y^2,x^4,x^2y^2,y^4, \ldots, y^{2K})\\
x_j^3 &= xy(1,x^2,y^2,x^4,x^2y^2,y^4, \ldots, y^{2K-2}),\\
X_j^0 &= (d_{00},d_{20},d_{02},d_{40},d_{22},d_{04}, \ldots, d_{0,2K})\\
X_j^1 &= (d_{10},d_{30},d_{12},d_{50},d_{32}, \ldots, d_{1,2K})\\
X_j^2 &= (d_{01},d_{21},d_{03},d_{41},d_{23}, \ldots, d_{0,2K+1}),\\
X_j^3 &= (d_{11},d_{31},d_{13},d_{51}, \ldots, d_{1,2K-1}),\\
Y_j^i &\text{ as } X_j^i, \text{ with } e_{pq} \text{ instead of } d_{pq},\\
u_j^i &\text{ as } X_j^i, \text{ with } a_{mn} \text{ instead of } d_{pq},\\
v_j^i &\text{ as } X_j^i, \text{ with } b_{mn} \text{ instead of } d_{pq},
\end{aligned}\right\} \qquad (4.67)$$

then, if we sum over repeated indices,

$$X' = X_j^i x_j^i,\quad Y' = Y_j^i x_j^i,\quad u = u_j^i x_j^i,\quad v = v_j^i x_j^i. \qquad (4.68)$$

We can write the load-displacement equations (2.56) as

$$\begin{bmatrix} u_j^i \\ v_j^{3-i} \end{bmatrix} = (A_{j\ell}^i) \begin{bmatrix} X_\ell^i \\ Y_\ell^{3-i} \end{bmatrix}, \text{ no sum over i; } i = 0,1,2,3. \qquad (4.69)$$

The matrices $A_{j\ell}^i$ are square and have a non-vanishing determinant, so that we can invert them:

$$\begin{bmatrix} X_j^i \\ Y_j^{3-i} \end{bmatrix} = (A_{j\ell}^i)^{-1} \begin{bmatrix} u_\ell^i \\ v_\ell^{3-i} \end{bmatrix}. \qquad (4.70)$$

According to (4.64), a great number of the u_j^i and v_j^i are zero, so that we can drop a number of columns of $(A_{j\ell}^i)^{-1}$, and we can write

$$
\left.\begin{aligned}
X^0_j &= B^0_{j,2n}\, a_{0,2n}, && (i=0 \text{ i.e. } \varepsilon=\omega=0),\\
X^1_j &= \tilde{C}^2_{j,2n+1}\, b_{0,2n+1} + D^1_j\, v_x, && (i=1, \text{ i.e. } \varepsilon=1,\ \omega=0),\\
X^2_j &= B^2_{j,2n+1}\, a_{0,2n+1} + \tilde{E}^1_j\, v_y, && (i=2, \text{ i.e. } \varepsilon=0,\ \omega=1),\\
X^3_j &= \tilde{C}^0_{j,2n}\, b_{0,2n} + F^3_j\, \phi, && (i=3, \text{ i.e. } \varepsilon=\omega=1).\\
Y^3_j &= \tilde{B}^0_{j,2n}\, a_{0,2n}, && (i=0 \text{ i.e. } \varepsilon=\omega=0),\\
Y^2_j &= C^2_{j,2n+1}\, b_{0,2n+1} + \tilde{D}^1_j\, v_x, && (i=1, \text{ i.e. } \varepsilon=1,\ \omega=0),\\
Y^1_j &= \tilde{B}^2_{j,2n+1}\, a_{0,2n+1} + E^1_j\, v_y, && (i=2, \text{ i.e. } \varepsilon=0,\ \omega=1),\\
Y^0_j &= C^0_{j,2n}\, b_{0,2n} + \tilde{F}^3_j\, \phi, && (i=3, \text{ i.e. } \varepsilon=\omega=1).
\end{aligned}\right\} \qquad (4.71)
$$

The quantities with the superscript $\sim$ vanish when $\sigma=0$, except $\tilde{F}^3_j$. This gives for (X',Y'):

$$
\left.\begin{aligned}
X' &= x^0_j\, B^0_{j,2n}\, a_{0,2n} + x^1_j\{\tilde{C}^2_{j,2n+1}\, b_{0,2n+1} + D^1_j\, v_x\} +\\
&\quad + x^2_j\{B^2_{j,2n+1}\, a_{0,2n+1} + \tilde{E}^1_j\, v_y\} + x^3_j\{\tilde{C}^0_{j,2n}\, b_{0,2n} + F^3_j\, \phi\},\\
Y' &= x^3_j\, \tilde{B}^0_{j,2n}\, a_{0,2n} + x^2_j\{C^2_{j,2n+1}\, b_{0,2n+1} + \tilde{D}^1_j\, v_x\} +\\
&\quad + x^1_j\{\tilde{B}^2_{j,2n+1}\, a_{0,2n+1} + E^1_j\, v_y\} + x^3_j\{C^0_{j,2n}\, b_{0,2n} + \tilde{F}^3_j\, \phi\}\ .
\end{aligned}\right\} \qquad (4.72)
$$

We can split X' and Y' in a part X_+, Y_+, even in y and a part X_-, Y_-, odd in y.

$$
\left.\begin{aligned}
\omega=0:\ X_+ &= x^0_j\, B^0_{j,2n}\, a_{0,2n} + x^1_j\{\tilde{C}^2_{j,2n+1}\, b_{0,2n+1} + D^1_j\, v_x\}\ ,\\
Y_- &= x^3_j\, \tilde{B}^0_{j,2n}\, a_{0,2n} + x^2_j\{C^2_{j,2n+1}\, b_{0,2n+1} + \tilde{D}^1_j\, v_x\}\ ,
\end{aligned}\right\} \qquad (4.73a)
$$

$$
\left.\begin{aligned}
\omega=1:\ X_- &= x^2_j\{B^2_{j,2n+1}\, a_{0,2n+1} + \tilde{E}^1_j\, v_y\} + x^3_j\{\tilde{C}^0_{j,2n}\, b_{0,2n} + F^3_j\, \phi\},\\
Y_+ &= x^1_j\{\tilde{B}^2_{j,2n+1}\, a_{0,2n+1} + E^1_j\, v_y\} + x^0_j\{C^0_{j,2n}\, b_{0,2n} + \tilde{F}^3_j\, \phi\}
\end{aligned}\right\} \qquad (4.73b)
$$

$$
X' = X_- + X_+,\quad Y' = Y_- + Y_+.\quad X_+(-y) = X_+(y),\ X_-(-y) = -X_-(y). \qquad (4.73c)
$$

We enter (4.73c) into the compensation condition (4.36):

$$
\left.\begin{aligned}
&\int_{-\pi/2}^{\pi/2} \{(X_+ + X_-)^2 + (Y_+ + Y_-)^2\}_{\text{edge}}\, d\psi =\\
&= \int_{-\pi/2}^{\pi/2} \{X_+^2 + Y_-^2\}|_{\text{edge}}\, d\psi + \int_{-\pi/2}^{\pi/2} \{X_-^2 + Y_+^2\}|_{\text{edge}}\, d\psi = \text{minimal.}
\end{aligned}\right\} \qquad (4.74)
$$

We see from (4.73a) that $\{X_+^2+Y_-^2\}$ depends only on υ_x, $a_{0,2n}$ and $b_{0,2n+1}$, and that $\{X_-^2+Y_+^2\}$ depends only on υ_y, ϕ, $a_{0,2n+1}$, and $b_{0,2n}$. So the system of compensation equations falls apart into two systems, one involving the quantities with $\omega = 0$, and one involving those with $\omega = 1$. Now, the total force is given by

$$F_x = G \iint_E \sqrt{1-(x/a)^2-(y/b)^2}^{-1} X' \,dxdy = G \iint_E \sqrt{1-(x/a)^2-(y/b)^2}^{-1} X_+ \,dxdy, \tag{4.75a}$$

so that, after removal of the singularity from the leading edge, F_x depends only on υ_x. Further we have that

$$F_y = G \iint_E \sqrt{1-(x/a)^2-(y/b)^2}^{-1} Y_+ \,dxdy, \tag{4.75b}$$

$$M_z = G \iint_E \sqrt{1-(x/a)^2-(y/b)^2}^{-1} (xY_+ - yX_-) \,dxdy, \tag{4.75c}$$

so that F_y and M_z depend only on υ_y and ϕ. This is completely in accordance with the findings of 4.2, since F_x, F_y and M_z are here linear in υ_x, υ_y, ϕ, owing to the linear character of the compensation condition, see (4.37).

Let us call

$$x^e = \begin{bmatrix} x_j^0 \\ x_j^1 \end{bmatrix}, \quad x^o = \begin{bmatrix} x_j^2 \\ x_j^3 \end{bmatrix}, \quad u^e = \begin{bmatrix} a_{0,2n} \\ b_{0,2n+1} \\ \upsilon_x \end{bmatrix}, \quad u^o = \begin{bmatrix} a_{0,2n+1} \\ b_{0,2n} \\ \upsilon_y \\ \phi \end{bmatrix} \tag{4.76}$$

and let us indicate a transpose by a ' over the letters. Then we have

$$X_+ = \begin{pmatrix} x_j^0 & x_j^1 \end{pmatrix} \begin{bmatrix} B_{j,2n}^0 & 0 & 0 \\ 0 & \tilde{C}_{j,2n+1}^2 & D_j^1 \end{bmatrix} \begin{bmatrix} a_{0,2n} \\ b_{0,2n+1} \\ \upsilon_x \end{bmatrix} = x'^e B^e u^e; \tag{4.77a}$$

$$Y_- = \begin{pmatrix} x_j^2 & x_j^3 \end{pmatrix} \begin{bmatrix} 0 & C_{j,2n+1}^2 & \tilde{D}_j^1 \\ \tilde{B}_{j,2n}^0 & 0 & 0 \end{bmatrix} \begin{bmatrix} a_{0,2n} \\ b_{0,2n+1} \\ \upsilon_x \end{bmatrix} = x'^o B^o u^e; \tag{4.77b}$$

$$X_- = \begin{pmatrix} x_j^2 & x_j^3 \end{pmatrix} \begin{bmatrix} B^2_{j,2n+1} & 0 & \tilde{E}^1_j & 0 \\ 0 & \tilde{C}^0_{j,2n} & 0 & F^3_j \end{bmatrix} \begin{bmatrix} a_{0,2n+1} \\ b_{0,2n} \\ v_y \\ \phi \end{bmatrix} = {}'x^o C^o u^o; \qquad (4.77c)$$

$$Y_+ = \begin{pmatrix} x_j^0 & x_j^1 \end{pmatrix} \begin{bmatrix} 0 & C^0_{j,2n} & 0 & \tilde{F}^3_j \\ \tilde{B}^2_{j,2n+1} & 0 & E^1_j & 0 \end{bmatrix} \begin{bmatrix} a_{0,2n+1} \\ b_{0,2n} \\ v_y \\ \phi \end{bmatrix} = {}'x^e C^e u^o \qquad (4.77d)$$

So,

$$\left.\begin{aligned} X_+^2 + Y_-^2 &= {}'u^e{}'B^e x^e{}'x^e B^e u^e + {}'u^e{}'B^o x^o{}'x^o B^o u^e = \\ &= {}'u^e \left({}'B^e x^e{}'x^e B^e + {}'B^o x^o{}'x^o B^o\right) u^e \ , \end{aligned}\right\} \qquad (4.78a)$$

$$X_-^2 + Y_+^2 = {}'u^o \left({}'C^o x^o{}'x^o C^o + {}'C^e x^e{}'x^e C^e\right) u^o. \qquad (4.78b)$$

We integrate (4.78a) and (4.78b) over the leading edge of the contact area $x=a\cos\psi$, $y=b\sin\psi$, $-\pi/2 \le \psi \le \pi/2$. Only the matrices $x^{e\prime}x^e$ and $x^{o\prime}x^o$ are position dependent. There are two types of integral:

$$\left.\begin{aligned} \int_{-\pi/2}^{\pi/2} x_k^i \, x_\ell^i \, d\psi &= \int_{-\pi/2}^{\pi/2} x^{2p} y^{2q} \, d\psi = \int_{-\pi/2}^{\pi/2} a^{2p} b^{2q} \cos^{2p}\psi \sin^{2q}\psi \, d\psi \\ &= a^{2p} b^{2q} \ \frac{\Gamma(p+\frac{1}{2})\Gamma(q+\frac{1}{2})}{(p+q)!} \ , \end{aligned}\right\} \qquad (4.79a)$$

$$\int_{-\pi/2}^{\pi/2} x_k^{2\omega} \, x_\ell^{2\omega+1} \, d\psi = \int_{-\pi/2}^{\pi/2} x^{2p+1} \, y^{2q} \, d\psi =$$

$$= \int_{-\pi/2}^{\pi/2} a^{2p+1} b^{2q} \cos^{2p+1}\psi \sin^{2q}\psi \, d\psi = a^{2p+1} b^{2q} \ \frac{\Gamma(q+\frac{1}{2})p!}{\Gamma(p+q+3/2)} \ . \qquad (4.79b)$$

Call

$$\int_{-\pi/2}^{\pi/2} x^{e\prime e} d\psi = F^e, \qquad \int_{-\pi/2}^{\pi/2} x^{o\prime o} d\psi = F^o, \qquad (4.80)$$

then

$$\int_{-\pi/2}^{\pi/2} \{X_+^2 + Y_-^2\}d\psi = \overset{'}{u}^e(\overset{'}{B}^e F^e B^e + \overset{'}{B}^o F^o B^o)u^e = \text{minimal},$$
$$\int_{-\pi/2}^{\pi/2} \{X_-^2 + Y_+^2\}d\psi = \overset{'}{u}^o(\overset{'}{C}^e F^e C^e + \overset{'}{C}^o F^o C^o)u^o = \text{minimal}, \tag{4.81}$$

and a typical compensation equation is found by differentiating (4.81) with respect to a_{on}, b_{on}:

$$2(0,0,1,0 \ \ldots \ 0)(\overset{'}{B}^e F^e B^e + \overset{'}{B}^o F^o B^o)u^e = 0, \tag{4.82}$$

or, in other terms

the first (2K+1) rows of $(\overset{'}{B}^e F^e B^e + \overset{'}{B}^o F^o B^o)u^e$ must vanish, (4.83a)

the first (2K+1) rows of $(\overset{'}{C}^e F^e C^e + \overset{'}{C}^o F^o C^o)u^o$ must vanish. (4.83b)

These equations are solved numerically, where we set $v_x=1$ in (4.83a), and by multiplying the resulting $(a_{0,2n}, b_{0,2n+1})$ by v_x; we set $v_y=1$, $\phi=0$ in (4.83b) and multiply the resulting $(a_{0,2n+1}, b_{0,2n})$ by v_y, and finally we set $v_y=0$, $\phi=1$ in (4.83b) and multiply the resulting $(a_{0,2n+1}, b_{0,2n})$ by ϕ.

In order to find the total force F_x, F_y and the torsional couple M_z, we first observe that

$$\left.\begin{aligned} F_x &= G \iint_E \sqrt{1-(x/a)^2-(y/b)^2}^{-1} \ X'dxdy = G \iint_E \sqrt{1-(x/a)^2-(y/b)^2}^{-1} \ X_j^o x_j^o dxdy, \\ F_y &= G \iint_E \sqrt{1-(x/a)^2-(y/b)^2}^{-1} \ Y_j^o x_j^o \ dxdy, \\ M_z &= G \iint_E \sqrt{1-(x/a)^2-(y/b)^2}^{-1} \ \left(xY_j^1 x_j^1 - yX_j^2 x_j^2\right) dxdy. \end{aligned}\right\} \tag{4.84}$$

By means of (4.71), we can determine X_j^o, Y_j^o, X_j^2, Y_j^1 from the (a_{on}, b_{on}) which we find from the solution of the compensation equations (4.83a,b). A typical integral of (4.84) is

$$\left.\begin{aligned} &\iint_E x^{2p} y^{2q} \sqrt{1-(x/a)^2-(y/b)^2}^{-1} \ dxdy = \\ &\quad = a^{2p+1} b^{2q+1} \int_0^{2\pi} \cos^{2p}\psi \sin^{2q}\psi d\psi \int_0^1 \frac{r^{2p+2q+1}}{\sqrt{1-r^2}} dr = \\ &\quad = a^{2p+1} b^{2q+1} \ \frac{\Gamma(p+\frac{1}{2})\Gamma(q+\frac{1}{2})\Gamma(\frac{1}{2})}{\Gamma(p+q+3/2)} \ . \end{aligned}\right\} \tag{4.85}$$

We obtain

$$F_x=Gc^2C_{11}\upsilon_x,\ F_y=Gc^2\left(C_{22}\upsilon_y + C_{23}c\phi\right),\ M_z=Gc^3\left(C_{32}\upsilon_y + C_{33}c\phi\right) \qquad (4.86)$$

where the creepage and spin coefficients C_{ij} are calculated with $c = \sqrt{ab}$ as unit of length. With (4.19), (4.20) and (3.50) we obtain for the dimensionless parameters of sec. 4.2:

$$\left(f_x,f_y,m_z\right)=\left(\frac{F_x}{\mu\Pi},\ \frac{F_y}{\mu\Pi},\ \frac{M_z}{\mu\Pi c}\right)=\frac{3(1-\sigma)E}{4\pi\sqrt{g}}\left(C_{11}\xi,\ C_{22}\eta + C_{23}\chi,\ C_{32}\eta + C_{33}\chi\right). \qquad (4.87)$$

4.33. Numerical results.

The creepage coefficients C_{ij} were calculated for a few values of a/b with $2K+\nu=3,5,7$. It was found that the solution with $2K+\nu=5$ had a relative error of less than 1% from the solution with $2K+\nu=7$. Therefore, we calculated the creepage coefficients C_{ij} for more values of a/b with $2K+\nu=5$. The results are shown in fig. 8a and 8b, and in Table 3.

For the case of a circular contact area (a/b = 1), the values found coincide with those given in KALKER [1]. In that paper, the values of C_{ij} were compared with JOHNSON's experimental results on the rolling of steel balls [1,3]. JOHNSON found that C_{11} lies between 3.8 and 4.4; we find for $\sigma = 0.28$ the value 4.22. Also, according to Johnson, $C_{22} = 3.47$ and $C_{23} = 1.53$; we find 3.71 and 1.49 respectively. Since according to JOHNSON the moment M_z due to elastic hysteresis is of a higher order of magnitude than the moment due to creepage and spin, when the latter are very small, we cannot compare C_{32} and C_{33} with the experiment; indeed, we conclude that the values of C_{23} and C_{33} are of little practical significance.

According to the theoretical results of JOHNSON and VERMEULEN [5],

$$\left.\begin{aligned} C_{22}(e) &= C_{22}(0)\ \psi_1(0)/\psi_1(e), \\ \psi_1(e) &= \underline{B} - \sigma g^2\underline{C} \quad \text{when } a \le b\ (e \ge 0), \\ &= \tfrac{1}{16}(4-\sigma)\pi \quad \text{when } a = b\ (e = 0), \\ &= g\underline{D} - \sigma g\underline{C} \quad \text{when } a \ge b\ (e \le 0); \end{aligned}\right\} \qquad (4.88a)$$

Table 3. The creepage and spin coefficients C_{ij}.

		C_{11}			C_{22}			$C_{23} = -C_{32}$			C_{33}		
	g	σ=0	1/4	1/2	σ=0	1/4	1/2	σ=0	1/4	1/2	σ=0	1/4	1/2
	0.0	$\pi^2/4(1-\sigma)$			$\pi^2/4$			$\pi\sqrt{g}/3$	-	-	$\pi^2/16(1-\sigma)g$		
b/a	0.1	2.51	3.31	4.85	2.51	2.52	2.53	0.334	0.473	0.731	6.42	8.28	11.7
	0.2	2.59	3.37	4.81	2.59	2.63	2.66	0.483	0.603	0.809	3.46	4.27	5.66
	0.3	2.68	3.44	4.80	2.68	2.75	2.81	0.607	0.715	0.889	2.49	2.96	3.72
	0.4	2.78	3.53	4.82	2.78	2.88	2.98	0.720	0.823	0.977	2.02	2.32	2.77
	0.5	2.88	3.62	4.83	2.88	3.01	3.14	0.827	0.929	1.07	1.74	1.93	2.22
	0.6	2.98	3.72	4.91	2.98	3.14	3.31	0.930	1.03	1.18	1.56	1.68	1.86
	0.7	3.09	3.81	4.97	3.09	3.28	3.48	1.03	1.14	1.29	1.43	1.50	1.60
	0.8	3.19	3.91	5.05	3.19	3.41	3.65	1.13	1.25	1.40	1.34	1.37	1.42
	0.9	3.29	4.01	5.12	3.29	3.54	3.82	1.23	1.36	1.51	1.27	1.27	1.27
a/b	1.0	3.40	4.12	5.20	3.40	3.67	3.98	1.33	1.47	1.63	1.21	1.19	1.16
	0.9	3.51	4.22	5.30	3.51	3.81	4.16	1.44	1.59	1.77	1.16	1.11	1.06
	0.8	3.65	4.36	5.42	3.65	3.99	4.39	1.58	1.75	1.94	1.10	1.04	0.954
	0.7	3.82	4.54	5.58	3.82	4.21	4.67	1.76	1.95	2.18	1.05	0.965	0.852
	0.6	4.06	4.78	5.80	4.06	4.50	5.04	2.01	2.23	2.50	1.01	0.892	0.751
	0.5	4.37	5.10	6.11	4.37	4.90	5.56	2.35	2.62	2.96	0.958	0.819	0.650
	0.4	4.84	5.57	6.57	4.84	5.48	6.31	2.88	3.24	3.70	0.912	0.747	0.549
	0.3	5.57	6.34	7.34	5.57	6.40	7.51	3.79	4.32	5.01	0.868	0.674	0.446
	0.2	6.96	7.78	8.82	6.96	8.14	9.79	5.72	6.63	7.89	0.828	0.601	0.341
	0.1	10.7	11.7	12.9	10.7	12.8	16.0	12.2	14.6	18.0	0.795	0.526	0.228

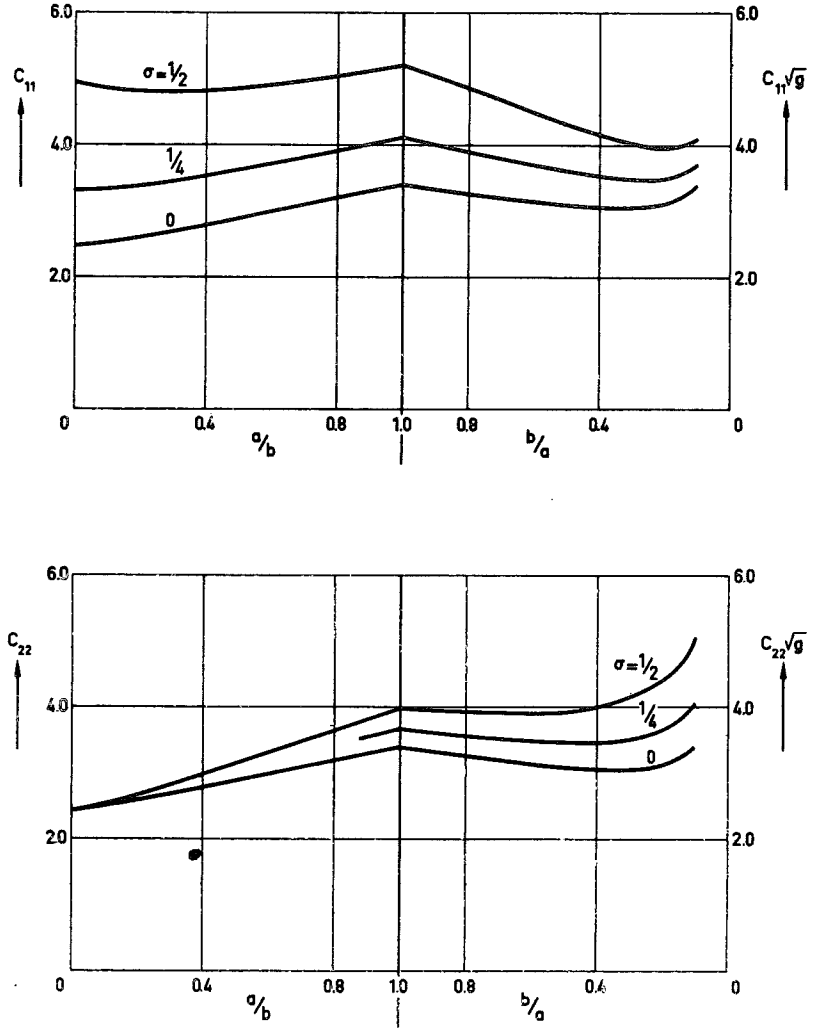

Fig. 3a. The creepage coefficients C_{11} and C_{22}.

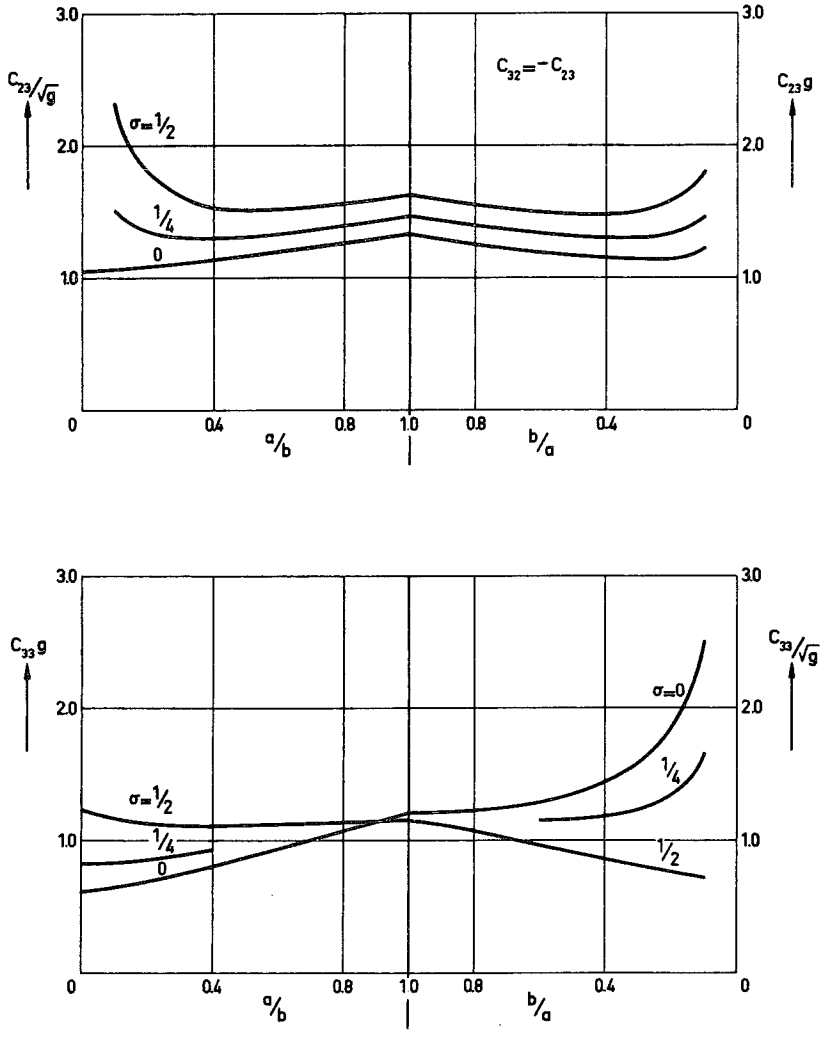

Fig. 8b. The creepage and spin coefficients C_{23}, C_{32}, C_{33}.

$$\left.\begin{aligned} C_{11}(e) &= C_{11}(0)\ \Phi(0)/\Phi(e), \\ \Phi(e) &= \underline{B} - \sigma(\underline{D} - \underline{C}) && \text{when } a \leq b\ (e \geq 0), \\ &= \frac{1}{16}(4-3\sigma)\pi && \text{when } a = b\ (e = 0), \\ &= g(1-\sigma)\underline{D} + \sigma g\underline{C} && \text{when } a \geq b\ (e \leq 0). \end{aligned}\right\} \tag{4.88b}$$

The experiments of JOHNSON and VERMEULEN on the dependence of F_y on v_y for different values of the axial ratio a/b, (see [5], fig. 3) show that the relationship

$$\left[\frac{F_y}{\mu N}\right]_{v_x=\phi=0} = f\left(\frac{\pi G a b v_y}{3\mu N \psi_1}\right), \quad \sigma = 0.28 \tag{4.89}$$

is very nearly satisfied. We compared the functions

$$\left.\begin{aligned} C'_{22}(e) &= C_{22}(0)\ \psi_1(0)/\psi_1(e), \\ C'_{11}(e) &= C_{11}(0)\ \Phi(0)/\Phi(e) \end{aligned}\right\} \tag{4.90}$$

with the values of $C_{22}(e)$ and $C_{11}(e)$ as we calculated them, for σ=0.25. In the range $0.2 \leq a/b \leq 1$, $0.2 \leq b/a \leq 1$ we found a discrepancy of at most 7% both in C_{22} and in C_{11}, the largest discrepancy occurring at the end of the ranges a/b = 0.2 or b/a = 0.2. In fact,

$$\left.\begin{aligned} a/b = 0.2: \quad C_{22}(0)\ \psi_1(0)/\psi_1(e) &= 1.07\ C_{22}(e), \\ C_{11}(0)\ \Phi(0)/\Phi(e) &= 1.05\ C_{11}(e), \\ b/a = 0.2: \quad C_{22}(0)\ \psi_1(0)/\psi_1(e) &= 0.94\ C_{22}(e), \\ C_{11}(0)\ \Phi(0)/\Phi(e) &= 0.93\ C_{11}(e). \end{aligned}\right\} \tag{4.91}$$

So here also the experimental results of JOHNSON are fairly close to our theoretical results on C_{22}.

We observe that in the calculations of C_{ij}, the smallest value of a/b and b/a with which we computed was a/b = 0.1, b/a = 0.1. The values of C_{ij} for a/b = 0.1 came close to those of the strip theory of KALKER [2], with the exception of $C_{32} = -C_{23}$, for $\sigma \neq 0$. So we ventured to put in the values of C_{ij} obtained by the strip theory at a/b = 0, and led the graphs through to a/b = 0.

Finally we note that the feature that $C_{32} = -C_{23}$ which was noted in KALKER [1], also persists in the case of elliptical contact

areas. No explanation has been given for this curious feature.

4.4. The limiting case of large creepage and spin. Numerical results.

When the creepage and the spin become very large, we may neglect the elastic deformation in the expression (4.15) for the relative slip:

$$\left.\begin{aligned} s_x &= v_x - \phi y + \frac{\partial u}{\partial x} - \frac{1}{V}\frac{\partial u}{\partial t} \approx v_x - \phi y, \\ s_y &= v_y + \phi x + \frac{\partial v}{\partial x} - \frac{1}{V}\frac{\partial v}{\partial t} \approx v_y + \phi x. \end{aligned}\right\} \qquad (4.92)$$

We can then regard the slip, with LUTZ [1,2,3] and WERNITZ [1,2] as a pure rigid body rotation with angular velocity ϕV about a point in the plane $z = 0$ which is called the spin pole by LUTZ and WERNITZ:

$$\text{spin pole} = (x', y'),\ x' = -v_y/\phi = -c\eta/\chi,\ y' = v_x/\phi = c\xi/\chi, \qquad (4.93)$$

see fig. 9. No adhesion area is assumed to form, not even when the

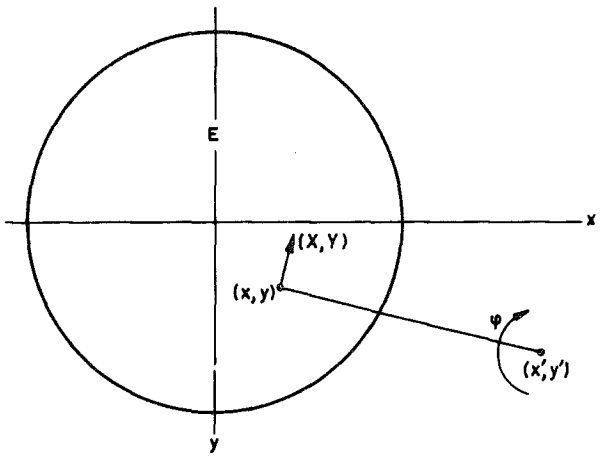

Fig. 9. Contact area with spin pole and traction vector.

spin pole lies inside the contact area. Note that the rolling direction is no longer a preferred direction. The surface traction transmitted by the upper body to the lower body has the magnitude

$$|(X,Y)| = \mu Z = \frac{3\mu N}{2\pi ab}\sqrt{1-(x/a)^2-(y/b)^2}, \qquad (4.94)$$

and the direction is perpendicular to the line between (x',y') and (x,y), with a positive moment with respect to (x',y') when ϕ is positive, and with a negative moment when ϕ is negative. It is easy to see from fig. 9 that

$$\left.\begin{aligned} df_x &= d(F_x/\mu N) = \frac{3\,\mathrm{sign}(\chi)}{2\pi ab}\sqrt{1-(x/a)^2-(y/b)^2}\;\frac{(y'-y)\,dxdy}{\sqrt{(x-x')^2+(y-y')^2}}\,, \\ df_y &= d(F_y/\mu N) = -\frac{3\,\mathrm{sign}(\chi)}{2\pi ab}\sqrt{1-(x/a)^2-(y/b)^2}\;\frac{(x'-x)\,dxdy}{\sqrt{(x-x')^2+(y-y')^2}}\,, \\ dm'_z &= d(M'_z/\mu Nc) = \frac{3\,\mathrm{sign}(\chi)}{2\pi ab}\sqrt{1-(x/a)^2-(y/b)^2}\;\sqrt{(x-x')^2+(y-y')^2}\;dxdy. \end{aligned}\right\} \tag{4.95}$$

Here M'_z is the moment about the spin pole. For the moment about the origin, we have the relation

$$M_z = M'_z + x'F_y - y'F_x. \tag{4.96}$$

We find the total force and moment by integrating (4.95),

$$\left.\begin{aligned} f_x &= \frac{3\,\mathrm{sign}(\chi)}{2\pi ab}\iint_E \sqrt{1-(x/a)^2-(y/b)^2}\;\frac{(y'-y)\,dxdy}{\sqrt{(x-x')^2+(y-y')^2}}\,, \\ f_y &= -\frac{3\,\mathrm{sign}(\chi)}{2\pi ab}\iint_E \sqrt{1-(x/a)^2-(y/b)^2}\;\frac{(x'-x)\,dxdy}{\sqrt{(x-x')^2+(y-y')^2}}\,, \\ m_z &= \frac{3\,\mathrm{sign}(\chi)}{2\pi abc}\iint_E \sqrt{1-(x/a)^2-(y/b)^2}\;\sqrt{(x-x')^2+(y-y')^2}\;dxdy - \frac{\eta}{\chi}f_y - \frac{\xi}{\chi}f_x. \end{aligned}\right\} \tag{4.97}$$

In the special case that the contact area is circular, these integrals were evaluated by LUTZ in [2], and in the special case that the contact area is an ellipse, and that the spin pole lies on one of the axes of the ellipse, they were evaluated by WERNITZ [1], p. 68-72. Since any line through the origin is an axis of the circle, LUTZ's results are a special case of WERNITZ's results. If, say, $x' = 0$, LUTZ and WERNITZ integrate with respect to x, and obtain as a result a form involving complete elliptic integrals of the first and second kind, which then has to be integrated with respect to y. This latter integration is done numerically. This process breaks down, however, when the spin pole does not lie on one of the axes, i.e. when $x' \neq 0$, $y' \neq 0$. The first integration with respect to x is still possible, but the resulting form contains also elliptic integrals of the third kind. We accordingly abandoned the attempt of analytically performing the first integration, and we treated the integrals as follows. We had:

$$f_x = \frac{3\mathrm{sign}(\chi)}{2\pi ab} \iint_E \sqrt{1-(x/a)^2-(y/b)^2}\, \frac{(y'-y)\,dxdy}{\sqrt{(x-x')^2+(y-y')^2}} =$$

$$= -\frac{3\mathrm{sign}(\chi)}{2\pi ab} \iint_E \frac{\sqrt{(x-x')^2+(y-y')^2}}{\sqrt{1-(x/a)^2-(y/b)^2}}\, \frac{y}{b^2}\, dxdy, \qquad (4.98)$$

by partial integration with respect to y. Then, we set

$$x = a\cos\psi, \quad y = br\sin\psi. \qquad (4.99)$$

This gives

$$f_x = \frac{-3\mathrm{sign}(\chi)}{2\pi b} \int_0^1 \frac{r^2 dr}{\sqrt{1-r^2}} \int_0^{2\pi} \sqrt{(a\cos\psi-x')^2+(br\sin\psi-y')^2}\, \sin\psi d\psi =$$

$$= -\frac{3\mathrm{sign}(\chi)}{2\pi b} \int_0^{\pi/2} \sin^2\theta d\theta \int_0^{2\pi} \sqrt{(a\sin\theta\cos\psi-x')^2+(b\sin\theta\sin\psi-y')^2}\sin\psi d\psi. \qquad (4.100a)$$

In the same way we find

$$f_y = \frac{3\mathrm{sign}(\chi)}{2\pi a} \int_0^{\pi/2} \sin^2\theta d\theta \int_0^{2\pi} \sqrt{(a\sin\theta\cos\psi-x')^2+(b\sin\theta\sin\psi-y')^2}\cos\psi d\psi, \qquad (4.100b)$$

$$m_z = \frac{3\mathrm{sign}(\chi)}{2\pi c} \int_0^{\pi/2} \sin\theta\cos^2\theta d\theta \int_0^{2\pi} \sqrt{(a\sin\theta\cos\psi-x')^2+(b\sin\theta\sin\psi-y')^2}\, d\psi +$$

$$- \frac{\xi}{\chi} f_x - \frac{\eta}{\chi} f_y. \qquad (4.100c)$$

By means of the substitution $\alpha = \pi-\psi$ in (4.100) it is easy to see from (4.93) that

$$\left.\begin{aligned} f_x(\xi/\chi, (-\eta)/\chi) &= f_x(\xi/\chi, \eta/\chi), \\ f_y(\xi/\chi, (-\eta)/\chi) &= -f_y(\xi/\chi, \eta/\chi), \\ m_z(\xi/\chi, (-\eta)/\chi) &= m_z(\xi/\chi, \eta/\chi). \end{aligned}\right\} \qquad (4.101a)$$

By means of the substitution $\alpha = -\psi$ in (4.100), it is easy to see from (4.93) that

$$\left.\begin{aligned} f_x((-\xi)/\chi, \eta/\chi) &= -f_x(\xi/\chi, \eta/\chi), \\ f_y((-\xi)/\chi, \eta/\chi) &= f_y(\xi/\chi, \eta/\chi), \\ m_z((-\xi)/\chi, \eta/\chi) &= m_z(\xi/\chi, \eta/\chi). \end{aligned}\right\} \qquad (4.101b)$$

By means of the substitution $\alpha = \pi/2-\psi$ in (4.100), it is easy to see that

$$\left.\begin{aligned} f_x(a,b, \xi/\chi, \eta/\chi) &= -f_y(b,a, \eta/\chi, \xi/\chi), \\ m_z(a,b, \xi/\chi, \eta/\chi) &= m_z(b,a, \eta/\chi, \xi/\chi). \end{aligned}\right\} \qquad (4.101c)$$

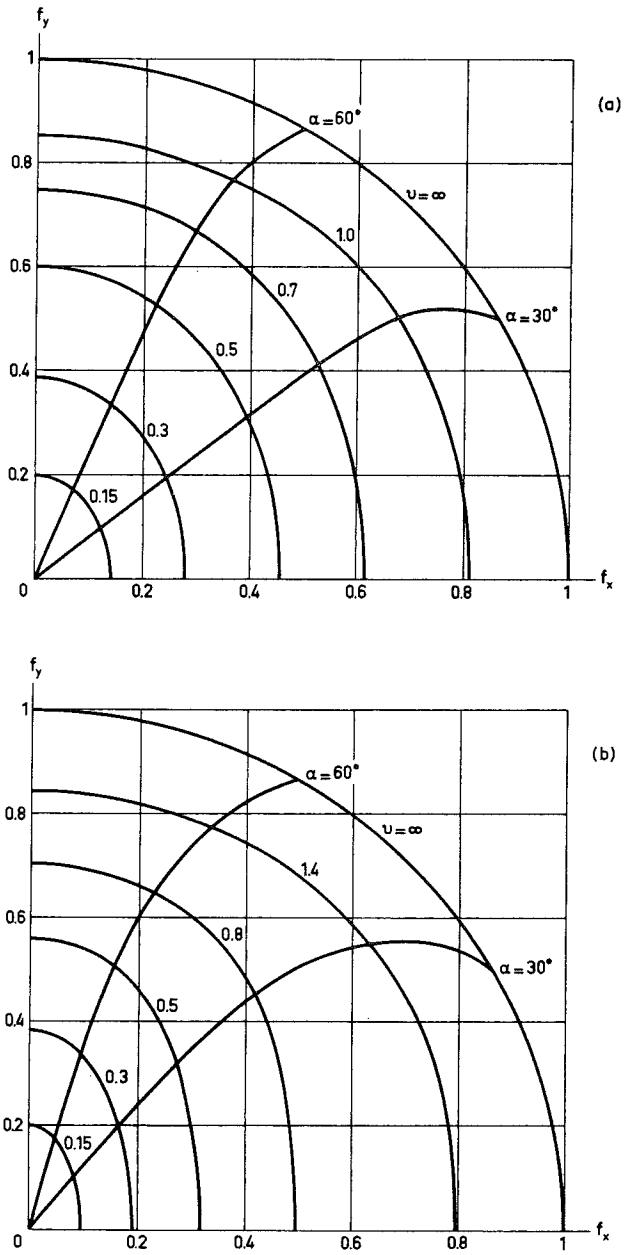

Fig. 10. The total force for large creepage and spin.
(a): g=0.5; (b): g=0.2.

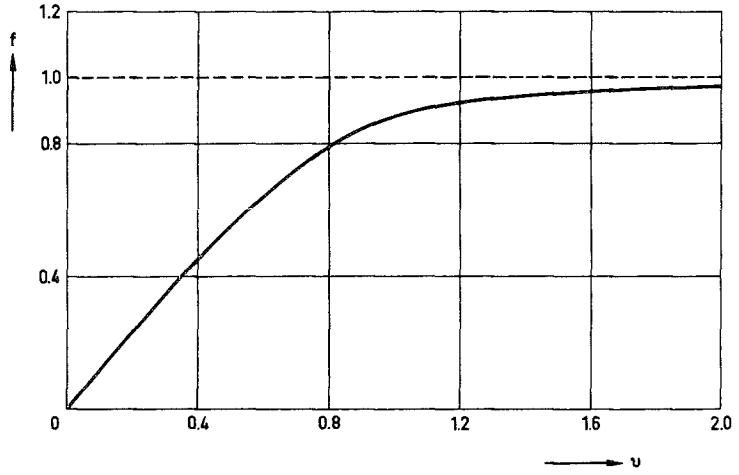

Fig. 11. The total force for large creepage and spin. g=1.

So we can confine ourselves for the purpose of calculations to the cases with

$$e \geq 0 \ (a \leq b), \ -x' = c\eta/\chi \geq 0, \ y' = c\xi/\chi \geq 0. \tag{4.102}$$

Under the conditions (4.102) we can eliminate a and b from (4.100). This gives

$$\left.\begin{aligned}
f_x &= -\frac{3\sqrt{g}\ \mathrm{sign}(\chi)}{2\pi}\int_0^{\pi/2}\sin^2\theta d\theta \times \\
&\quad \times \int_0^{2\pi}\sqrt{\left(\sqrt{g}\,\sin\theta\cos\psi + \eta/\chi\right)^2 + \left(\frac{\sin\theta\sin\psi}{\sqrt{g}} - \xi/\chi\right)^2}\,\sin\psi d\psi, \\
f_y &= \frac{3\ \mathrm{sign}(\chi)}{2\pi\sqrt{g}}\int_0^{\pi/2}\sin^2\theta d\theta \times \\
&\quad \times \int_0^{2\pi}\sqrt{\left(\sqrt{g}\,\sin\theta\cos\psi + \eta/\chi\right)^2 + \left(\frac{\sin\theta\sin\psi}{\sqrt{g}} - \xi/\chi\right)^2}\,\cos\psi d\psi, \\
m_z &= \frac{3\ \mathrm{sign}(\chi)}{2\pi}\int_0^{\pi/2}\sin\theta\cos^2\theta d\theta \times \\
&\quad \times \int_0^{2\pi}\sqrt{\left(\sqrt{g}\,\sin\theta\cos\psi + \eta/\chi\right)^2 + \left(\frac{\sin\theta\sin\psi}{\sqrt{g}} - \xi/\chi\right)^2}\,d\psi + \\
&\quad - (\eta/\chi)f_y - (\xi/\chi)f_x
\end{aligned}\right\} \tag{4.103}$$

$\chi \neq 0$; if $\chi = 0$ then $f_x = \xi/\upsilon$, $f_y = \eta/\upsilon$, $\upsilon = \sqrt{\xi^2+\eta^2}$.

The repeated integrals of (4.103) are easy to integrate numerically. The total force has been calculated for g = 0.5 and g = 0.2, see fig. 10, and for g = 1, see fig. 11. In the figures, we use the symbols υ and α:

$$\xi, \chi = \upsilon\cos\alpha, \quad \eta/\chi = \upsilon\sin\alpha. \tag{4.104}$$

As to fig. 11, we observe that the force is always in the direction of the creepage. So fig. 11 could have a simpler form than fig. 10.

We finally observe that the three integrals of (4.97) can be written as a sum of integrals of the form

$$I = P_2(x',y') \iint_E P_4(x,y) J(x,y) \frac{dxdy}{R}, \tag{4.105}$$

where P_2 and P_4 are polynomials and $J(x,y)$ and R have their usual meaning. Hence GALIN's theorem of sec. 2.2 can be applied, and the I can be evaluated by means of DOVNOROVICH's method. This gives after some calculation:

$$\left.\begin{aligned}
f_x &= \frac{3y\,\mathrm{sign}(\chi)}{ab}\left[F^{1;00}_{02} + \frac{1}{6}y^2 F^{1;00}_{04} + \frac{1}{2}x^2 F^{1;00}_{22}\right],\\
f_y &= -\frac{3x\,\mathrm{sign}(\chi)}{ab}\left[F^{1;00}_{20} + \frac{1}{6}x^2 F^{1;00}_{40} + \frac{1}{2}y^2 F^{1;00}_{22}\right],\\
m_z &= \frac{3\,\mathrm{sign}(\chi)}{abc}\left[F^{1;00}_{00} + \frac{1}{2}x^2 F^{1;00}_{20} + \frac{1}{2}y^2 F^{1;00}_{02} + \right.\\
&\qquad \left. + \frac{1}{24}x^4 F^{1;00}_{40} + \frac{1}{4}x^2y^2 F^{1;00}_{22} + \frac{1}{24}y^4 F^{1;00}_{04}\right] +\\
&\qquad + \frac{x}{c} f_y - \frac{y}{c} f_x
\end{aligned}\right\}$$

(x,y): spin pole, $x = -c\eta/\chi$, $y = c\xi/\chi$.

$F^{1;00}_{ij}$: see (3.22). (4.106)

It should be kept in mind that (4.106) is valid only when the spin pole lies inside the contact area, so that (4.106) has only limited applicability.

5. Steady rolling with arbitrary creepage and spin: a numerical theory.

In the present chapter we apply the theory of the load-displacement equations to the problem of rolling with arbitrary creepage and spin. In section 5.1 and its subsections we present the numerical process. In section 5.2 and its subsections we discuss a computer programme based on the method of section 5.1. Finally we present the numerical results in section 5.3 and its subsections. In 5.31 they are compared with the experiments of JOHNSON and HAINES and OLLERTON. In the two remaining subsections of 5.3, we discuss the solutions obtained.

5.1. The numerical method.

In 5.11, we reformulate the boundary conditions so, that the solution becomes equivalent to minimizing a certain integral. The numerical analysis of the minimalization is presented in 5.12, and some details concerning the minimalization and the formulation of the problem are discussed in 5.13 and 5.14.

5.11. Formulation as a variational problem.

Since the tangential traction is at most equal to a finite multiple of the normal Hertzian traction, the latter vanishing at the edge of the contact area, we will use the theory of section 3.1. We can rewrite the results of that section as follows:

$$\left.\begin{aligned}
&\text{Let } Z = G f_{00} \sqrt{1-(x/a)^2-(y/b)^2} && \text{inside E,}\\
&\qquad = 0 && \text{on } z=0\text{, outside E;}\\
&\text{If } (X,Y) = G\mu f_{00}\sqrt{1-(x/a)^2-(y/b)^2} \sum_{k=1}^{p} (x_k^M \tau_k, y_k^M \tau_k) && \text{inside E,}\\
&\qquad = (0,0) && \text{on } z=0\text{, outside E,}\\
&\text{with } (x_k^M) = (1,x,y,x^2,xy,y^2,\ldots,y^M,\ 0,0,0,\ldots,\ 0),\\
&\qquad (y_k^M) = (0,0,0,\ldots,\ 0,1,x,y,x^2,xy,y^2,\ldots,\ y^M),\\
&\qquad (\tau_k) = (d_{00},d_{10},d_{01},d_{20},\ldots,\ d_{0M},e_{00},e_{10},e_{01},e_{20},\ldots,e_{0M}),\\
&\qquad p = (M+1)(M+2),
\end{aligned}\right\} \qquad (5.1)$$

$$\left.\begin{aligned}
&\text{then } [u(x,y),\ v(x,y)] = f_{00} \sum_{k=1}^{p} \sum_{j=1}^{q} (z_j u_{jk}\tau_k, z_j v_{jk}\tau_k),\\
&\text{with } u_{jk}, v_{jk}\text{: coefficients of the load-displacement}\\
&\qquad\qquad \text{equations (3.5)},\\
&(z_j) = (1,x,y,x^2,xy,y^2,\ldots,xy^{M+1},y^{M+2}),\\
&\quad q = \tfrac{1}{2}(M+3)(M+4).
\end{aligned}\right\} \qquad (5.1)$$

The derivatives of u and v with respect to x, which we need to calculate the slip, are readily found. They are:

$$\left.\begin{aligned}
&\left(\frac{\partial u}{\partial x}, \frac{\partial v}{\partial x}\right) = \mu f_{00} \sum_{k=1}^{p} \sum_{j=1}^{q} (z_j' u_{jk}\tau_k, z_j' v_{jk}\tau_k),\\
&\text{with } (z_j') = \left(\frac{\partial z_j}{\partial x}\right) = (0,1,0,2x,y,0,3x^2,\ldots,y^{M+1},0).
\end{aligned}\right\} \qquad (5.2)$$

The relative slip due to the traction distribution of (5.1) in steady rolling is then according to (4.15c),

$$(s_x, s_y) = \left(v_x - \phi y + \frac{\partial u}{\partial x},\ v_y + \phi x + \frac{\partial v}{\partial x}\right),$$

$$s_x = \mu f_{00}\left\{ \frac{v_x}{\mu f_{00}} - \frac{\phi y}{\mu f_{00}} + \sum_{k=1}^{p} \sum_{j=1}^{q} z_j' u_{jk}\tau_k \right\},$$

$$s_y = \mu f_{00}\left\{ \frac{v_y}{\mu f_{00}} + \frac{\phi x}{\mu f_{00}} + \sum_{k=1}^{p} \sum_{j=1}^{q} z_j' v_{jk}\tau_k \right\}.$$

According to (3.51),

$$\mu f_{00} = \frac{3\mu N}{2\pi abG} = \frac{2\mu c\sqrt{g}}{(1-\sigma)\rho \underline{E}},$$

and according to (4.20),

$$\xi = \frac{v_x \rho}{\mu c},\quad \eta = \frac{v_y \rho}{\mu c},\quad \chi = \frac{\phi \rho}{\mu},$$

so that the relative slip due to the tractions of (5.1) becomes

$$\left.\begin{aligned}
s_x &= \mu f_{00}\left(A\xi - A\chi\frac{y}{c} + \sum_{k=1}^{p} \sum_{j=1}^{q} z_j' u_{jk}\tau_k\right),\\
s_y &= \mu f_{00}\left(A\eta + A\chi\frac{x}{c} + \sum_{k=1}^{p} \sum_{j=1}^{q} z_j' v_{jk}\tau_k\right),\\
A &= \frac{(1-\sigma)\underline{E}}{2\sqrt{g}},\quad \underline{E} = \int_0^{\pi/2} \sqrt{1-e^2\sin^2\theta}\,d\theta.
\end{aligned}\right\} \qquad (5.3)$$

When we use the X and Y of (5.1), and we calculate the surface displacement differences also in the manner of (5.1), we accomplish that the surface of the half-space outside the contact area is free of traction, and that the displacement and stress vanish at infinity. In terms of the boundary conditions (4.16), this means that (4.16c) and (4.16a) are satisfied. Also, the normal pressure of (5.1) is the same as the one in (4.16b). So, only condition (4.16d) remains for the slip region E_g and condition (4.16e) for the locked region E_h. We repeat these boundary conditions here:

$$\left.\begin{aligned} &s_x=\upsilon_x-\phi y+\frac{\partial u}{\partial x},\ s_y=\upsilon_y+\phi x+\frac{\partial v}{\partial x},\\ &w_x=s_x/s,\ w_y=s_y/s,\ s=\sqrt{s_x^2+s_y^2};\\ &(X,Y)=\mu G f_{00}\sqrt{1-(x/a)^2-(y/b)^2}\ (w_x,w_y) \qquad \text{in slip area } E_g,\\ &s_x=s_y=0,\ |(X,Y)|\leq \mu Z=\mu G f_{00}\sqrt{1-(x/a)^2-(y/b)^2} \ \text{in locked area } E_h. \end{aligned}\right\} \tag{5.4}$$

We set

$$(X',Y')=(X,Y)/\mu Z=(X,Y)/\{\mu f_{00}G\sqrt{1-(x/a)^2-(y/b)^2}\}. \tag{5.5}$$

Then we can reformulate the boundary conditions:

$$\left.\begin{aligned} &T=(X'-w_x)^2+(Y'-w_y)^2,\quad S=\frac{1}{\mu^2 f_{00}^{\,2}}\left(s_x^2+s_y^2\right),\\ &T=0 \text{ in } E_g,\\ &S=0,\ |(X',Y')|\leq 1 \text{ in } E_h, \end{aligned}\right\} \tag{5.6}$$

where E_g and E_h are unknown, and follow from the solution of the problem. We defined S so that it is independent of the factor μf_{00} which represents the normal load and the coefficient of friction. We eliminate E_g and E_h from the equations by demanding that the product TS vanishes everywhere in E. Moreover, $|(w_x,w_y)|=1$, so that the inequality $|(X',Y')|\leq 1$ must hold throughout E. So we obtain for (5.6):

$$TS = 0,\ |(X',Y')|\leq 1 \quad \text{in E.} \tag{5.7}$$

If (5.7) is satisfied, we have found the solution of the problem. Since $TS \geq 0$ for any choice of (X',Y'), we can integrate (5.7) to obtain

$$\left.\begin{aligned} &I = \iint_E WTS\ dxdy = 0,\ |(X',Y')| \leq 1 \text{ in } E, \\ &W = \text{weightfunction} > 0 \text{ in } E\ . \end{aligned}\right\} \tag{5.8}$$

Here we have put in a positive weightfunction W. Again, since WTS ≥ 0, the integral $I \geq 0$ for any choice of (X',Y'), so that the value zero of the integral is actually a minimum. So we can reformulate (5.8):

$$I = \iint_E WTS\ dxdy = \text{minimal},\ |(X',Y')| \leq 1 \text{ in } E. \tag{5.9}$$

The two conditions of (5.9) are completely equivalent to the boundary conditions (5.4), but (5.9) can be used to obtain an approximate solution, namely by introducing the tractions of (5.1) into it, with the corresponding relative slip (5.3), and minimizing the integral with respect to the τ_k. The inequality $|(X',Y')| \leq 1$ is verified afterwards.

5.12. Numerical analysis.

We summarize the new formulation of the problem:

$$\left.\begin{aligned} &I = \iint_E WTS\ dxdy \text{ is minimal},\ |(X',Y')| \leq 1 \text{ in } E; \\ &T = (X'-w_x)^2+(Y'-w_x)^2,\ \mu^2 f_{00}{}^2 S = s_x^2+s_y^2, \\ &(X',Y') = \sum_{k=1}^{p} \left(x_k^M\ \tau_k, y_k^M\ \tau_k\right), \\ &w_x = s_x/s,\ w_y = s_y/s,\ s = |(s_x,s_y)|, \\ &s_x = \mu f_{00}\left(A\xi - A\chi\ \frac{y}{c} + \sum_{k=1}^{p}\sum_{j=1}^{q} z_j'\ v_{jk}\ \tau_k\right), \\ &s_y = \mu f_{00}\left(A\eta + A\chi\ \frac{x}{c} + \sum_{k=1}^{p}\sum_{j=1}^{q} z_j'\ v_{jk}\ \tau_k\right), \\ &A = (1-\sigma)\underline{E}/2\sqrt{g}\ . \end{aligned}\right\} \tag{5.10}$$

(5.10) is an approximation in the sense that we take along only $p=(M+1)(M+2)$ parameters τ_k, so that X' and Y' are arbitrary M-th degree polynomials in x and y, the coefficients of which are determined from condition (5.9).

In order to determine the τ_k from the condition I = minimal, we

seek the stationary value of I with respect to the τ_k by iteration. We are not certain that the stationary value we find in actually the absolute minimum or even a relative minimum. In practice, however, we determined I after each iteration step and we found in practically all cases that at the stationary value, I was indeed the smallest as compared with the series of values of I obtained during the iteration. In the cases where this was not so, the solution was grossly at fault. So there is a strong presumption to believe that we indeed find a minimum.

At the stationary value,

$$\frac{\partial I}{\partial \tau_k} = \frac{\partial}{\partial \tau_k} \iint_E WTS \, dxdy = \iint_E W \frac{\partial (TS)}{\partial \tau_k} \, dxdy = 0. \qquad (5.11)$$

This is a difficult equation, as a consequence, principally, of the complicated dependence of (w_x, w_y) on τ_k. We find the solution by NEWTON's method: we start with an arbitrary τ_k^o, and proceed by iteration, as follows:

$$(\tau_k^o) = \text{arbitrary}; \qquad (5.12a)$$

$$\left.\begin{aligned} &\left(\frac{\partial I}{\partial \tau_k}\right)_{\tau_k=\tau_k^n+\Delta\tau_k} \iint_E W \left(\frac{\partial TS}{\partial \tau_k}\right)_{\tau_k=\tau_k^n} dxdy + \\ &\quad + \iint_E W \sum_{\ell=1}^{p} \left(\frac{\partial^2 TS}{\partial \tau_k \partial \tau_\ell}\right)_{\tau_k=\tau_k^n, \tau_\ell=\tau_\ell^n} \Delta\tau_\ell \, dxdy = 0, \\ &k = 1,2,3,\ldots, \; p = (M+1)(M+2); \end{aligned}\right\} (5.12b)$$

$$\left.\begin{aligned} &\tau_k^{n+1} = \tau_k^n + \Delta\tau_k; \text{ if } \max_k |\Delta\tau_k| < \delta \max_k |\tau_k^{n+1}| \text{ then solution is found;} \\ &\delta: \text{ a small positive number which can be chosen arbitrarily.} \end{aligned}\right\} (5.12c)$$

The equations of (5.12b) are p linear equations in the p unknowns $\Delta\tau_\ell$.

The integrals are evaluated numerically, by replacing them by unweighted sums over a fairly large number of points. This was done for two reasons. The most important reason is that the integrals have no physical meaning, so that we are not interested in their precise value. In fact, one could directly have used finite sums instead of integrals in the original equations. Secondly, the function T, containing as it does the discontinuous functions w_x and

w_y, is a function with locally large gradients. This does not render it very suitable for numerical integration methods involving higher order differences.

The process (5.12) of successive approximations converges fairly rapidly: it depends on the behaviour of the resulting function WTS, and to some extent also on the starting value τ_k^o. When in the calculation of several cases we work in a chainlike fashion, by slowly increasing the creepage and the spin, and using the previous result as a starting value, the number of iterations for δ=0.001 (see 5.12c) is about 5, sometimes increasing to 7 or 8 when the adhesion area is large, or dropping down to 3 when the adhesion area is small. The number of iterations increases slowly with the degree M of the polynomials X' and Y'. In the calculation performed on a series of 33 different values of creepage and spin, we needed an average of 3.9 iterations per case for M=2 (12 τ's), 4.4 iterations per case for M=3 (20 τ's), and 4.7 iterations per case for M=4 (30 τ's). The number δ of (5.12c) was taken equal to 0.001.

In the contact area we took 80 points to approximate the integral when M=2 or M=3, and about 100 points when M=4. The calculations proved to be exceedingly lengthy. On the fast Telefunken TR4 computer of Delft Technological University, each iteration step (5.12b), which consists of the evaluation of the coefficients of the linear equations and their subsequent solution, took the following amount of machine time:

$$\left.\begin{array}{l} \text{M=2, 12 equations, 80 points in the contact area} \quad \ldots 18 \text{ sec.} \\ \text{M=3, 20 equations, 80 points in the contact area} \quad \ldots 35 \text{ sec.} \\ \text{M=4, 30 equations, 100 points in the contact area} \quad \ldots 87 \text{ sec.} \end{array}\right\} \quad (5.13)$$

Most of the time was used in setting up the equations. These long calculating times are due to the complicated character of $\partial^2(TS)/\partial\tau_k\partial\tau_\ell$ (see sec. 5.23), and to the fact that these calculations have to be performed for every point, that is, they must be repeated about a hundred times for each iteration step.

In the calculation outlined above, the inequality $|(X',Y')| \leq 1$ is ignored. After the τ_k have been determined, we inspect the solution to see whether $|(X',Y')| \leq 1$ in each point (x,y) of the

contact area. The output of the computer programme has been especially designed to facilitate this verification, see sec. 5.24. We found that generally $|(X',Y')| > 1$ at some points. In judging this aberration, we distinguish three cases, viz. T<S, T>S, and (x,y) near the edge of the contact area.

In the case T<S, the reduced tangential tractions (X',Y') are closer to the Coulomb value than the slip is to zero. That means that the solution at a point where T<S approximates slip area conditions, in which $|(X',Y')|$ should be equal to unity. That means that the traction $|(X',Y')|$ we actually find should be regarded as a more or less succesful approximation of unity. The situation $|(X',Y')| > 1$, T<S indeed occurred very frequently in our numerical work, but for the reason just mentioned should not be used to throw doubt on the validity of the solution.

Points with $|(X',Y')| > 1$, T>S do throw doubt on the validity of the solution. A point of this type we call an aberration of the solution. Aberrations also occurred in our numerical work, but much less frequently, and mostly concentrated in a small portion of the contact area. Solutions with aberrations occur mostly at values of the spin close to the peaks of fig. 23, sec. 5.33. The argument of the case T<S does not apply, since the solution at a point with T>S approximates adhesion area conditions, where $|(X',Y')|$ should be smaller than unity. One might be tempted to think that where $|(X',Y')|$ passes the value 1, a slip area with small T should be found. This is, however, not always the case, since a small value of T implies not only that $|(X',Y')| \approx 1$, but also that the angle between slip and traction must be small. Mostly this angle is not small in an aberration.

As to the case that (x,y) is near the edge of the contact area while $|(X',Y')| > 1$, we observe that for reasons discussed in sec. 5.13, we used the weight function

$$W = W_1 \equiv 1-x^2/a^2-y^2/b^2. \qquad (5.14)$$

As a consequence, little weight is attached during the minimalisation process to the behaviour of the solution near the edge of the contact area where W_1 is small, and hence in judging the solution in the

light of the requirement that $|(X',Y')| \leq 1$, little importance should be attached to the behaviour near the edge.

5.13. The choice of the weight function.

The weight function of (5.14) was chosen, because then WT is proportional to the square of the absolute value of the difference between the actual tractions (X,Y) and the COULOMB traction $\mu Z(w_x,w_y)$, with the proportionality constant $\mu^2 f_{00}{}^2 G^2$. As a consequence, $\mu^4 f_{00}{}^4 G^2 V^2 (W_1 TS)$ is the square of the rate of work per unit area done by the difference of the actual tractions (X,Y) and the COULOMB traction $\mu Z(w_x,w_y)$ on the slip $V(s_x,s_y)$, if the latter were in the same direction as the traction difference $(X-\mu Z w_x,\ Y-\mu Z w_y)$.

We also tried W=1, and compared the total force obtained with $W=W_1$ with the total force obtained with W=1 for the degree M of the traction polynomials (X',Y') equal to 2 (12 τ's), to 3 (20 τ's), and to 4 (30 τ's). We did not use higher degrees M, because of the large amount of machine time, see (5.13). We calculated the force $f_y=F_y/\mu N$ for a circular contact area, POISSON's ratio $\sigma=0.28$, and for pure lateral creepage $(\upsilon_x=\phi=0,\ \upsilon_y\neq 0)$, and also for pure spin $(\upsilon_x=\upsilon_y=0,\ \phi\neq 0)$. The results of the comparison are given in Tables 4 and 5. In reading the tables it should be remembered that the maximum value of

Table 4. A comparison of f_y with W=1 and with $W=W_1$, for M=4.

	$\upsilon_x=\phi=0$		$\upsilon_x=\upsilon_y=0$	
	Max	Mean	Max	Mean
$\lvert f_{y,W=1} - f_{y,W=W_1} \rvert$	0.016	0.009	0.046	0.016

Table 5. A comparison of f_y with W=1, $W=W_1$, with the conjectured value of f_y.

	$\upsilon_x=\phi=0$			$\upsilon_x=\upsilon_y=0$		
	W	Max	Mean	W	Max	Mean
$\lvert \frac{1}{2} f_{y,W=1,M=4} + \frac{1}{2} f_{y,W=W_1,M=4} - f_{y,M=3} \rvert$	1	0.022	0.009	1	0.044	0.023
	W_1	0.033	0.011	W_1	0.029	0.018

f_y is 1.

We see from Table 4 that there is a distinct difference between $f_{y,W=W_1}$ and $f_{y,W=1}$ for M=4. This indicates that we should have used a higher value of M in our calculation. The large amount of machine time precluded that, however.

In table 5 we assume that $\left(\frac{1}{2}f_{y,W=1,M=4}+\frac{1}{2}f_{y,W=W_1,M=4}\right)$ is the correct value of f_y with which we want to compare the performance of polynomials with degree M=3. We see from Table 5 that the polynomials with M=3 give passable results. The weightfunction W=1 performed better than $W=W_1$ in the case of pure lateral creepage, and $W=W_1$ performed better than W=1 in the case of pure spin. In view of the fact that the largest errors occur in the case of pure spin, and in view of the amount of machine time available, we decided to adopt M=3, $W=W_1$, in all our further calculations.

5.14. Final remarks on the method.

It should be observed that the formulation of the boundary value problem as a minimalization problem is by no means unique. In fact, one could also minimize the integral $\iint_E WT^mS^n dxdy$, but we preferred the integral (5.9), since the integrand is the square of a rate of work per unit area. A possibility to be considered is $m=n=\frac{1}{2}$: the integrand is then a rate of work per unit area. We tried it for a single case in which the integrand W_1TS gave good results, but it turned out that the iteration did not converge. We suspect that this is because $\sqrt{TS}$ has too large gradients near T=0 and S=0 to be workable.

A possibility which has been investigated more fully is the minimalization of

$$\left.\begin{aligned} &\iint_{E_g} W_2\, T\, dxdy + \iint_{E_h} W_3\, S\, dxdy = \text{minimal}, \\ &|(X',Y')| \leq 1 \text{ in } E_h . \end{aligned}\right\} \qquad (5.15)$$

This form has the drawback that the adhesion area and the slip area explicitly enter into the minimalization problem. It has the advantage that for fixed E_g and E_h, for fixed w_x and w_y and if W_2

and W_3 are functions of (x,y) only, it is a least squares problem, since S and T are then quadratic in τ_k. So it has a single stationary value which is actually the absolute minimum. A situation which approaches fixed (w_x,w_y) is that of pure creepage with vanishing POISSON's ratio σ. The variation of E_g and E_h in all cases turns out to be simple: if at a certain point of the boundary $W_2T>W_3S$, then E_h should be increased, if $W_2T<W_3S$, E_g should be increased. In the final solution $W_2T=W_3S$ on the boundary. So, assuming that the solution continuously changes with the creepage, we see that in the case of pure creepage with $\sigma=0$ we find the best solution in the sense of least squares, and assuming that this feature of (5.15) does not change when $\sigma\neq0$ and $\phi\neq0$, we see that there is a strong presumption, that we will find the solution from the stationary value of (5.15).

Now, by a special choice of W_2 and W_3 we can obtain (5.9) back. One must then take $W_2=WS$, and $W_3=WT$. Note that now W_2 and W_3 depend also on T and S, which is different from what we assumed before. Seen in this light one can say that in (5.9) WT serves as a weight function on S in the adhesion area, so that the larger is the difference of the approximation of the traction and the COULOMB traction at a certain point, the more importance is attached to a small value of S at that point, while in the slip area S serves as a weight function on WT, so that the larger the slip at a certain point, the more importance is attached to a small difference between the approximation of the traction and the COULOMB traction at that point.

It was found that the results of (5.12) compared better with the experiment than those of (5.15). In view of the fact that by making (5.15) stationary one probably finds the absolute minimum, we conclude that the process (5.12) of making (5.9) stationary probably leads to the absolute minimum of (5.9).

Let us finally return for a moment to the fact that we have used the tractions of ch. 3, which are so that they vanish at the edge of the contact area. One might argue that this choice is not a necessary one, and that one could use any set of tractions which form a complete set of functions. So one could also use the tractions of ch. 2, which are infinite at the edge of the contact area. In that

case the displacement differences can be chosen arbitrarily, for instance

$$u = -v_x x + \phi xy, \quad v = -v_y x - \tfrac{1}{2}\phi x^2.$$

We see that u and v are second degree polynomials, and hence the corresponding traction in the contact area has the form

$$X = G\{1-(x/a)^2-(y/b)^2\}^{-\frac{1}{2}} \left(d_{00}+d_{10}x+d_{01}y+d_{20}x^2+d_{11}xy+d_{02}y^2\right),$$
$$Y = G\{1-(x/a)^2-(y/b)^2\}^{-\frac{1}{2}} \left(e_{00}+e_{10}x+e_{01}y+e_{20}x^2+e_{11}xy+e_{02}y^2\right).$$

Moreover, we see from (4.15c) that the relative slip $(s_x,s_y)=(0,0)$ throughout the contact area, so that the integral I of (5.9) actually vanishes. However, $|(X,Y)|>>\mu Z$ near the edge, from which it appears that we must reject this solution. So we see that the inequality $|(X,Y)|\leq\mu Z$ is indeed essential for the solution of the problem, and we see that we cannot use the tractions of ch. 2 in a calculation in which the inequality is verified afterwards. Instead, we use the tractions of ch. 3, which, as we recall, have the form

$$(X,Y) = G\{1-(x/a)^2-(y/b)^2\}^{+\frac{1}{2}} \sum \left(d_{pq},e_{pq}\right)x^p y^q.$$

These tractions already reflect something of the inequality $|(X,Y)|\leq\mu Z$, namely, they behave correctly at the edge of the contact area, and the inequality reduces to

$$\left|\left(\sum d_{pq}x^p y^q, \sum e_{pq}x^p y^q\right)\right| \leq \frac{3\mu N}{2\pi abG}.$$

This relationship is much easier to satisfy that the inequality

$$\left|\left(\sum d_{pq}x^p y^q, \sum e_{pq}x^p y^q\right)\right| \leq \frac{3\mu N}{2\pi abG}\{1-(x/a)^2-(y/b)^2\}$$

which obtains in the case that we use the tractions of ch. 2. Indeed, the tractions of ch. 3 lead to an acceptable approximative solution in a great many cases, while, as we saw, the tractions of ch. 2 do not.

5.2. The computer programme.

In the subsections of the present section, we discuss several features of the ALGOL-60 computer programme which was written to perform the iteration described by (5.12). The input is described in

5.21, in order to give some impression of the degree of generality of the programme. The possibility to use several forms of the integrand is described in 5.22, the optimalization of the programme is discussed in 5.23, and in 5.24 the output is described with the aid of an example (fig. 12).

5.21. The input.

To be specified at input are:

a) The degree M of the traction polynomials;
b) The ratio of the axes a/b of the contact ellipse;
c) POISSON's ratio σ;
d) The points for the calculation of the integral;
e) The number δ of (5.12c);
f) The maximum number of iterations;
g) Creepage and spin;
h) If necessary, the starting values τ_k^o;
i) Several features of the output.

a) The importance of the generality of M hardly needs adstruction. Owing to the large amount of machine time involved, (see (5.13)), only small values of M (say, up to 6) are of interest. So the load-displacement equations can be kept in core storage, which is important with a view to calculating speed.

a,b,c) The most difficult to adapt to the demand of variable M, a/b, and σ was the construction of the load-displacement equations. They are constructed by the machine in such a way that use is made of the fact that they fall apart into four independent systems of equations. This was done to avoid the occurrence of unnecessary zeros in the equations. The load-displacement equations are computed only once for a whole series of calculations. After they have been computed, the lengthy procedure needed for their calculation is placed on tape and the memory space occupied by it is again free for use.

d) The points needed for the calculation of the integral are taken so that they form a rectangular network, the meshlength of which in the x and y directions can be specified separately.

e) Ordinarily, we took $\delta=0.001$. It should be noted that $\max_k|\Delta\tau_k|$ in (5.12c) is an approximation of the error present in τ_k^n. Since in (5.12b) terms of order $\Delta\tau_k\Delta\tau_\ell$ are neglected, the τ_k^{n+1} which we obtain at the end of the iteration contains errors of order

$$\left\{\frac{\max_k|\Delta\tau_k|}{\max_k|\tau_k|}\right\}^2$$

, that is, of order $\delta^2 = 10^{-6}$.

f) Ordinarily, we set the maximum number of iterations equal to 12. If after these 12 iterations the inequality (5.12c) is not satisfied, the machine concludes that the calculation diverges, and proceeds to another case.

g) Creepage and spin are put in in terms of the significant data of the following triple loop:

```
for χ:= χ_o step Δχ until χ_e do
for α:= α_o step Δα until α_e do
for ℓ:= 1 step 1 until ℓ_e do
begin ξ:= υ[ℓ] cos α; η:= υ[ℓ] sin α;
      perform the calculation;
end;
```

(5.16)

Here, $\upsilon[1:\ell_e]$ is an array the dimension ℓ_e elements of which are given in the input. α is the angle between the vector (ξ,η) and the x-axis; it is given in degrees.

h) The programme works in a chainlike fashion, taking the resulting τ_k as the starting value τ_k^o for the next case. In the first case to be treated, τ_k^o is set equal to zero, unless it is specified otherwise. The presence of a set of starting values $\{\tau_k^o\}$ in the input is indicated by a control word in the input.

i) The features of the output which are under control of the input are discussed in sec. 5.24.

5.22. The form of the integrand.

It was the object during the writing of the programme to put as

few restrictions on the form of the integrand of I as was possible in view of the fact that hardly any loss of machine time may be suffered. So we chose as a general form of the integrand the function f(x,y,a,b,T,S). f is calculated by a procedure which gives the values of

$$\left.\begin{aligned} &f,\ f^{*},\ f^{\cdot},\ f^{**},\ f^{\cdot\cdot},\ f^{\cdot *},\\ &{}^{\cdot}\text{: differentiation with respect to S,}\\ &{}^{*}\text{: differentiation with respect to T,} \end{aligned}\right\} \qquad (5.17)$$

which are all that is needed from f in the course of the calculation, as we will see in sec. 5.23. Another function f can easily be tried by a modification of the body of the f-procedure alone. In order to facilitate this, the f-procedure is kept separate from the rest of the programme. More specifically, it is a pretranslated procedure in the Delft TR4.

Up to now, we have extensively tried f=TS and f=W_1TS. We also tried f=$\sqrt{W_1 TS}$. It should be noted in this connection that the form (5.15) is not caught in this way: a separate programme was written for it, which actually preceeded the present programme in time.

5.23. Optimalisation of the programme.

With a view to the formidable amount of machine time, the programme had to be optimalized as much as possible. Consequently, the first demand is that the load-displacement equations, which are constantly referred to in the course of the calculation, should be immediately available at all times. Hence they were placed in core storage. The procedure which computes them is used only once for a whole series of cases, so it was placed on magnetic tape in order to save space.

Since every point of the network covering the contact area gives its contribution to every one of the $(M+1)^2(M+2)^2$ coefficients of the linear equations (5.12b), the generation of these equations takes up most of the machine time. Consequently, these equations are placed in core storage, and special case is taken to perform the calculation as efficiently as possible. This optimalisation took the

form of reducing the number of operations in the innermost loop of the programme as much as possible. We will give here the analysis involved.

We introduce the following notations:

$$\left.\begin{aligned} &P = s_x/\mu f_{00},\ Q = s_y/\mu f_{00} \Longrightarrow S = P^2+Q^2;\\ &,k\text{: differentiation with respect to } \tau_k;\\ &^*\text{: differentiation with respect to T;}\\ &^\cdot\text{: differentiation with respect to S.} \end{aligned}\right\} \tag{5.18}$$

Hence, by (5.10),

$$\left.\begin{aligned} &w_x = P/\sqrt{S},\ w_y = Q/\sqrt{S},\ P_{,k} = \sum_{j=1}^{q} z'_j\, u_{jk},\\ &Q_{,k} = \sum_{j=1}^{q} z'_j\, v_{jk},\ X'_{,k} = x_k,\ Y'_{,k} = y_k. \end{aligned}\right\} \tag{5.19}$$

Also, we set

$$U = X'-w_x,\ V = Y'-w_y \Longrightarrow T=U^2+V^2. \tag{5.20}$$

We differentiate $f(x,y,a,b,T,S)$ with respect to τ_k. That gives

$$f_{,k} = f^* T_{,k} + f^\cdot S_{,k}. \tag{5.21}$$

We differentiate (5.21) with respect to τ_ℓ,

$$\left.\begin{aligned} f_{,k\ell} &= f^* T_{,k\ell} + f^\cdot S_{,k\ell} +\\ &+ f^{**} T_{,k} T_{,\ell} + f^{*\cdot}\left(T_{,k} S_{,\ell} + T_{,\ell} S_{,k}\right) + f^{\cdot\cdot} S_{,k} S_{,\ell}. \end{aligned}\right\} \tag{5.22}$$

We observe that in $f_{,k}$ and $f_{,k\ell}$ occur only the quantities (5.17) which are produced by the f-procedure.

In order to be able to evaluate (5.21) and (5.22), we must have the derivatives $T_{,k}$, $S_{,k}$, $T_{,k\ell}$, $S_{,k\ell}$:

$$\left.\begin{aligned} S_{,k} &= 2PP_{,k} + 2QQ_{,k},\\ S_{,k\ell} &= 2P_{,k}P_{,\ell} + 2Q_{,k}Q_{,\ell}, \end{aligned}\right\} \tag{5.23}$$

the latter, since according to (5.19) $P_{,k}$ and $Q_{,k}$ are independent of τ_ℓ. Also,

$$
\left.\begin{aligned}
T_{,k} &= 2UU_{,k} + 2VV_{,k}\ , \\
U_{,k} &= X'_{,k} - (P/\sqrt{S})_{,k} = X'_{,k} + \frac{1}{S\sqrt{S}}\left(PQQ_{,k} - Q^2P_{,k}\right) = \\
&= X'_{,k} + \frac{1}{\sqrt{S}}\left(w_x w_y Q_{,k} - w_y^2 P_{,k}\right), \\
V_{,k} &= Y'_{,k} - (Q/\sqrt{S})_{,k} = Y'_{,k} + \frac{1}{S\sqrt{S}}\left(PQP_{,k} - P^2Q_{,k}\right) = \\
&= Y'_{,k} + \frac{1}{\sqrt{S}}\left(w_x w_y P_{,k} - w_x^2 Q_{,k}\right).
\end{aligned}\right\} \qquad (5.24)
$$

We differentiate $T_{,k}$ with respect to τ_ℓ. That gives after some calculation, if we recall that $X'_{k\ell}=Y'_{k\ell}=0$:

$$
\begin{aligned}
T_{,k\ell} &= 2U_{,k}U_{,\ell} + 2V_{,k}V_{,\ell} + 2UU_{,k\ell} + 2VV_{,k\ell}\ , \\
U_{,k\ell} &= \frac{1}{S}P_{,\ell}\left[3w_x w_y^2 P_{,k} + \left(w_y - 3w_y w_x^2\right)Q_{,k}\right] + \\
&\quad + \frac{1}{S}Q_{,\ell}\left[\left(w_y - 3w_y w_x^2\right)P_{,k} + \left(w_x - 3w_x w_y^2\right)Q_{,k}\right]; \qquad (5.25) \\
V_{,k\ell} &= \frac{1}{S}P_{,\ell}\left[\left(w_y - 3w_y w_x^2\right)P_{,k} + \left(w_x - 3w_x w_y^2\right)Q_{,k}\right] + \\
&\quad + \frac{1}{S}Q_{,\ell}\left[\left(w_x - 3w_x w_y^2\right)P_{,k} + 3w_y w_x^2\, Q_{,k}\right].
\end{aligned}
$$

We introduce (5.23), (5.24), and (5.25) into (5.22). Clearly, $f_{,k\ell}$ is a bilinear form in $\left(X'_{,k},\ Y'_{,k},\ P_{,k},\ Q_{,k}\right)$ and $\left(X'_{,\ell},\ Y'_{,\ell},\ P_{,\ell},\ Q_{,\ell}\right)$. We write it in matrix form, as follows:

$$
f_{,k\ell} = \left(X'_{,\ell}\ Y'_{,\ell}\ P_{,\ell}\ Q_{,\ell}\right)\begin{bmatrix} A_{11} & A_{12} & A_{13} & A_{14} \\ A_{21} & A_{22} & A_{23} & A_{24} \\ A_{31} & A_{32} & A_{33} & A_{34} \\ A_{41} & A_{42} & A_{43} & A_{44} \end{bmatrix}\begin{bmatrix} X'_{,k} \\ Y'_{,k} \\ P_{,k} \\ Q_{,k} \end{bmatrix}, \qquad (5.26a)
$$

with

$$
A_{ij}=A_{ji},\ X'_{,\ell}=x_\ell,\ Y'_{,\ell}=y_\ell,\ P_{,\ell}=\sum_{j=1}^{q} z'_j\, u_{j\ell},\ Q_{,\ell}=\sum_{j=1}^{q} z'_j\, v_{j\ell}\ , \qquad (5.26b)
$$

and

$$
\left.\begin{aligned}
A_{11} &= 2f^* + 4f^{**}U^2, \qquad A_{12} = 4f^{**}UV, \\
A_{13} &= -\frac{2}{\sqrt{S}}f^* w_y^2 + 4f^{**}UP - 4f^{**}Uw_y\left(Uw_y - Vw_x\right)/\sqrt{S}, \\
A_{14} &= \frac{2}{\sqrt{S}}f^* w_x w_y + 4f^{**}UQ + 4f^{**}Uw_x\left(Uw_y - Vw_x\right)/\sqrt{S}, \\
A_{22} &= 2f^* + 4f^{**}V^2,
\end{aligned}\right\} \qquad (5.26c)
$$

$$
\left.
\begin{aligned}
A_{23} &= \frac{2}{\sqrt{S}} f^{*} w_x w_y + 4f^{**} PV - 4f^{**} Vw_y (Uw_y - Vw_x)/\sqrt{S}, \\
A_{24} &= -\frac{2}{\sqrt{S}} f^{*} w_x^2 + 4f^{**} VQ + 4f^{**} Vw_x (Uw_y - Vw_x)/\sqrt{S}, \\
A_{33} &= \frac{2}{S} f^{*} \{w_y^2 + 3Uw_x w_y^2 + V(w_x - 3w_x w_y^2)\} + 2f^{\cdot} + \\
&\quad + \frac{4}{S} f^{**} w_y^2 (Uw_y - Vw_x)^2 - 8f^{**} w_x w_y (Uw_y - Vw_x) + 4f^{\cdot\cdot} P^2, \\
A_{34} &= \frac{2}{S} f^{*} \{-w_x w_y + U(w_y - 3w_y w_x^2) + V(w_x - 3w_x w_y^2)\} + \\
&\quad - \frac{4}{S} f^{**} w_x w_y (Uw_y - Vw_x)^2 + 4f^{**} (w_x^2 - w_y^2)(Uw_y - Vw_x) + 4f^{\cdot\cdot} PQ, \\
A_{44} &= \frac{2}{S} f^{*} \{w_x^2 + 3Vw_y w_x^2 + U(w_y - 3w_y w_x^2)\} + 2f^{\cdot} + \\
&\quad + \frac{4}{S} f^{**} w_x^2 (Uw_y - Vw_x)^2 + 8f^{**} w_x w_y (Uw_y - Vw_x) + 4f^{\cdot\cdot} Q^2.
\end{aligned}
\right\} \quad (5.26c)
$$

It should be noted that all three factors of (5.26a) are position dependent. It should also be observed that if $f=W_1 TS$ or $f=TS$, only $A_{21}=A_{12}$ vanishes identically. So, very little is gained by writing a special programme dealing with these cases only. The greater generality of f in the present programme is thus obtained at hardly any cost.

A programme which computes the coefficients $\int f_{,k\ell} = \int f_{,\ell k}$ of the equations (5.12b) in a way which is based on the form (5.26a) of $f_{,k\ell}$, is easily given. Its innermost loop might look as follows:

```
Generate the 4 arrays X'_,k, Y'_,k, P_,k, Q_,k;
comment here and only here the load-displacement
equations are used;
Generate the A_ij;
comment no array to save time;
p:= (M+1)(M+2);
for k:= 1 step 1 until p do                                   (5.27)
begin C1:= A11X'_,k + A12Y'_,k + A13P_,k + A14Q_,k;
      C2:= ...; C3:= ...; C4:= ...;
      comment the C_i form no array to save time;
      for ℓ:= k step 1 until p do
      ∫f_,kℓ:= ∫f_,kℓ + C1X'_,ℓ + C2X'_,ℓ + C3P_,ℓ + C4Q_,ℓ;
end;
```

By making use of the fact that half of the numbers $X'_{,\ell}$ and $Y'_{,\ell}$

vanish, (see (5.26b) and (5.1)), more calculation time can be saved. We avoid the use of subscripted variables as much as possible, since the call of a subscripted variable takes more time than the call of an ordinary variable.

5.24. The output.

In the course of time, the output underwent a number of changes. We will discuss here only the final version, which was introduced when 75% of the calculations described in sec. 5.33 were finished. A page of this output is reproduced in fig. 12. We will discuss this figure in some detail, in order to give an impression of the verification of the inequality in (5.9).

The format of the numbers in fig. 12 has three forms:

$$\left.\begin{array}{ll} \pm.\times\times\times_{10}\pm\times\times: & \text{a floating number with exponent at the right (fl);} \\ \pm\times\times\times.\times\times: & \text{a fixed point number (fi);} \\ \pm\times\times\times: & \text{an integer (in).} \end{array}\right\} \quad (5.28)$$

It should be remembered that throughout the programme the major semi-axis ℓ is unit of length.

SPIN, MICROSLIP, HOEK: a_1(fi) a_2(fi) a_3(fi)
with $a_1=\chi$, $a_2=\upsilon$, $a_3=\alpha$, see (5.16).
Specification of creepage and spin.

UPSX, UPSY, PHI: a_1(fi) a_2(fi) a_3(fi)
with $a_1=\upsilon_x/\mu f_{00}$, $a_2=\upsilon_y/\mu f_{00}$, $a_3=\phi\ell/\mu f_{00}$.
TOEG GEV a_1(fl) a_2(fl) GEMAFW a_3(fl)
with $a_1 = \delta \max_k |\tau_k^{n+1}|$, $a_2 = \max_k |\Delta\tau_k|$, see (5.12c),

$a_3 = \frac{1}{m}\sum_1^m f^{(n)}(x,y,a,b,T,S)$, m: number of points in contact area.

We can see from the series of lines TOEG GEV etc. how fast the iteration process converges. It should be noted that a_2 gives an approximation of the error in the previous iteration. In combination with the fast convergence when a_2 gets small (here even faster than quadratic, when $a_2 \ll 1$) this justifies us to give δ the

```
SPIN,MICROSLIP,HOEK:  2.0000   1.7000 - 30.00
UPSX,UPSY,PHI      :  0.9077 - 0.5241   1.7439
TOEG GEV+.310202512545E-  2 +.825463503290E+  0 GEMAFW!+.124967846743E-  1
TOEG GEV+.325191548046E-  2 +.196467231468E+  0 GEMAFW!+ 055982139915E-  2
TOEG GEV+.325668086279E-  2 +.243485761775E-  1 GEMAFW!+.636476356704E-  2
TOEG GEV+.325667730896E-  2 +.223328902182E-  3 GEMAFW!+.636289979821E-  2
CONVER
FX FY MZ: 0.6249 -0.1220   0.3437
TAU
+.908286119491E+  0 -.349367884271E+  0 -.598682684580E+  0 -.713134273210E+  0 -.412520882910E+  0 -.123865208988E+  1
+.196130755753E+  1 -.166438669774E+  0 +.339905894663E+  0 -.764905620933E+  0 +.363984163655E-  1 +.122234826366E+  1
+.281355484607E+  0 -.166314884292E+  1 +.591234429808E+  0 -.376036296511E+  0 -.106033963398E+  1 -.325667730905E+  1
+.153874845084E+  0 -.432568316460E+  0
UVX
+.488529460241E+  0 -.131612477230E+  1 -.920601446923E+  0 +.976207865077E+  0 +.891314656189E+  0 +.107945629140E+  0
+.102304109863E+  1 +.381601540534E+  0 +.156971880339E+  1 +.35412772  02E-  1 -.316159336356E+  1 +.795568278409E+  1
-.117220861720E+  1 +.806106721342E+  0 -.621773461409E-  1 +.186643 96240E-  1 +.460620005888E+  0 +.204563654266E+  0
-.270534609240E+  1 -.111786684778E+  1 -.203120076839E+  0 +.3072405363 9 E+  1 -.129517249693E+  1 +.803580199801E+  0
-.162104008915E+  0 +.213857179240E+  1 +.587589341798E+  1 - 110478684091E+  0  .119064418005E+  1 -.622240009372E-  1
AFWIJKINGEN:
T,S,Y,X,F,S,HOEK:+.996538670152E-  1 +.782010710173E-  1   5    2   1.2865  0.2796    7.3
G,H,A,OPP:  1    1    1    22
CONTACTVLAK:
- 4         . . . .                    0   0   0  -1  -1  -1  -1   0   0   0
- 3       . . . . . . . .              0  -1  -1  -1  -1  -1  -1  -1  -1   0
- 2       . . . . . . . .              0  -1  -1  -1  -1  -1  -1  -1  -1   0
- 1   . . . . . . . . . .             -1  -1  -1  -1  -1  -1  -1  -1  -1  -1
  0   . . . . . . . . . H            -1  -1  -1  -1  -1  -1  -1  -1  -1   1
  1   . . . . . . . H H H            -1  -1  -1  -1  -1  -1  -1   1   1   1
  2   . . . . H H H H H H H          -1  -1  -1  -1   1   1   1   1   1   1
  3     . . H H H H H H H             0  -1  -1   1   1   1   1   1   1   0
  4       . . H H H H H H             0  -1  -1  -1   1   1   1   1   1   0
  5           . . . A                 0   0   0  -1  -1  -1   1   0   0   0
T,S,INT,X,F,FW,ANF,WS,ARS:
Y:-0.5000
+.166133321545E-  2 +.961605765187E+  1 +.415362375452E-  2 -0.3500  0.9599  0.4894 - 27.3  3.1010 - 27.8
+.151439686365E-  3 +.736778676230E+  1 +.557887658033E-  3 -0.2500  1.0088  0.7134 - 21.6  2.7144 - 22.1
+.500945898238E-  3 +.538701820158E+  1 +.178167988342E-  2 -0.1500  1.0224  0.8366 - 16.3  2.3218 - 16.3
+.260215543676E-  3 +.382747524121E+  1 +.737016727598E-  3 -0.0500  1.0131  0.8715 - 10.9  1.9564 - 10.4
+.172421023367E-  3 +.267835781729E+  1 +.341735844771E-  3  0.0500  0.9940  0.8551 -  5.6  1.6366 -  4.9
+.514759714861E-  3 +.184769929270E+  1 +.627739966291E-  3  0.1500  0.9773  0.7940 -  0.2  1.3593 -  0.2
+.138197710111E-  2 +.122851534459E+  1 +.848890038696E-  3  0.2500  0.9735  0.6884    4.6  1.1084    3.1
+.294273050531E-  2 +.736370221307E+  0 +.563404169512E-  3  0.3500  0.9907  0.5051    8.4  0.8581    5.3
Y: 0.5000
+.124776151060E-  1 +.191754441562E+  1 +.622085910368E-  2 -0.3500  0.8932  0.4555 - 77.9  1.3848 - 79.9
+.168548618210E+  0 +.429966799773E+  0 +.362351549890E-  1 -0.2500  0.5998  0.4241 - 66.3  0.6557 - 73.1
+.417216103353E+  0 +.389698802534E-  1 +.107308486478E-  1 -0.1500  0.3714  0.3018 - 47.8  0.1974 - 61.8
+.122841013490E-  1 +.239830621166E-  2 +.218011670564E-  2 -0.0500  0.2321  0.1996 - 14.2  0.0490   97.9
+.111114408529E+  1 +.170290990747E-  1 +.140021192089E-  1  0.0500  0.2038  0.1753   28.9  0.0305  128.7
+.110524486022E+  1 +.174456342756E-  1 +.127259204268E-  1  0.1500  0.2213  0.1798   56.6  0.1321  153.9
+.117756519309E+  1 +.144254949480E-  1 +.849348037218E-  2  0.2500  0.2869  0.1463   71.1  0.1201  180.1
+.102047302975E+  1 +.111194503863E-  1 +.295024579860E-  2  0.3500  0.1276  0.0651   78.5  0.1054  169.4
```

Fig. 12. A page of the output. a/b=0.5, σ=0.28.

modest value of 0,001. It should also be noted that a_3 gives the mean value of f for $\tau_k = \tau_k^n$ rather than τ_k^{n+1}, which is the one generated by the iteration. When the last value of a_3 is smaller than all the previous ones, we conjecture that the stationary value is a minimum. It is seen that in the present case this condition is satisfied.

CONVER

After the machine concludes that the iteration is finished according to the criterium (5.12c), the word "conver" is printed. If the iteration is not finished after the number of iterations specified at input, the word "cycle" is printed and a new case is taken up.

FX FY MZ: $a_1(fi)$ $a_2(fi)$ $a_3(fi)$

with $a_1=f_x=F_x/\mu N$, $a_2=f_y=F_y/\mu N$, $a_3=m_z=M_z/\mu Nc$.
The total force and the torsional couple exerted on the lower body by the upper body.

TAU

(a number of lines of floating numbers)

The τ_k of the solution. Taking the inner product with x_k^M and y_k^M (see (5.1)) gives the traction polynomials X'=X/μZ, and Y'=Y/μZ respectively. It should be recalled in computing X' and Y' that the major semi-axis of the ellipse is the unit of length.

UVX

(a number of lines of floating numbers)

The slip polynomials. Taking the inner product with $2x_k^{M+1}$ and $2y_k^{M+1}$ (see (5.1)) gives P and Q. The contributions of the creepage and the spin, which are first degree polynomials, are accounted for in UVX.

AFWIJKINGEN:

T,S,Y,X,F,S,HOEK: $a_1(fl)a_2(fl)a_3(in)a_4(in)a_5(fi)a_6(fi)a_7(fi)$

with a_1=T, a_2=S, (a_4,a_3) = coordinates in the network of the point under consideration, $a_5=\sqrt{X'^2+Y'^2}$, $a_6=\sqrt{S}$, a_7= angle between traction and slip in degrees.
This is a list of all the aberrations, i.e. the points of the network with T>S, $|(X',Y')|>1$, that is, the points in which the inequality of (5.9) is not satisfied in the critical case that T>S. In the present

case, we have that the aberration occurs at the edge of the contact area, while T is only a little larger than S. So the solution is acceptable.

G,H,A,OPP: a_1(in) a_2(in) a_3(in) a_4(in)

with a_1=number of separate areas of slip; a_2=number of separate areas of adhesion; a_3=number of aberrations; a_4=number of points in E_h. This line gives some statistics regarding the solution. It should be observed that the solution itself does not specify the division of the contact area in areas of slip and locked areas. One can only say that a point with T<<S belongs to the area of slip, while a point with T>>S belongs to the area of adhesion. Quite arbitrarily, we set the boundary between an area of slip and an area of adhesion at the line T=S. It will be seen later on that in the case represented by fig. 12 the region where T≈S is narrow, so that there is in fact a sharp distribution between the locked region E_h and the slip region E_g.

CONTACTVLAK:

-4 ... 0 0 0 -1 -1 -1 -1 0 0 0

etc. etc.

This is a crude picture of the division of the contact area in areas of slip and adhesion. The numbers at the right were only used to generate the picture on the left, and to compute the statistics of G,H, etc. In the picture on the left, the column of integers indicates the line number (y-coordinate). A point indicates that the point belongs to the area of slip, an H indicates that it belongs to the locked area, and an A indicates an aberration. Complete data regarding the solution at an aberration are found in the AFWIJKINGEN list. It is seen from the picture in fig. 12 that we took a rectangular mesh of points which has at most 10 points in the x-direction and 10 points in the y-direction giving a total of 80 points in the contact area.

T,S,INT,X,F,FW,ANF,WS,ARS:

Y: a_0(fi)

a_1(fl) a_2(fl) a_3(fl) a_4(fi) a_5(fi) a_6(fi) a_7(fi) a_8(fi) a_9(fi)

etc.

with a_o = y-coordinate of the points listed below; a_1=T, a_2=S, a_3=f, a_4 = x-coordinate of the point, $a_5 = \sqrt{X'^2+Y'^2}$, $a_6 = \sqrt{X^2+Y^2}/\mu f_{00}G$, a_7 = angle between traction and x-axis in degrees, $a_8 = \sqrt{S}$, a_9 = angle between slip and x-axis in degrees. The angles a_7 and a_9 are between 0° and 90°, when X'>0, Y'>0; S_x>0, S_y>0. This is a specification of the solution at the point (a_4,a_o), where it should be recalled that the major semi-axis is unit of length. The values of (a_4,a_o) are specified in the input. From this list we can judge the quality of the solution. In the case represented by fig.12 one can see from the T and S of the points (-0.35, 0.5), (-0.25, 0.5), and (-0.15, 0.5) that the distinction between locked area and slip area is sharply defined. It is also seen that the solution at y = -0.5 is of good quality. The angle between slip and traction is satisfactorily small (up to 3°), and the traction is quite close to the COULOMB value (error up to 4%). The values of f are all below average, see GEMAFW. The values of f at y = + 0.5 are above average, and it is seen that the quality of the solution is much worse than at y = - 0.5. It is worst at the separatrix T = S.

5.3. Numerical results.

The present section is divided into three parts. In 5.31, we calculate several cases with the object of comparing them with the experiments of JOHNSON [1,3], and of HAINES and OLLERTON [1]. In 5.31 we treat only cases with circular contact area, since most of the experimental evidence is so confined.

In 5.32, we try to give a qualitative survey of the behaviour of the surface stresses occurring under conditions of rolling with creepage and spin.

Finally, we direct our attention in 5.33 to the total force exerted by the upper body on the lower body.

5.31. Comparison with the experiment.

We calculated the cases of pure creepage in the x and y directions respectively, of pure spin and of combined lateral creepage and spin all for a circular contact area, with the object of comparing them with the experiments. The results are shown in

figs. 13 to 17.

In fig. 13, the dimensionless forces $f_x = F_x/\mu N$ and $f_y = F_y/\mu N$ are plotted against the creepage parameters $\xi = \upsilon_x \rho/\mu c$, and $\eta = \upsilon_y \rho/\mu c$, respectively. Also plotted in fig. 13 are JOHNSON's experimental values taken from [1]. As the theoretical curves for the degrees M=2,3,4 nearly coincide, we show only one viz. M=2 for the ξ-f_x diagram, and M=4 for the η-f_y diagram. The weight function W=1. The agreement is quite satisfactory.

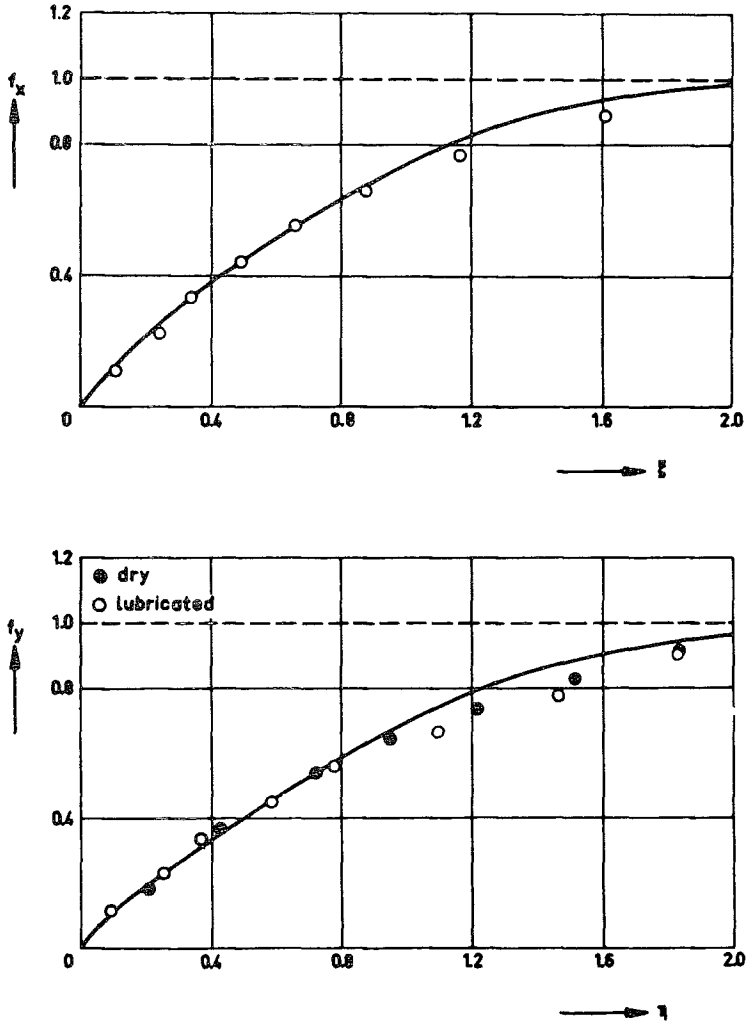

Fig. 13. The total force due to longitudinal and lateral creepage. a/b=1, σ=0.28, χ=0.

In fig. 14, f_y is plotted as a function of the spin parameter $\chi=\phi\rho/\mu$, for zero creepage. The weight function $W=W_1$. Curves for M=2,3,4 are shown; where not drawn, the curve for M=2 follows the curve for M=3. Also given are experimental results taken from K.L. JOHNSON [3, fig. 8]. The coefficient of friction was not known; it was adjusted to fit the curve M=4 best (μ=0.094). It is seen that the curve of M=3 lies markedly higher in the region χ=0.7 to χ=2. In this region, a change in the coefficient of friction has little effect upon the fit of theory and experiment. The curve of M=4 in that region lies somewhat lower than the curve of M=3, but still above the experimental values.

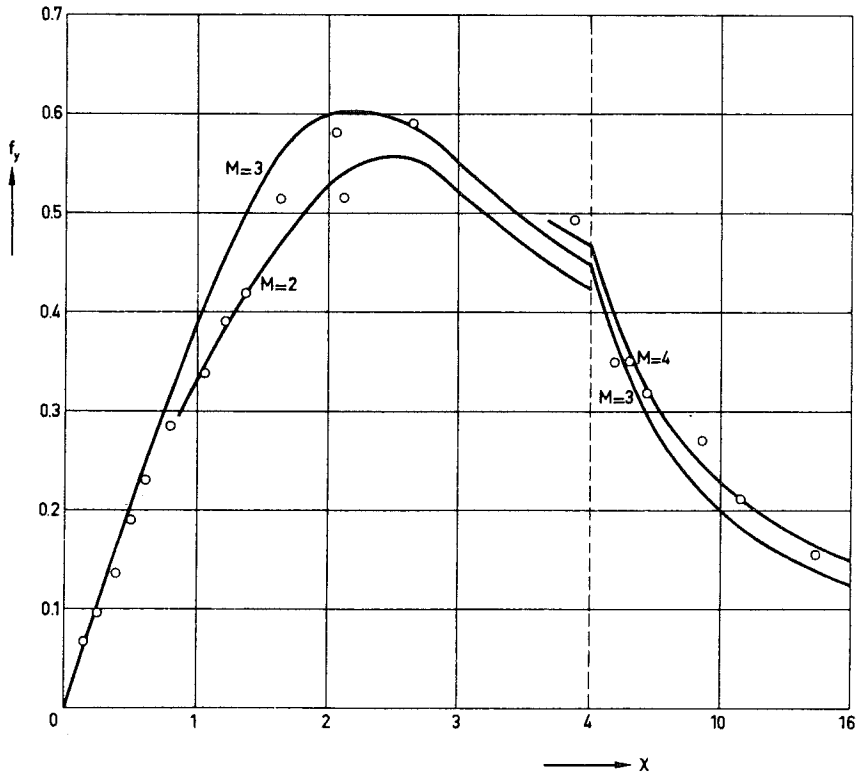

Fig. 14. The total force due to pure spin for various degrees M in comparison with experiments by JOHNSON. a/b=1, σ=0.28, μ=0.094 (estimated).

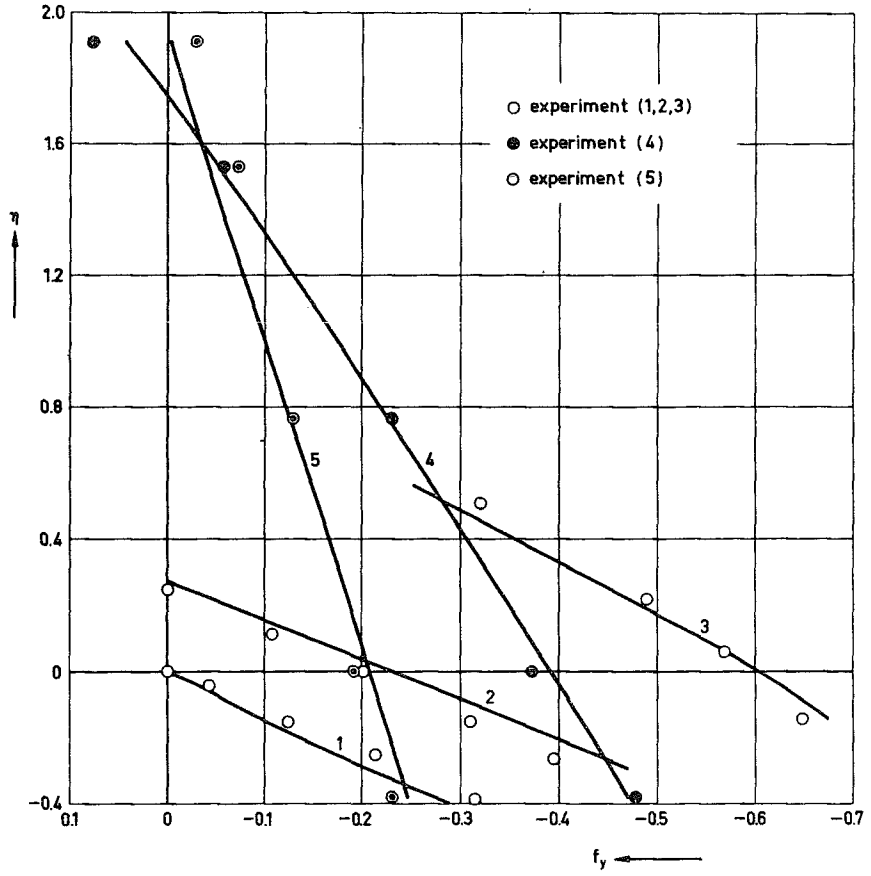

Fig. 15. The total force due to combined lateral creepage and spin in comparison with experiments by JOHNSON. a/b=1, σ=0.28.
1: χ=0; 2: χ=-0.561; 3: χ=-2.25; 4: χ=-4.78; 5: χ=-9.58.
1,2,3: μ=0.0845; 4,5: μ=0.1044.

In fig. 15, the results of the numerical theory are compared with the experimental evidence of JOHNSON [3] on combined lateral creepage and spin, i.e. $v_x=0$, $(v_y,\phi)\neq(0,0)$. The numerical results were obtained with the weight function $W=W_1$ and the degree M=3. Here also, the coefficient of friction μ was not known; however, the differences between theory and experiment are rather insensitive to

changes in μ for the curves 1 and 2 of fig. 15 which represent small values of the spin, so that they give a clear impression of the deviation of theory and experiment for small spin. The curves 1,2,3 were measured with the same apparatus, so that it seemed natural to suppose that the coefficient of friction was the same in all three cases. It was adjusted so as to minimize the difference between theory and experiment for the curve 3(μ=0.085). As a consequence of the way in which μ was estimated, the correlation between experiment and theory for curve 3 is not necessarily as good as the one shown in fig. 15. JOHNSON performed the experiments for the curves 4 and 5 (large spin) by means of a different apparatus, so that it seems justified in assuming for curves 4 and 5 a coefficient of friction which differs from the one taken in curves 1,2,3. The μ for 4 and 5 was chosen so as to minimize the differences between theory and experiment in those curves (μ=0.104). The differences appeared to be very sensitive to changes in μ. Consequently the correlation between experiment and theory is not necessarily as good for the curves 4 and 5 as the one shown in fig. 15.

The moment M_z agreed badly with the experiments. However, it was pointed out by JOHNSON [3] that a moment due to elastic hysteresis is present in the experiments, which is of the same, or even larger order of magnitude than the moment due to surface friction. So there is little practical significance attached to the moment M_z as we calculate it, and consequently we omit it from our further considerations.

In fig. 16, the results for pure longitudinal creepage, calculated with $W=W_1$ and $M=3$, are compared with the photoelastic work of HAINES and OLLERTON [1]. In the upper left part of fig. 16, the circular contact area is divided into an area of adhesion and an area of slip, the separatrix being assumed to be the line T=S. The distinction between E_g and E_h is quite sharp. Also shown is the separatrix according to HAINES and OLLERTON. It is seen that the lines are quite close. Also shown in fig. 16 is a comparison between HAINES and OLLERTON's surface stress and our results. The agreement is best for y=0, and worst for y=0.80. The value of P (see (5.18)) is shown for y=0. It is seen that it rises sharply in the slip

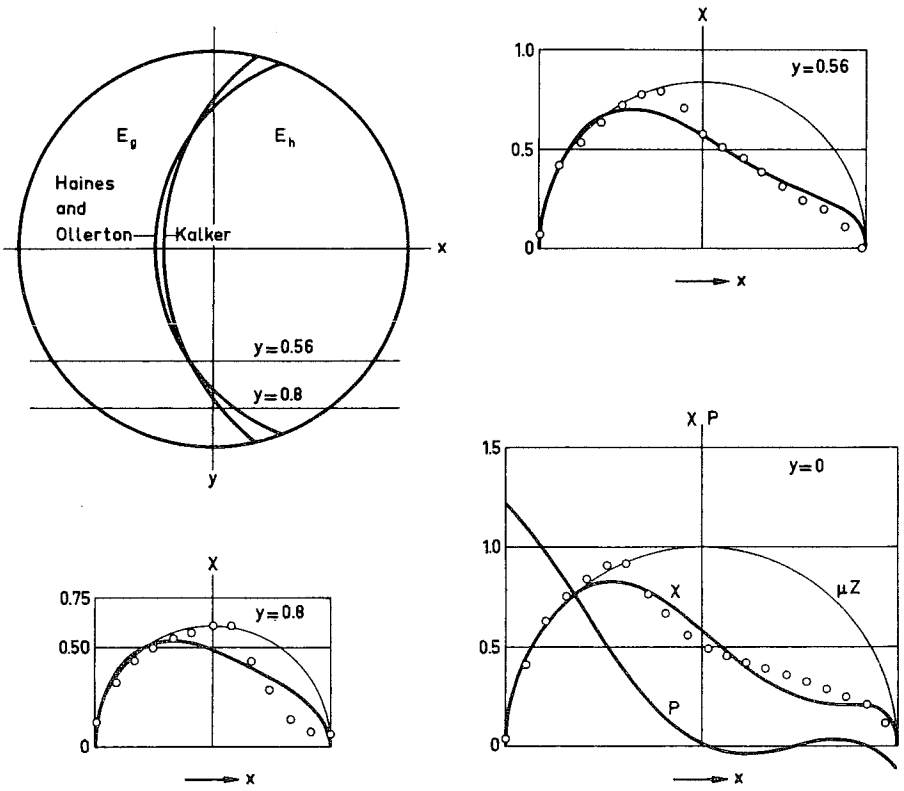

Fig. 16. A comparison with the photoelastic results of HAINES and OLLERTON. a/b=1, σ=0.5, η=χ=0, ξ=0.90.

zone, and winds itself about zero in the adhesion zone.

In fig. 17, we show the division of the contact area in areas of slip and adhesion according to the numerical theory, the strip theory (KALKER [2]), and the experimental evidence of JOHNSON [4], which consists of a photograph of the track of a rubber ball rolling over a sooted transparent plate (JOHNSON [4], fig.8b). The value of the spin parameter χ=1.20, and POISSON's ratio σ=0.50 (for, taking the rubber ball as the upper body, we have that $G^{+}>>G^{-}$, σ^{-}=0.50; hence, according to (2.10), $G=2G^{+}$, σ=0.50, κ=0). The longitudinal creepage v_x=0, so that F_x=0, and v_y is chosen so that F_y also vanishes: that is, we are in fig. 15 at the intersection of the line

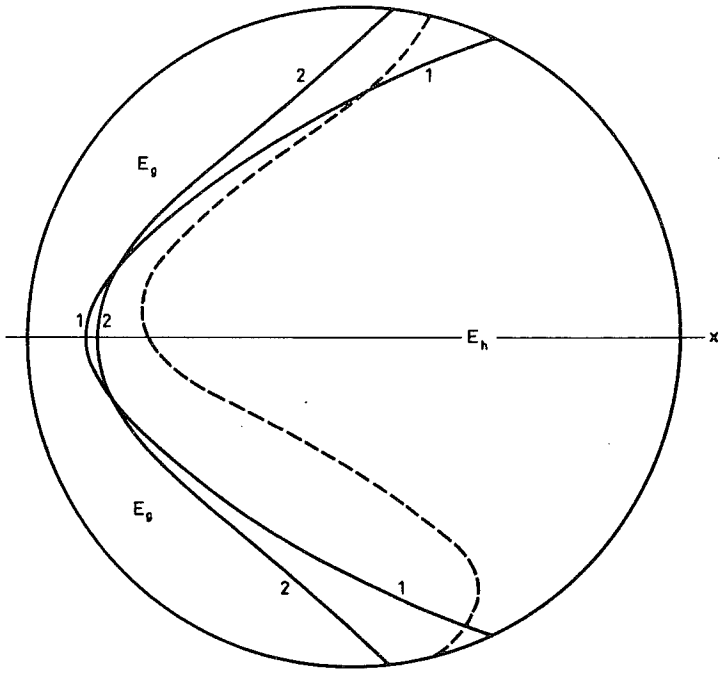

Fig. 17. The separatrix for combined lateral creepage and spin.
σ=0.5, f_y=0, χ=1.20, η= -0.57.
1: strip theory. 2: numerical theory.
Broken line: a photograph by JOHNSON.

χ=1.20 (not shown) with the η-axis. The theoretical separatrix is the line T=S, the degree M=3, the weight function $W=W_1$. It is seen that JOHNSON's contour is asymmetric with respect to the x-axis, while our contour is symmetric, as it should be with $\upsilon_x=0$, see (4.26). This is attributed by JOHNSON to the fact that the soot is swept into the adhesion area in the lower part of the figure, while it is swept away from the adhesion area in the upper part.

5.32. Qualitative behaviour of the solution.

In the present section and its subsections, we will make some observations on the qualitative behaviour of the solution in the case of pure creepage (ϕ=0, sec. 5.321), pure spin ($\upsilon_x=\upsilon_y=0$, sec. 5.322), and arbitrary creepage and spin (sec. 5.323).

5.321. Pure creepage.

In the case of pure creepage, the area of adhesion borders on the leading edge of the contact area, and it is, according to the numerical theory, approximately symmetric about the x-axis. In the cases of purely longitudinal or purely lateral creepage, the form of the area of adhesion is well predicted by the strip theory of KALKER [2], which is a generalization of the strip theory due to HAINES and OLLERTON [1]. According to KALKER [2], the separatrix is found by shifting the trailing edge of the contact area parallel to itself along the x-axis, see fig. 18, where the case of a circular contact

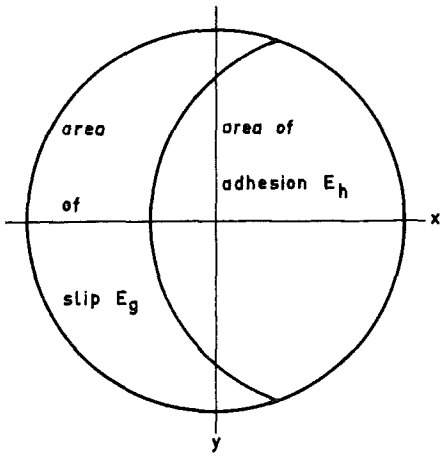

Fig. 18. Separatrix according to KALKER [2] for pure creepage.

area is shown. So, in the theory of KALKER [2], the area of adhesion is symmetric about the x-axis when there is combined longitudinal and lateral creepage, but no spin. When the total creepage increases, the separatrix comes to lie further and further from the trailing edge, until there is no area of adhesion left and gross sliding commences. Adhesion areas of this type have been observed by HAINES-OLLERTON [1] for pure longitudinal creepage, and by HAINES [2] for pure lateral creepage.

The behaviour of the absolute value of the traction can be seen from fig. 16. Going in the rolling direction along a line parallel to

the x-axis, the tangential traction first increases according to $|(X,Y)|=\mu Z$ in the slip area, then falls below μZ near the separatrix, and stays below μZ in the locked area. According to the strip theory of HAINES and OLLERTON [1] and of KALKER [2], the curve representing the traction would have a vertical tangent at the separatrix.

The traction vectors are in general not parallel to each other. In the case of pure longitudinal creepage, the traction direction behaves qualitatively as sketched in fig. 19a. The division of the contact area in areas of adhesion and slip is not shown, our considerations are valid both for the area of slip and for the area of adhesion. γ is the angle between the traction and the x-axis. It is seen that the angle γ vanishes on the x-axis, since the traction is mirror-symmetric about the x-axis, see (4.27). When the longitudinal creepage changes sign, the direction of the traction is reversed, that is, the arrows in fig. 19a are reversed. To give an idea of the magnitude of γ, we give some values for $\xi=0.8$, $\eta=\psi=0$, $a/b=1$, $\sigma=0.28$. Then $\gamma_3 = -\gamma_1 = 3^\circ$, and $\gamma_4 = -\gamma_2 = 3^\circ$. For increasing $|y|$, the absolute value of γ increases. For increasing longitudinal creepage $|\xi|$, $|\gamma|$ decreases. For increasing values of POISSON's ratio σ, $|\gamma|$ increases up to values of about 20° for $\sigma=0.5$. For values near unity of the excentricity $|e|$ of the contact ellipse,

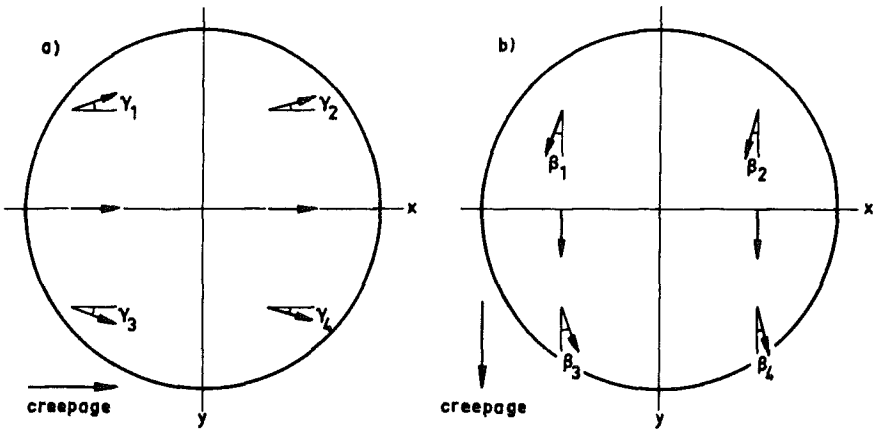

Fig. 19. An impression of the direction of the traction for a) longitudinal, b) lateral creepage, without spin.

$|\gamma|$ decreases. It should be remarked that the foremost points of fig. 19a lie in the area of adhesion or close to it, when $|\xi|=0.8$. Deeper in the adhesion area, and for smaller values of $|\xi|$, the traction becomes much smaller than the COULOMB value, and its direction according to the numerical method tends to be erratic. One should not place undue reliance on the fact that the direction of (X',Y') is erratic when $|(X',Y')|\ll 1$, since the error in the numerical method may drown the information. We also meet this phenomenon later on.

In the case of pure lateral creepage $(\upsilon_x=\phi=0)$, the traction direction behaves qualitatively as sketched in fig. 19b. It is seen from fig. 19b that on the x-axis the angle $\beta=0$, since according to (4.26), the traction and slip are mirror anti-symmetric about the x-axis, whenever $\upsilon_x=0$. Also, when under the conditions of fig. 19b the lateral creepage changes sign, traction and slip are reversed. If $\eta=0.8$, $\xi=\psi=0$, $a/b=1$, $\sigma=0.28$, then $\beta_1=-\beta_3=7^\circ$, and $\beta_2=-\beta_4=3^\circ$. $|\beta|$ increases for increasing $|y|$; $|\beta|$ decreases for $|e|\uparrow 1$, and for increasing $|\eta|$. The foremost points of fig. 19b lie in the area of adhesion or close to it when $|\eta|=0.8$. Deeper in the adhesion area, and for smaller values of $|\eta|$, the traction becomes much smaller than the COULOMB value, and its direction according to the numerical theory tends to be erratic.

We finally observe that the maximum values of $|\gamma|$ and $|\beta|$ found here are of the same order of magnitude as the angle θ_m of (4.46), which is the maximum angle between slip and traction in the problem of infinitesimal creepage and spin. The same values also occur in the strip theory of KALKER [2], fig. 4.

We leave the discussion of the total force exerted on the lower body to section 5.33.

5.322. Pure spin.

In the case of pure spin, the area of adhesion is symmetric about the x-axis, in accordance with the symmetry relations (4.26). In fig. 20, we sketched the division of the contact area into areas of slip and adhesion for different values of the spin parameter χ. The separatrix is assumed to be the line T=S. All three figures correspond to $a/b=1$, $\sigma=0.28$, $\upsilon_x=\upsilon_y=0$. The adhesion areas are shown

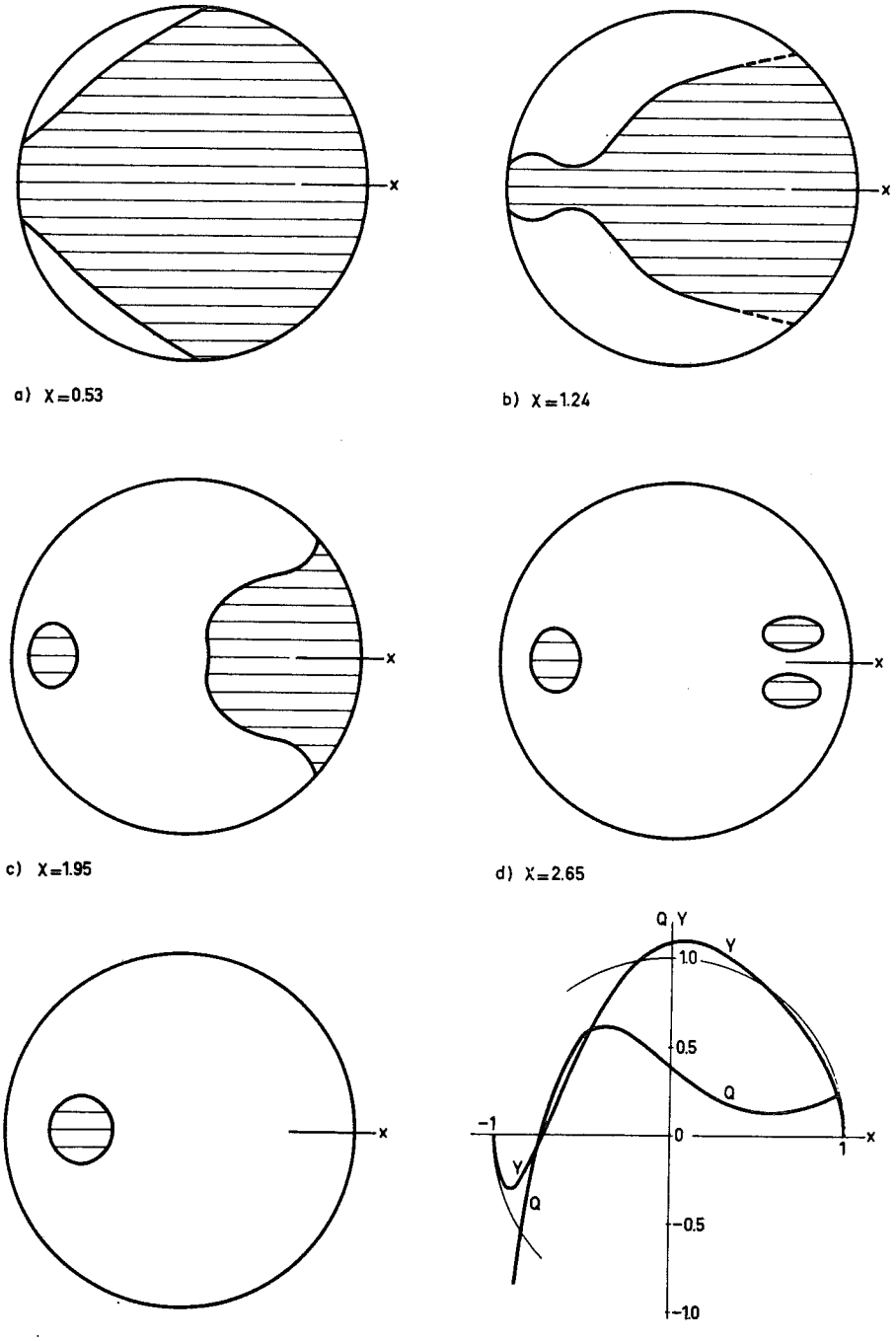

Fig. 20. a/e: Areas of adhesion (shown shaded) and slip for pure spin. a/b=1, σ=0.28. f: Traction Y and slip Q on the x-axis for χ=2.65.

shaded. The trivial case $\psi=0$ has not been sketched; the adhesion area then covers the whole of the contact area (free rolling). In fig. 20a, the case $\chi=0.53$ has been sketched. It is seen that slip commences at the trailing edge of the contact area, but that the x-axis lies entirely in the adhesion zone. For increasing values of the spin, the areas of slip grow, while the x-axis remains in the adhesion zone; the adhesion area becomes narrow in the y-direction (see fig. 20b, $\chi=1.24$), and finally splits into two parts (fig.20c $\chi=1.95$). The island on the left is the adhesion area about the point with $X=Y=s_x=s_y=0$. The traction vectors from a rotating field about this adhesion area, see fig. 21. Both slip and traction have a large gradient there in the numerical solution, see fig. 20f. With further increasing spin, the adhesion area on the right of fig. 20c decreases in size; then it breaks up into small parts (fig. 20d, $\chi=2.65$), and finally vanishes (fig. 20e, $\chi > 3$). The island on the left remains, retains the character outlined above, but moves inward toward the centre of the contact area, where the spin pole of LUTZ [1,2,3] and WERNITZ [1,2] is situated (see (4.93)). The behaviour of the solution on the x-axis, upon which the island lies, can be gathered from fig. 20f, in which is sketched the relative slip Q (see (5.18)) and the distribution of the traction Y, both on the x-axis. The circle represents the COULOMB value of the traction. It is seen that slip and traction vanish at about the same point in the adhesion island on the left. It is also seen that going in the rolling direction the relative slip Q increases sharply with increasing x, attains a maximum, and decreases again with a much smaller gradient. This clearly shows the influence of the two small adhesion areas on the right of fig. 20d. It should be observed, finally, that it is doubtful whether the two small adhesion areas on the right of fig. 20c actually exist. Indeed $T > S$, but the difference is small, and, moreover, the largest contribution to T stems from the fact that the angle between slip and traction is rather large (up to 14°). In fact, for slightly different values of ψ, η , and ξ, aberrations occur in that region, in the sense that $|(X,Y)|>\mu Z$, and $T > S$. The occurrence of the island on the left is also somewhat doubtful. It is entirely possible that the tractions have a discontinuity there, and that the

slip has there a simple zero.

In fig. 21, the traction distribution in the contact area is shown for various values of the spin. Only half of the contact area has been drawn. The traction distribution is given in the form of curves of constant ratio between the resultant surface stress $|(X,Y)|$ and the COULOMB traction μZ in percents. These lines are symmetric about the x-axis. The arrows represent the direction of the traction exerted on the lower body; according to (4.26), the tangential traction is mirror anti-symmetric about the x-axis, see fig. 19b.

It is seen from fig. 21 that the tractions form a rotating field with somewhat varying centre of rotation. The spin pole of LUTZ and WERNITZ lies in the centre of the contact area, but it is seen that there is no point X=Y=0 inside the contact area when $\chi=0.53$ (fig. 21a), such a point enters the contact area, (fig. 21b, $\chi=1.24$), and slowly moves towards the centre of the contact area with increasing spin (fig. 21c, $\chi=2.65$).

5.323. Arbitrary creepage and spin.

The case of arbitrary creepage and spin lies between the cases of the spin pole at infinity (pure creepage) and of the spin pole at the center of the contact area (pure spin). An example is sketched in fig. 22, in the manner of fig. 21. The determining parameters of fig. 22 are: $\chi=0.70$, $\xi=-\eta=0.50$, $a/b=1$, $\sigma=0.28$, $M=3$, $W=W_1$. The spin pole of LUTZ and WERNITZ lies on the circle, and has the coordinates (0.71a, 0.71a), where a is the radius of the contact circle. The point X=Y=0 lies approximately at (0.25a, 0.50a). Since the traction is small near this point, it is not clearly defined. Also, when the parameters ξ,η,ψ get larger in absolute value in such a way that the spin pole retains its position, the absolute value $|(X,Y)|$ of the traction has a minimum inside the contact area, but no zero. However, the accuracy of the numerical method is not so that one can come to a decision on the point whether there is a zero or not. It is seen from fig. 22 that the traction again forms a rotating field with the centre somewhere in the first quadrant $x>0$, $y>0$. In this quadrant, the values of the traction are small, and, especially near the point X=Y=0, the direction is erratic; this is possibly a case of the error

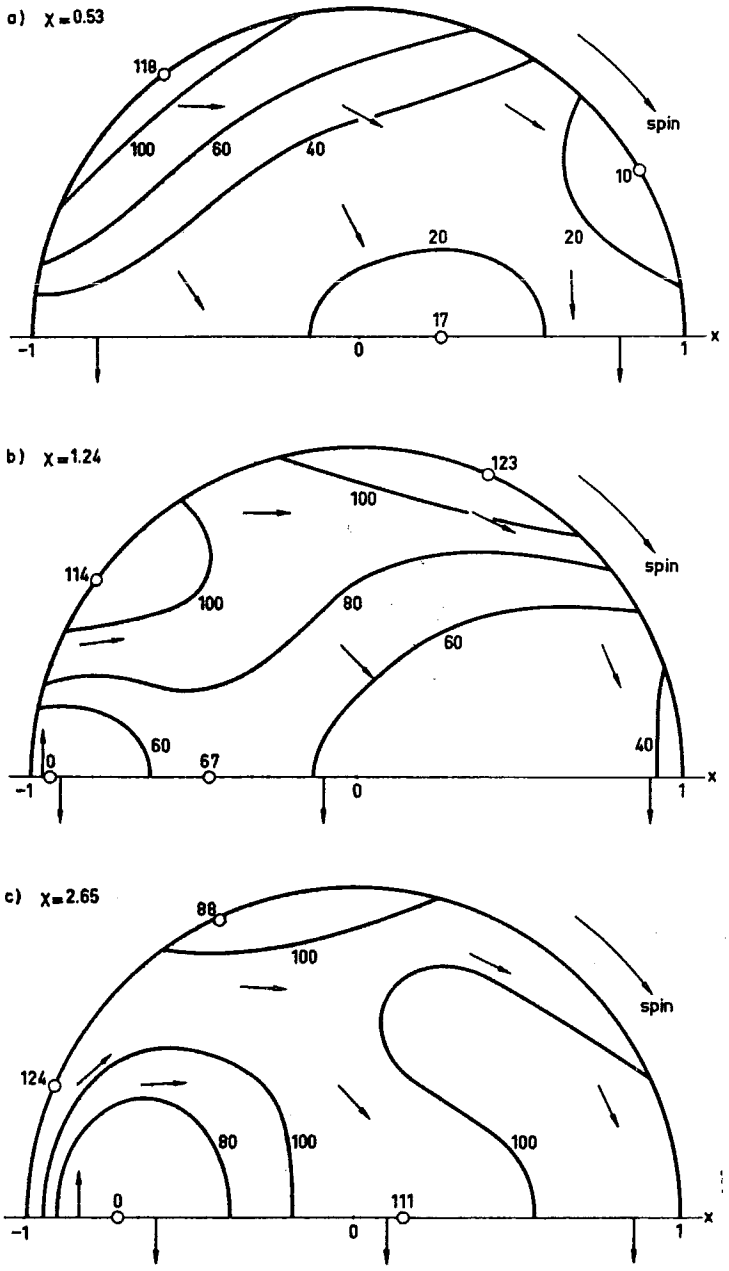

Fig. 21. Traction distribution for various values of the spin. a/b=1, σ=0.28, ξ=η=0.

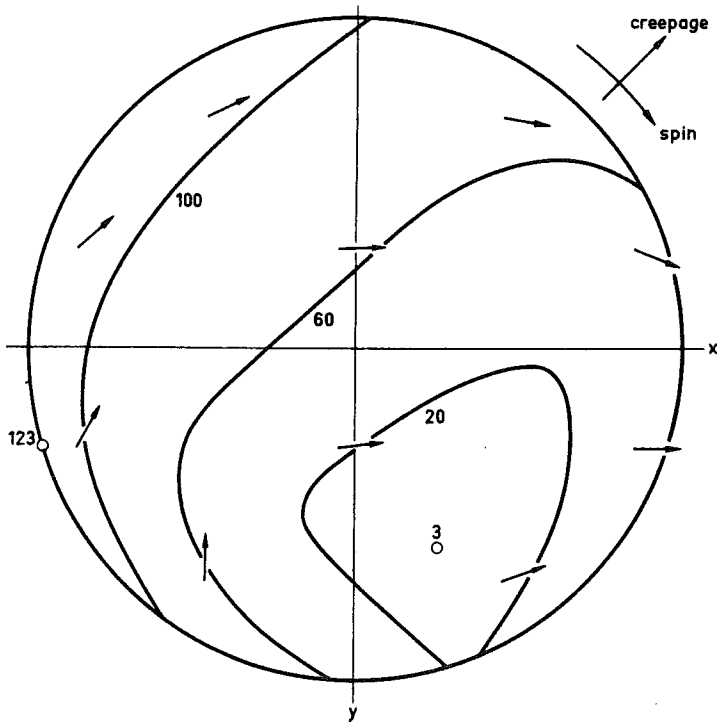

Fig. 22. Traction distribution for a case of combined creepage and spin.
a/b=1, σ=0.28, χ=υ=0.7, α = -45°.

in the calculation drowning the information.

5.33. The total force transmitted to the lower body.

For fixed ratio of the axes a/b and fixed POISSON's ratio σ, one can imagine surfaces of constant creepage $\upsilon=\sqrt{\xi^2+\eta^2}$ in the three-dimensional (f_x,f_y,χ)-space. The surfaces of constant creepage all lie inside the cylinder $f_x^2 + f_y^2 = 1$, or, equivalently, $F_x^2 + F_y^2=\mu^2N^2$. This cylinder represents the limiting case that $\xi^2+\eta^2\to\infty$, see fig. 24a,b,c. It was found that the surfaces υ=constant form tubes in the χ-direction which lie inside each other, and which have a roughly circular intersection with the planes χ=constant, the radius of the tube increasing as υ increases. The radius decreases when the spin

becomes larger, i.e. as $|\chi|$ increases, see fig. 24a,b,c, In the limit $\chi \to \infty$, the force is determined solely by the parameters $c\xi/\chi$, and $-c\eta/\chi$, which are the coordinates of the spin pole, see (4.93). So the "radius" of the tube is roughly determined by the quantity $v/|\chi|$, as $\chi \to \infty$.

It follows from the considerations of symmetry of sec. 4.2 that the (χ,f_y)-plane is a plane of symmetry of the tubes, for when the point (f_x,f_y,χ) corresponds to (ξ,η), then $(-f_x,f_y,\chi)$ corresponds to $(-\xi,\eta)$, see (4.23f). It follows from (4.22e) that the tubes are symmetric about the origin, for if the point (f_x,f_y,χ) corresponds to (ξ,η), then $(-f_x,-f_y,-\chi)$ corresponds to $(-\xi,-\eta)$. Hence we need for the construction of the tubes only the pertinent information in the quarter space $f_x \geq 0$, $\chi \geq 0$. When $\xi=\eta=0$, the tube degenerates into a line in the (f_y,χ)-plane. This is the case of pure spin, which is given in fig. 23 for four values of the parameter a/b, with POISSON's ratio $\sigma=0.28$.

The total force transmitted to the lower body was calculated in a great number of cases, with the degree M=3, the weight function $W=W_1$, and $\sigma=0.28$. First, we calculated the case of pure spin $\xi=\eta=0$ for a/b=2, 1, 0.5, 0.2. The results are shown in fig. 23. Then we calculated f_x and f_y as functions of ξ and η, for fixed values of spin, POISSON's ratio, and ratio of the axes a/b. The values of χ were chosen so that we obtain the plane of pure creepage ($\chi=0$), then two values of χ before the peak in fig. 23, one at the peak, and two after. In fact, we calculated

$$\left.\begin{array}{l} \sigma=0.28,\ a/b=2;\quad \chi=0,\tfrac{1}{2},1,2,3\tfrac{1}{2},7;\ \text{variable } \xi \text{ and } \eta. \\ \sigma=0.28,\ a/b=1;\quad \chi=0,\tfrac{1}{2},1,2,5,10;\ \text{variable } \xi \text{ and } \eta. \\ \sigma=0.28,\ a/b=0.5;\ \chi=0,1,2,3,5,10;\ \text{variable } \xi \text{ and } \eta. \\ \sigma=0.28,\ a/b=0.2;\ \chi=0,\tfrac{1}{2},1,2,5,10;\ \text{variable } \xi \text{ and } \eta. \end{array}\right\} \qquad (5.29)$$

The case $\chi = \infty$ has been treated in sec. 4.4, fig. 10 and 11.
The results of these calculations will be laid down in a report of the Laboratorium voor Technische Mechanica of the Delft Technological University. Some results of the calculations with χ = constant are given in fig. 24, all for a/b=1, $\sigma=0.28$.

We also attempted to calculate the case a/b=5, but here the

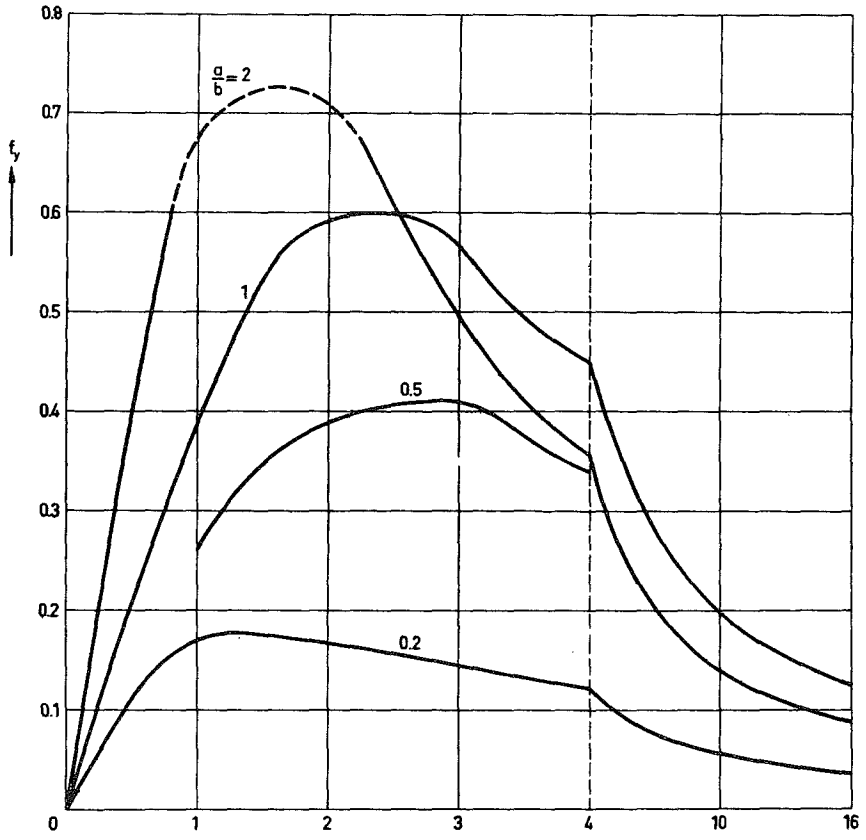

Fig. 23. f_y-χ diagram for various values of a/b.
$\sigma=0.28$, $\xi=\eta=0$.

numerical method failed to give results in a large portion of the curve of pure spin, situated around the peak. Either the iteration process (5.12) failed to converge, or it gave incorrect results, with aberrations covering nearly the entire contact area, and with $f_x^2+f_y^2$ exceeding unity. By taking special care in the choice of the initial value τ_k^o, the trouble could be concentrated in a smaller position of the curve of pure spin, but even so the solutions obtained showed many aberrations. We decided to drop the case altogether in view of the formidable amount of machine time needed to obtain any results at all, which would be of poor quality as well. Also, the case would

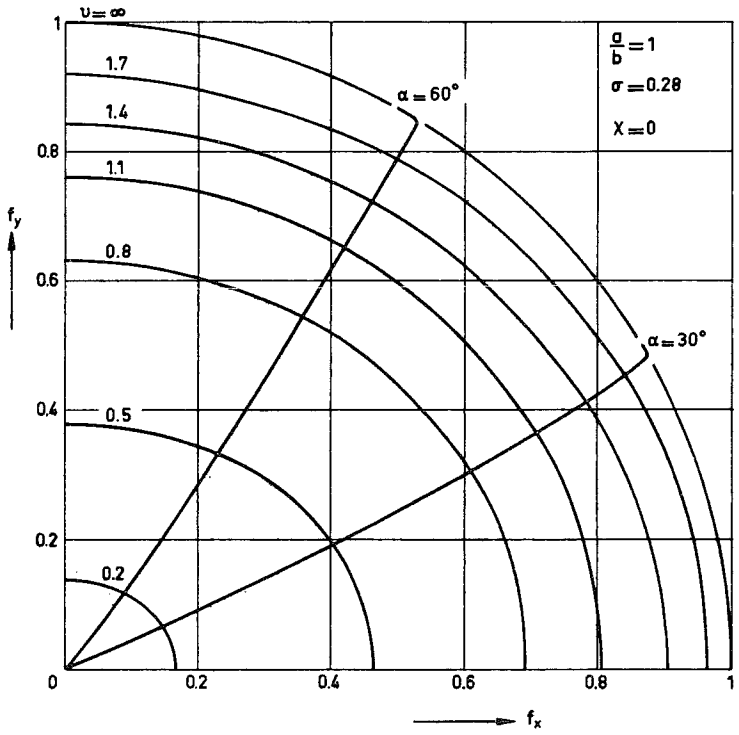

Fig. 24a. Lines of constant υ and α as functions of f_x and f_y, a/b=1, σ=0.28, X=0.

seem to have little practical interest: it is the case of a contact area which is narrow in the lateral direction, an extreme case of which is a circular knife rolling over a plane. The trouble in the case a/b=5 was already foreshadowed in the calculations of the case a/b=2, where near the peak many aberrations T > S, $|(X,Y)|>\mu Z$ occurred. In pure spin also, the resulting values near the peak of f_y for a/b=2 were somewhat erratic, which is the reason why that portion of the curve of f_y for a/b=2 is given in fig. 23 with a broken line.

In fig. 23 we show the case of pure spin, for different values of a/b. The curve for a/b=0.5 is shown only partially; it goes through the origin in the same way as the other curves, and on the right the curve a/b= 0.5 is very close to the curve a/b=2. In fact,

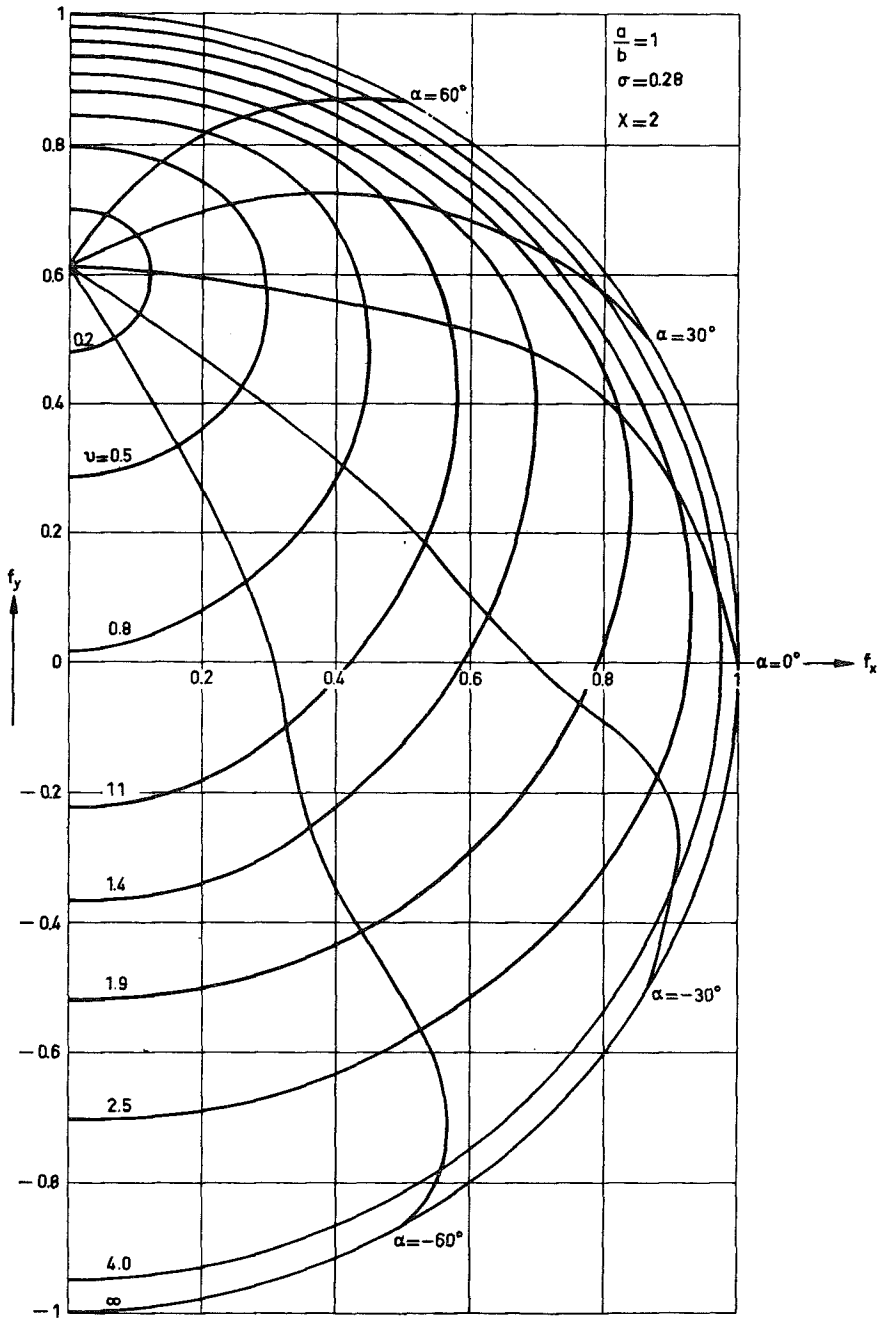

Fig. 24b. Lines of constant υ and α as functions of f_x and f_y.
a/b=1, σ=0.28, χ=2.

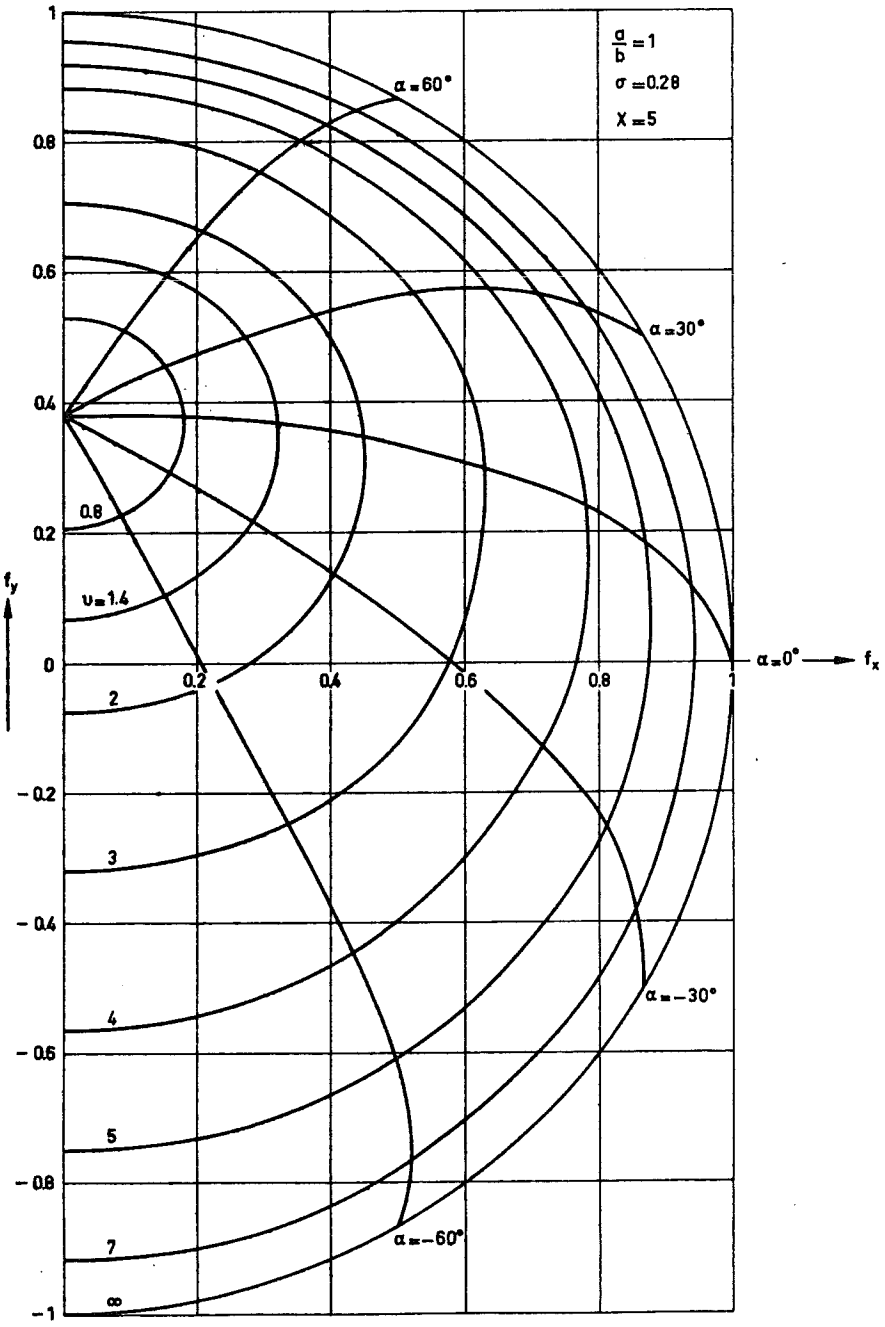

Fig. 24c. Lines of constant υ and α as functions of f_x and f_y.
a/b=1, σ=0.28, X=5.

the values of f_y lie slightly higher in the case a/b=0.5, but not significantly so. It is seen that the curves of f_y as functions of χ increase from zero to a maximum, then decrease again, approaching zero asymptotically. Two competing mechanisms are at work. For small values of $|\chi|$, the effective spin pole lies far from the origin, see fig. 21. However, the area of adhesion is large, which keeps the mean absolute value of the traction down as a consequence of elastic deformation. As $|\chi|$ increases, the area of adhesion becomes smaller, and the mean absolute value of the tractions grows. At the same time, however, the effective spin pole moves towards the origin. Consequently, the direction of the traction becomes diversified, which tends to diminish the total force. Especially for small values of a/b, the effects appear to keep each other in check for a large range of values of χ around the maximum, for the maximum is very flat.

It is seen from fig. 23, that the value of the maximum decreases when a/b decreases, that is, when the ellipse becomes narrower in the rolling direction. If we assume tentatively that the effective spin pole lies in the point $(-\alpha a, o)$, where α is some function of χ independent of the ratio a/b, it is clear that with decreasing a/b the area occupied by points with a large x-component of the traction increases, while in the determination of the total force the x-components cancel each other, owing to the mirror antisymmetry of the traction.

It is also seen from fig. 23 that the value of χ at which the maximum is reached, first increases with decreasing a/b, reaches a maximum at $a/b \approx 0.5$, when $\sigma=0.28$, and then decreases again. This is partially because for the same value of the spin parameter ϕc, a slender ellipse has a larger area of slip than a non-slender ellipse, so that the effect of the elastic deformation described above, dies out for a smaller value of ϕc.

We now turn our attention to the figures 24. They represent the case $\sigma=0.28$, a/b=1. In the three-dimensional (f_x, f_y, χ)-space introduced above, they are planes of constant χ. In fig. 24a, $\chi = 0$ (pure creepage). Fig. 24b represents a value of χ near the peak of fig. 23 ($\chi = 2$). Fig. 24c represents a value of χ beyond the peak,

for which $f_y(\upsilon_x=0,\ \upsilon_y=0) \approx \frac{1}{2} \max_{\chi} f_y$: $\chi = 5$. In the figures, the tangentials are lines of constant creepage $\upsilon \equiv \sqrt{\xi^2+\eta^2}$ = constant. The radials are lines of constant α, where

$$\xi = \upsilon\cos\alpha,\ \eta = \upsilon\sin\alpha,\ \upsilon = \sqrt{\xi^2+\eta^2},\ \alpha \text{ in degrees}, \tag{5.30}$$

in accordance with (5.16).

In fig. 24a, only the first quadrant is shown because when $\chi = 0$, there is symmetry about both the f_x and f_y axes. It is seen that the lines $\alpha = 30^\circ$ and $\alpha = 60^\circ$ are nearly straight, except at the end $\upsilon \to \infty$, where they make a sharp turn. This means that the ratio f_x/f_y depends principally on the ratio ξ/η for values of υ up to 1.7. In fact,

$$\left.\begin{aligned} &25^\circ < \tan^{-1}(f_y/f_x) < 27.6^\circ \text{ when } \alpha = 30^\circ,\ 0 < \upsilon < 1.7; \\ &53^\circ < \tan^{-1}(f_y/f_x) < 56.7^\circ \text{ when } \alpha = 60^\circ,\ 0 < \upsilon < 1.7. \end{aligned}\right\} \begin{array}{l} a/b=1 \\ \sigma=0.28 \end{array} \tag{5.31a}$$

According to the theory of JOHNSON and VERMEULEN [5], these angles are constant, and

$$\left.\begin{aligned} &\tan^{-1}(f_y/f_x) = 25.8^\circ \text{ when } \alpha = 30^\circ,\ \upsilon > 0; \\ &\tan^{-1}(f_y/f_x) = 55.4^\circ \text{ when } \alpha = 60^\circ,\ \upsilon > 0; \\ &a/b=1,\ \sigma=0.28. \end{aligned}\right\} \tag{5.31b}$$

In figs. 24b and 24c, only the first and fourth quadrants are shown, since the f_y-axis is a line of symmetry. The curves υ=constant are egg-shaped, with the flat end up. In fig. 24b ($\chi = 2.0$), the curves for $\alpha = -30^\circ$ and $\alpha = -60^\circ$ show some waviness. It is not at all certain whether this waviness actually occurs in practice: it is quite possible that it is due to errors in the numerical calculation. It is seen from fig. 24c that the waviness is completely gone for $\chi = 5$. In fig. 24c, the effect of the diminishing radius of the tube υ=constant with increasing χ is clearly shown.

6. Conclusion.

In this final chapter we will review in 6.1 the results which have been achieved in this thesis, and in 6.2 we will make some observations on further research.

6.1. Results achieved.

In this thesis, we confine ourselves to contact problems between purely elastic bodies which can be approximated by half-spaces, while the contact area is elliptic in form. The method for the solution of contact problems with friction which is discussed in this thesis is, strictly speaking, only valid when the elastic constants of the bodies are the same, or when both bodies are incompressible. The method gives an approximation in case that these conditions are not satisfied. A crude estimate of the error of this approximation is given in sec. 2.1.

In chapters 2 and 3, we discuss the general theory. It was shown in 2.2 that a generalized version of GALIN's theorem (GALIN [1], ch. 2, sec. 8) can be established without recourse to LAME's ellipsoidal harmonics. As a consequence of this, DOVNOROVICH's method [1] for the calculation of contact problems without friction on the basis of GALIN's theorem could be adapted in 2.3 to contact problems in which there are also frictional forces. DOVNOROVICH's method was generalized in 2.4 sqq. in the sense that the connection between tractions and displacement differences was given explicitly for any degree M of the determining polynomials. In 3.1, the theory is worked out for the case without traction singularity at the edge of the contact area. DOVNOROVICH also considered this problem, but he did not arrive at the simple relationship (3.15). The examples treated in 3.2 sqq. are all well-known.

In chapters 4 and 5, we discuss the problem of contact in steady rolling. The boundary conditions are well established, see e.g. DE PATER [1] and KALKER [1]; they are set up in section 4.1. In 4.2., we derive a number of symmetry relations between the surface tractions and the slip on the one hand, and creepage and spin on the other hand. These relations lead to a number of symmetry properties of the

total force and the total torsional moment as functions of creepage and spin. It is also found that the determining parameters of the problem are a/b, ξ, η, χ, and σ. We have not found the symmetry relations in this form in the literature.

The limiting case of infinitesimal creepage and spin (sec. 4.3 sqq.) was treated before in the literature, but we generalized it to elliptic contact areas. KALKER's proof (see [1], p. 168-169) that no slip takes place at the leading edge of the contact area when creepage and spin are infinitesimal, and which is valid for circular contact areas and vanishing POISSON's ratio, was extended in sec. 4.31 to elliptic contact areas and arbitrary POISSON's ratio. The creepage and spin coefficients C_{ij} (p.91 to 93) coincided with those obtained in KALKER [1], pg. 174, when the contact area is circular. It was found in KALKER [1] that the creepage and spin coefficients agree with JOHNSON's experiments [1,2,3], when the contact area is a circle. In a comparison with the experiments of JOHNSON and VERMEULEN [5], it was found that C_{22} agrees well with the experiment when the contact area is an ellipse. The curious and unexplained phenomenon that $C_{23} = -C_{32}$, which was noted in KALKER [1], occurred also with elliptic contact areas.

The theory of LUTZ [1,2,3] and WERNITZ [1,2] for very large creepage and spin, which is confined to the case that $v_x=0$ or $v_y=0$ when the contact area is an ellipse, was generalized in sec. 4.4 to the case that $v_x \neq 0$, $v_y \neq 0$.

The numerical theory of ch. 5 for steady rolling with arbitrary creepage and spin, which consists of the minimalization of a certain integral, appeared to work reasonably well for the degree $M=3$, and the weight function $W=W_1$. The error in the total force is at most about 10%, see fig. 15. The error in the traction distribution is larger, see fig. 16. A qualitative description of the tractions in steady rolling is given in sec. 5.32 sqq. The calculations were carried out for a large number of the defining parameters a/b, ξ, η, χ (see (5.29)); POISSON's ratio was kept at $\sigma=0.28$ throughout. The calculations proved to be exceedingly lengthy, so that in our opinion the main significance of the theory of ch. 5 lies in the possibility that existing approximate theories (JOHNSON [1,2,3,4,5],

LUTZ [1,2,3] - WERNITZ [1,2], DE PATER [1] - KALKER (sec. 4.3 sqq.), HAINES - OLLERTON [1], KALKER [2]) or theories that will be developed yet can be tested with the numerical theory.

6.2. Further research.

It would be of interest to have a deeper insight in the interaction between the normal and the tangential problem, when $\kappa \neq 0$.

Such an interest is mainly academic in the case of the influence of the tangential traction on the normal problem. An interesting aspect of such a theory is the change of the contact area as a consequence of tangential tractions. A simple, non-trivial problem of this sort is the problem of gross sliding in Hertzian contact. In that case, the boundary conditions are

$$\left.\begin{aligned} w &= -Ax^2-By^2 + \alpha, \\ X &= \mu Z,\ Y = 0 \end{aligned}\right\} \text{ in } E, \tag{6.1}$$

$$\left.\begin{aligned} w &> -Ax^2-By^2 + \alpha, \\ X &= Y = Z = 0 \end{aligned}\right\} \text{ on } z = 0, \text{ outside } E, \tag{6.2}$$

Displacements and stresses vanish at infinity. (6.3)

In the rotationally symmetric case of pure spin about the z-axis, $X = -\frac{\mu yZ}{\sqrt{x^2+y^2}}$, $Y = +\frac{\mu xZ}{\sqrt{x^2+y^2}}$, the normal problem is unaffected by the tangential tractions, see SNEDDON [1], ch. V, sec. 31.

The case of the normal problem influencing the tangential problem is of greater practical interest, especially in the case of a small coefficient of friction μ. This would be an investigation into the second approximation of sec. 2.1. This has already been carried out for the two-dimensional case of two cylinders rolling freely over each other, see JOHNSON [4]. In the general three-dimensional case of rolling contact, the treatment would differ only slightly from the one given in chapter 5. The only new thing needed is

$$\frac{\partial u^H}{\partial x} = \left[\frac{\partial u}{\partial x}\right]_{X=Y=0}, \quad \frac{\partial v^H}{\partial x} = \left[\frac{\partial v}{\partial x}\right]_{X=Y=0} \tag{6.4}$$

which can be given as a surface integral derived from (2.11a,b), with the Hertzian normal pressure

$$Z(x',y') = G\, f_{00} \sqrt{1-(x'/a)^2-(y'/b)^2}. \tag{6.5}$$

By means of the substitutions of the fundamental lemma of sec. 2.2, the double integral derived from (2.11) can be reduced to a single integral with periodic continuous integrand which is integrated over the period. So the quantities (6.4) are brought in a numerically accessible form. The relative slip is then given by (4.15c):

$$\left.\begin{aligned} s_x &= v_x-\phi y+\left[\frac{\partial u}{\partial x}\right] = v_x-\phi y+\left[\frac{\partial u}{\partial x}\right]_{X=Y=0}+\left[\frac{\partial u}{\partial x}\right]_{Z=0}, \\ s_y &= v_y+\phi x+\left[\frac{\partial v}{\partial x}\right] = v_y+\phi x+\left[\frac{\partial v}{\partial x}\right]_{X=Y=0}+\left[\frac{\partial v}{\partial x}\right]_{Z=0}; \end{aligned}\right\} \tag{6.6}$$

the only difference with the theory of ch. 5 is, that a known function is added to s_x and s_y at each point.

An analytical investigation into JOHNSON's problem of free rolling is also feasible in the case of a circular contact area. The problem is:

Determine v_x, v_y and ϕ so, that

$$\left.\begin{aligned} s_x &\equiv v_x-\phi y+\left[\frac{\partial u}{\partial x}\right]_{X=Y=0}+\left[\frac{\partial u}{\partial x}\right]_{Z=0} = 0 \text{ in E}, \\ s_y &\equiv v_y+\phi x+\left[\frac{\partial v}{\partial x}\right]_{X=Y=0}+\left[\frac{\partial v}{\partial x}\right]_{Z=0} = 0 \text{ in E}; \end{aligned}\right\} \tag{6.7}$$

No singularity at the edge of the contact area;

$Z = f_{00}\, G \sqrt{1-x^2/a^2-y^2/a^2}$.

This investigation could be based on potential theory, using the methods developed in KALKER [1].

As a final project we mention the case of instationary rolling: it is perhaps possible that the theory of ch. 5 can be adapted to some problems of unsteady rolling.

References.

CAIN, B.S. [1] Discussion of the paper by H. PORITSKY: Stresses and deflections of cylindrical bodies in contact, with application to contact of gears and of locomotive wheels. Discussion: J. Appl. Mech. (1950) p. 465.

CARTER, F.W. [1] On the action of a locomotive driving wheel. Proc. Roy. Soc. A112 (1926) p. 151-157.

CATTANEO, C. [1] Sul contatto di due corpi elastici: distribuzione locale degli sforzi. Rend. Acad. Lincei, ser. 6, vol. XXVII, 1938 pp. 342-348, 434-436, 474-478.

DOVNOROVICH, V.I. [1] Three-dimensional contact problems in the theory of elasticity. Minsk (1959) (in Russian).

ERDELYI, A. et al. [1] Higher transcendental functions Vol. 1, Mc.Graw-Hill, 1953.

GALIN, A.L. [1] Contact problems in the theory of elasticity. Moscow (1953) (in Russian). Also in English translation, at the North Carolina State College, 1961.

HAINES, D.J. and E. OLLERTON [1] Contact stress distributions on elliptical contact surfaces subjected to radial and tangential forces. Proc. Inst. Mech. Engrs. Vol. 177 (1963) p. 95-114.

HAINES, D.J. [2] Contact stresses in flat elliptical contact surfaces which support radial and shearing forces during rolling. Proc. Inst. Mech. Engrs. 1964-65, Vol. 179, part 3.

JAHNKE, E. and F. EMDE [1] Tables of functions. Dover publications, New York, 1943.

JOHNSON, K.L. [1] The effect of a tangential contact force upon the rolling motion of an elastic sphere on a plane. J. Appl. Mech. 25 (1958) p. 339-346.

[2] The effect of spin upon the rolling motion of an elastic sphere upon a plane. J. Appl. Mech.

JOHNSON, K.L. 25 (1958) p. 332-338.

[3] The influence of elastic deformation upon the motion of a ball rolling between two surfaces. Proc. Inst. Mech. Engrs. 173 (1959) 34 p. 795-810.

[4] Tangential tractions and microslip in rolling contact, Proc. Symp. Rolling Contact Phenomena ed. J.B. BIDWELL, Elsevier 1962, p. 6-28.

JOHNSON, K.L. and P.J. VERMEULEN [5] Contact of nonspherical bodies transmitting tangential forces. J. Appl. Mech. (1964) p. 338-340.

KALKER, J.J. [1] The transmission of force and couple between two elastically similar rolling spheres. Proc. Kon. Ned. Akad. Wet. Amsterdam, B67 (1964) p. 135-177.

[2] A strip theory for rolling with slip and spin, Proc. Kon. Ned. Akad. Wet. Amsterdam, B70 (1967) p. 10-62.

LEE, A.J.C. and E. OLLERTON [1] The photcelastic investigation of rolling with spin. VDI-Berichte nr. 102, 1966, S. 25/28.

LOVE, A.E.H. [1] A treatise on the mathematical theory of elasticity. 4th ed. Cambridge U.P. 1952.

LUTZ, O. [1] Grundsätzliches über stufenlos verstellbare Wälzgetriebe. Konstruktion 7 (1955) 9, p. 330-335.

[2] Same title. Konstruktion 9 (1957) 5, p. 169-171.

[3] Same title. Konstruktion 10 (1958) 11, p. 424-427.

MINDLIN, R.D. [1] Compliance of elastic bodies in contact. J. Appl. Mech. 16 (1949) p. 259 sqq.

DE PATER, A.D. [1] On the reciprocal pressure between two bodies. Proc. Symp. Rolling Contact Phenomena. ed. J.B. BIDWELL, Elsevier 1962 p. 29-75.

POON, S.Y. [1] An experimental study of the shear traction distribution in rolling with spin. Wear,

10 (1967) no. 1, p. 61-69.

SNEDDON, I.N. [1] The use of transform methods in elasticity, Techn. Rept. AFOSR 64-1789. North Carolina State College, (1964).

WERNITZ, W. [1] Wälz-Bohrreibung. F. Vieweg & Sohn, Braunschweig 1958, p. 68-81.

[2] Friction at Hertzian contact with combined roll and twist. Proc. Symp. Rolling Contact Phenomena, ed. J.B. BIDWELL, Elsevier 1962, p. 132-156.

Notations.

Underlined symbols designate vectors. A superscript $^+$ indicates that the quantity belongs to the lower body. A superscript $^-$ indicates that the quantity belongs to the upper body. We list only symbols the meaning of which extends beyond the section where they are defined.

Symbol	Meaning	Definition, etc.
a	In sec. 1.1: half width of contact area	Fig. 2
	Elsewhere: semi-axis of contact ellipse in x-direction	(1.5a)
a_{mn}	Coefficient of u-polynomial	(1.10)
$\underline{B}$	(No vector) A complete elliptic integral	(3.17)
b	In sec. 1.1: coordinate of trailing edge of locked area	Fig. 2
	Elsewhere: semi-axis of contact ellipse in y-direction	(1.5a)
b_{mn}	Coefficient of v-polynomial	(1.10)
C_{ij}	In sec. 4.32: creepage coefficient	(4.36), Fig. 8 Table 3
$\underline{C}$	(No vector) A complete elliptic integral	(3.17), Table 1
c	$= \sqrt{ab}$, geometric mean of semi-axes of contact ellipse	(3.50)
c_{mn}	Coefficient of w-polynomial	(1.10)
$\underline{D}$	(No vector) A complete elliptic integral	(3.17), Table 1
d	Integer with special meaning	(2.67)
d_{pq}	Coefficient of X'-polynomial	(1.9), (4.63)
E	(Elliptic) contact area	(1.5a)
E_g	Slip area	
E_h	Area of adhesion, also called locked area	

Symbol	Meaning	Definition, etc.
$E^{h;pq}_{mn}$	A certain integral	(2.35),(2.48),(2.53)
$E^{h;2p+\varepsilon,2q+\omega}_{2m+\varepsilon,2n+\omega}$	Expressed in complete elliptic integrals	(2.73),(2.74),(3.22)
$\underline{E}$	(No vector) Complete elliptic integral of the 2nd kind	(3.17), Table 2
e	Signed excentricity of contact ellipse	(2.63), Table 2
e_{pq}	Coefficient of Y'-polynomial	(1.9),(4.63),(5.1)
(F_x,F_y)	(x,y) components of total tangential force on lower body. See also (f_x,f_y)	(4.24)
$F^{h;pq}_{mn}$	Coefficients derived from $E^{h;pq}_{mn}$	(3.4),(3.15)
$F^{h;2p+\varepsilon,2q+\omega}_{2m+\varepsilon,2n+\omega}$	Expressed in complete elliptic integrals	(3.12),(3.13),(3.22)
f	In 5.22, 5.23: integrand of I	sec. 5.22
(f_x,f_y)	Components of dimensionless total force exerted on lower body	(4.19), Figs. 3, 8, 10, 11, 13, 14, 15, 23, 24
G, G^+, G^-	Modulus of rigidity: combined, upper body, lower body	(2.4),(2.10)
g	=min(a/b,b/a). Ratio of axes of contact ellipse	(2.63), Table 2
I	In ch. 5: an integral to be minimized	(5.9)
I(d,i,j,e)	A complete elliptic integral	(2.74),(3.14),(3.21)
J(x,y)	"Square root singularity"	(2.21a)
J(d,i,j,e)	A complete elliptic integral	(3.13),(3.14),(3.21)
K	Integer connected with the degree: M=2K+ν	(2.54)
$\underline{K}$	(No vector) Complete elliptic integral of the 1st kind	(3.17), Table 2
ℓ	Integer; also: major semi-axis of contact ellipse max(a,b)	

Symbol	Meaning	Definition, etc.
M	Degree of traction polynomial	(1.9)
M_z	Total moment about the z-axis on lower body	(4.24)
m_z	Dimensionless total moment about z-axis	(4.19)
N	Total normal force	(3.50)
O	Origin of cartesian coordinate system, centre of contact area. Also: order of magnitude symbol	
P	Proportional to x-component of relative slip	(5.18)
p	In ch. 5 only: number of degrees of freedom	(5.1)
Q	Proportional to y-component of relative slip	(5.18)
q	In ch. 5 only: summation limit	(5.1)
R	Distance between two points on the surface	(2.9)
$R_x^+, R_y^+, R_x^-, R_y^-$	Radii of curvature of bodies in xz, yz plane	sec. 3.221
r	Distance from origin to a point of the plane z=0 (except in sec. 2.1)	(2.33)
S	Positive definite function of relative slip	(5.6)
s	Minor semi-axis of contact ellipse min(a,b)	(2.63)
$\underline{s}(s_x, s_y)$	Relative slip (vector end components) of upper body over lower	(4.15)
T	Positive definite function of traction difference	(5.6)
t	Time	

Symbol	Meaning	Definition, etc.
(u,v,w)	Displacement differences, except in 2.41 and 4.31	(1.4), (1.6b)
$\underline{u}^{\pm}(u^{\pm},v^{\pm},w^{\pm})$	Elastic displacement of lower/ upper body	
V	Magnitude of rolling velocity, except in sec. 5.23	(4.9), (4.10)
W	Weight function	(5.8)
W_1	A special weight function	(5.14)
(w_x,w_y)	Components of unit vector in the direction of the slip	(1.8a)
(X,Y,Z)	(x,y,z) components of surface tractions on lower body	
(X,Y)	Tangential traction components	
(X',Y')	Traction polynomials	(4.40), (4.63), (5.5)
(x,y,z)	Cartesian coordinate system	sec. 2
x-direction	(Nearly the) rolling direction	(4.10)
y-direction	Lateral direction	
z-direction	Inner normal on lower body at centre of contact area	
Z	Normal pressure distribution, mostly Hertzian	(1.5b)
z_j	Standard polynomial	(5.1)
z_j'	x-derivative of z_j	(5.2)
α	Angle between creepage and x-axis in degrees	(4.104), (5.30)
δ	A small positive number with several meanings	(2.38); (4.10); (5.12c)
ε,ε'	Parity numbers (0 or 1); $\varepsilon+\varepsilon'=1$	(2.54)
η	Lateral creepage parameter	(4.20)
κ	An elastic constant (neglected in the present work)	(2.10)
μ	Coefficient of friction, assumed	

Symbol	Meaning	Definition, etc.
	to be constant	
ν,ν'	Parity numbers (0 or 1); $\nu+\nu'=1$	(2.54)
ξ	Longitudinal creepage parameter	(4.20)
ρ	Characteristic length of the bodies	(3.38)
σ,σ^+,σ^-	Poisson's ratio: combined, upper body, lower body	(2.4),(2.10)
τ_k	Coefficients of traction polynomials	(5.1)
υ	Creepage. In ch. 5:	(5.16),(5.30)
$\underline{\upsilon}(\upsilon_x,\upsilon_y)$	Creepage vector, longitudinal and lateral creepage	(4.11),(4.14a)
ϕ	Spin	(4.12),(4.14a)
χ	Spin parameter	(4.20)
ω,ω'	Parity numbers (0 or 1); $\omega+\omega'=1$	(2.54)